Ministry of Higher Education and Scientific Research
Hassiba Ben Bouali University of Chlef
Faculty of Science and Technology
Department of Electrical Engineering

THESIS

Submitted in fulfillment of the requirements for the degree of

DOCTORATE(LMD)

Field : Electrotechnics

Specialty : Electrical Networks

by

Mohamed CHENOUI

Title:

Carbon Dioxide Treatment Using Electrical Discharges

(Traitement de Dioxyde de Carbonne par l'utilisation des décharges électriques)

Defended on 28/04/2026, in front of the jury composed of :

Toufik TAHRI	Professor	University of Chlef	Chair
Hocine TEBANI	MCA	University of Chlef	Supervisor
Djilali BENYOUCEF	Professor	University of Chlef	Co-Supervisor
Mohamed MOSTEFAOUI	MCA	University of Chlef	Examiner
Aicha AISSA BOKHTACHE	MCA	University of Chlef	Examiner
Abdelatif GADOUM	MCA	University of Ouargla	Examiner
Ismail BOUYAKOUB	MCA	University of Chlef	Guest

In the name of Allah, the Beneficent, the Merciful

Acknowledgment

First and foremost, I thank God for granting me the health, strength, and perseverance necessary to complete this work.

I would like to express my sincere gratitude and deep appreciation to my professors at University of Chlef and to all those who contributed to the realization of this thesis.

My heartfelt thanks go to my supervisors, **Dr. Hocine TEBANI** and , **Pr. Djilali BENYOUCEF** from the Department of Electrical Engineering at the University of Chlef for their guidance, constant support, valuable advice, and availability throughout the course of this work, despite his numerous commitments.

I am also honored to thank **Pr. Toufik TAHRI** for kindly agreeing to preside over the jury of this thesis.

I would like to extend my sincere thanks to **Dr. Mohamed MOSTEFAOUI, Dr. Aicha AISSA BOUKHTACHE** and **Dr. Abdelatif GADOUM** for accepting to examine this work and for their valuable comments and suggestions.

Finally, I would like to express my heartfelt gratitude to my family for their unconditional love, patience, and unwavering support, and to my friends, whose encouragement and companionship have been a great source of motivation throughout this journey.

إهداء

الحمد لله حمدًا يليق بجلاله وعظيم سلطانه، على ما أولاني من نعمٍ وتوفيق، وعلى ما منحني من صبرٍ وعزيمة حتى أتممت هذا العمل

إلى من كانا أساس هذا النجاح، ومن غرسا في نفسي حبّ العلم والاجتهاد، وبذلا من أجلي الغالي والنفيس دون انتظار مقابل،
إلى والديّ الكريمين، حفظهما الله وأطال في عمرهما، وجزاهما عني خير الجزاء،

إلى من كانت دعواتها نورًا لطريقي، وحنانها ملاذًا في كلّ حين، وصبرها سرّ قوتي،
إلى أمي الغالية، أطال الله عمرها ومتّعها بالصحة والعافية،

إلى من شاركوني رحلة البحث والتعب والسهر، وكانوا عونًا لي في الشدائد،
إلى إخوتي وعائلتي الكريمة، جزاهم الله عني كلّ خير،

إلى أساتذتي الأفاضل، الذين كان لعلمهم وتوجيههم الأثر البالغ في إنجاز هذه الأطروحة،
وإلى كل من قدّم لي يد العون والدعم، من قريب أو بعيد،

أهدي هذا العمل المتواضع، راجيًا من الله تعالى أن يجعله إضافة نافعة للعلم والمعرفة، وأن يتقبّله خالصًا لوجهه الكريم

والحمد لله ربّ العالمين.

محمد شنوي

Abstract

This thesis investigates the application of non-thermal dielectric barrier discharge (DBD) plasma for the conversion of carbon dioxide (CO_2) at atmospheric pressure, with the objective of improving CO_2 activation and conversion efficiency under controlled operating conditions. Non-thermal plasmas offer a promising alternative to conventional thermal processes by enabling efficient energy transfer to electrons while maintaining low gas temperatures, thereby favoring selective chemical reactions. A self-consistent plasma model is developed to describe the electrical and physicochemical behavior of CO_2/Ar DBD discharges. The model accounts for electron kinetics, plasma chemistry, charge transport, and electric field evolution within the reactor. Particular attention is given to the role of gas composition and dielectric properties in shaping discharge dynamics and stability. The influence of key operating parameters, including applied voltage, excitation frequency, gas pressure, argon concentration, and dielectric material characteristics, is systematically analyzed through numerical simulations. The results demonstrate that the addition of argon significantly enhances electron density and promotes more stable discharge behavior by reducing the breakdown voltage and facilitating electron impact processes. Optimal CO_2 conversion performance is obtained at intermediate excitation frequencies and applied voltages, where a balance between discharge intensity and stability is achieved. In contrast, increasing the gas pressure leads to reduced conversion efficiency due to enhanced collisional losses and reduced electron mean free path. The simulated electrical characteristics and plasma behavior show good agreement with experimental observations, validating the reliability of the proposed model. Overall, this work provides valuable insights into the mechanisms governing CO_2 activation in DBD plasmas and highlights the importance of operating parameter optimization for the development of efficient plasma-based CO_2 conversion and environmental technologies.

Keywords: Dielectric barrier discharge; Non-thermal plasma; Carbon dioxide conversion; CO_2 splitting; Plasma modeling; Argon admixture; Electrical discharges; Environmental applications.

Résumé

Cette thèse étudie l'application des plasmas non thermiques de type décharge à barrière diélectrique (DBD) pour la conversion du dioxyde de carbone (CO_2) à pression atmosphérique, dans le but d'améliorer l'activation du CO_2 et l'efficacité globale de conversion sous des conditions de fonctionnement contrôlées. Les plasmas non thermiques constituent une alternative prometteuse aux procédés thermiques conventionnels, car ils permettent un transfert d'énergie efficace vers les électrons tout en maintenant une température du gaz relativement basse, favorisant ainsi des réactions chimiques sélectives. Un modèle plasma auto-cohérent est développé afin de décrire le comportement électrique et physico-chimique des décharges DBD CO_2/Ar. Ce modèle prend en compte la cinétique électronique, la chimie du plasma, le transport des charges et l'évolution du champ électrique au sein du réacteur. Une attention particulière est portée au rôle de la composition du gaz et des propriétés diélectriques dans la dynamique et la stabilité de la décharge. L'influence des principaux paramètres opératoires, tels que la tension appliquée, la fréquence d'excitation, la pression du gaz, la concentration en argon et les caractéristiques du matériau diélectrique, est analysée de manière systématique à travers des simulations numériques. Les résultats montrent que l'ajout d'argon améliore significativement la densité électronique et favorise un comportement plus stable de la décharge en réduisant la tension de claquage et en facilitant les processus d'impact électronique. Des performances optimales de conversion du CO_2 sont obtenues pour des valeurs intermédiaires de fréquence et de tension appliquée, où un compromis entre intensité et stabilité de la décharge est atteint. En revanche, l'augmentation de la pression du gaz entraîne une diminution de l'efficacité de conversion en raison de l'intensification des pertes collisionnelles et de la réduction du libre parcours moyen des électrons. Les résultats numériques présentent un bon accord avec les observations expérimentales, ce qui confirme la validité du modèle proposé. Dans l'ensemble, ce travail apporte des connaissances approfondies sur les mécanismes gouvernant l'activation du CO_2 dans les plasmas DBD et souligne l'importance de l'optimisation des paramètres opératoires pour le développement de technologies plasma efficaces dédiées à la conversion du CO_2 et aux applications environnementales.

Mots-clés: Décharge à barrière diélectrique ; Plasma non thermique ; Conversion du dioxyde de carbone ; Dissociation du CO_2 ; Modélisation plasma ; Ajout d'argon ; Décharges électriques ; Applications environnementales.

ملخص

تتناول هذه الأطروحة دراسة استخدام البلازما غير الحرارية من نوع التفريغ ذي الحاجز العازل (DBD) في تحويل ثاني أكسيد الكربون (CO_2) عند الضغط الجوي، وذلك بهدف تحسين تنشيط جزيئات CO_2 ورفع كفاءة التحويل الكلية تحت ظروف تشغيل محكومة. وتُعد البلازما غير الحرارية بديلاً واعدًا للتقنيات الحرارية التقليدية، إذ تُمكّن من نقل الطاقة بشكل انتقائي إلى الإلكترونات مع الحفاظ على درجة حرارة منخفضة نسبيًا للغاز، مما يسمح بتحفيز التفاعلات الكيميائية بكفاءة عالية ودون الحاجة إلى ظروف تشغيل قاسية.تم تطوير نموذج بلازما ذاتي الاتساق لوصف السلوك الكهربائي والفيزيائي–الكيميائي لتفريغات DBD في خليط CO_2/Ar.ويأخذ هذا النموذج بعين الاعتبار حركية الإلكترونات، وكيمياء البلازما، وانتقال الشحنات، وتطور المجال الكهربائي داخل المفاعل. كما أُولي اهتمام خاص بدراسة تأثير تركيب الغاز وخصائص المواد العازلة على ديناميكية التفريغ واستقراره. وتم تحليل تأثير المعلمات التشغيلية الأساسية، بما في ذلك الجهد المطبق، وتردد الإثارة، وضغط الغاز، ونسبة الأرجون، وخصائص الحاجز العازل، وذلك بشكل منهجي اعتمادًا على المحاكاة العددية.تُظهر النتائج أن إضافة غاز الأرجون تؤدي إلى زيادة ملحوظة في كثافة الإلكترونات وتحسين استقرار التفريغ من خلال خفض جهد الانهيار وتعزيز عمليات التصادم الإلكتروني. كما تبيّن أن أفضل أداء لتحويل ثاني أكسيد الكربون يتحقق عند قيم متوسطة لكل من الجهد والتردد، حيث يتم الوصول إلى توازن مناسب بين شدة التفريغ واستقراره. في المقابل، يؤدي ارتفاع ضغط الغاز إلى انخفاض كفاءة التحويل نتيجة ازدياد الخسائر التصادمية وانخفاض متوسط المسار الحر للإلكترونات. وقد أظهرت النتائج العددية توافقًا جيدًا مع المعطيات التجريبية المتوفرة، مما يؤكد موثوقية وصلاحية النموذج المقترح.بوجه عام، يقدّم هذا العمل إسهامًا علميًا في فهم الآليات الفيزيائية والكيميائية التي تحكم تنشيط ثاني أكسيد الكربون في بلازما التفريغ ذي الحاجز العازل، ويبرز أهمية تحسين شروط التشغيل من أجل تطوير تقنيات بلازما فعّالة ومستدامة لتحويل CO_2 وتطبيقاته البيئية.

الكلمات المفتاحية: التفريغ ذو الحاجز العازل؛ البلازما غير الحرارية؛ تحويل ثاني أكسيد الكربون؛ تفكك ثاني أكسيد الكربون؛ نمذجة البلازما؛ إضافة الأرجون؛ التفريغات الكهربائية؛ التطبيقات البيئي.

List of Abbreviation

AC	Alternating Current
DC	Direct Current
CCS	Carbon Capture and Storage
CCU	Carbon Capture and Utilization
CO_2	Carbon Dioxide
CO	Carbon Monoxide
Ar	argon
CaO	calcium oxide
NO_x	nitrogen oxides
DBD	Dielectric Barrier Discharge
EEDF	Electron Energy Distribution Function
GHG	greenhouse gas
HV	High Voltage
MCC	Monte Carlo Collision
NTP	Non-Thermal Plasma
PIC	Particle-in-Cell
GWP	Global Warming Potential
PDE	Partial differential equations
VOC	Volatile Organic Compound
V–I	Voltage–Current
FEM	Finite Element Method
1D	One-Dimensional

List of Symbols

A	Electrode surface area	(m^2)
C	Capacitance	(F)
C_d	Dielectric capacitance	(F)
C_g	Gas gap capacitance	(F)
d	Electrode gap distance	(mm)
E	Electric field strength	($V \cdot m^{-1}$)
e	Elementary charge	(C)
f	Frequency	(Hz)
$f(\varepsilon)$	Electron energy distribution function	(eV^{-1})
I	Discharge current	(A)
k_j	Reaction rate coefficient	($m^3 \cdot s^{-1}$)
k_B	Boltzmann constant	($J \cdot K^{-1}$)
n	Number density	(m^{-3})
n_e	Electron density	(m^{-3})
n_ε	Electron energy density	($eV \cdot m^{-3}$)
μ_e	Electron mobility	($m^2 \cdot V^{-1} \cdot s^{-1}$)
μ_i	Ion mobility	($m^2 \cdot V^{-1} \cdot s^{-1}$)
D_e	Electron diffusion coefficient	($m^2 \cdot s^{-1}$)
D_i	Ion diffusion coefficient	($m^2 \cdot s^{-1}$)
Γ_e	Electron flux	($m^{-2} \cdot s^{-1}$)
Γ_i	Ion flux	($m^{-2} \cdot s^{-1}$)

P	Discharge power	(W)
R	resistance	(Ω)
t	Time	(s)
T_e	Electron temperature	(eV) or(°K)
T_g	Gas temperature	(K)
V	Applied voltage	(V)
ε	Mean electron energy	(eV)
ε_0	Vacuum permittivity	($F \cdot m^{-1}$)
ε_r	Relative permittivity	(–)
Q	Accumulated surface charge	(C)

List of Figures

CHAPTER I : GENERAL OVERVIEW OF PLASMAS AND ELECTRICAL DISCHARGES

CHAPTER II : FUNDAMENTALS OF DIELECTRIC BARRIER DISCHARGES

CHAPTER III : PLASMA MODEL PARAMETERS AND COMPUTATIONAL APPROACH

CHAPTER IV:MODELING AND ELECTRICAL CHARACTERIZATION OF CO_2/AR DIELECTRIC BARRIER DISCHARGES

List of Table

CHAPTER I : GENERAL OVERVIEW OF PLASMAS AND ELECTRICAL DISCHARGES

CHAPTER II : FUNDAMENTALS OF DIELECTRIC BARRIER DISCHARGES

CHAPTER IV: MODELING AND ELECTRICAL CHARACTERIZATION OF CO_2/AR DIELECTRIC BARRIER DISCHARGES

Table of Contents

CHAPTER II:FUNDAMENTALS OF DIELECTRIC BARRIER DISCHARGES

CHAPTER III:PLASMA MODEL PARAMETERS AND COMPUTATIONAL APPROACH

CHAPTER IV:MODELING AND ELECTRICAL CHARACTERIZATION OF CO_2/AR DIELECTRIC BARRIER DISCHARGES

General Introduction

General Introduction

The continuous increase in global carbon dioxide (CO_2) emissions resulting from fossil fuel combustion, industrial activities, and transportation has become one of the most critical environmental issues worldwide[1]. Elevated atmospheric CO_2 concentrations are widely recognized as a major driver of climate change, global warming, ocean acidification, and ecosystem degradation[2]. Consequently, considerable scientific and technological efforts have been directed toward the development of effective carbon capture, conversion, and utilization strategies aimed at reducing greenhouse gas emissions and enabling a transition toward sustainable energy systems[3,4].

Conventional CO_2 conversion technologies, including thermochemical reforming and catalytic hydrogenation, typically require high operating temperatures and pressures, leading to significant energy consumption and limited economic viability[5]. In response to these challenges, non-thermal plasma technologies have emerged as promising alternatives for CO_2 activation and conversion[6,7]. Unlike thermal processes, non-thermal plasmas enable selective energy transfer to electrons, which can efficiently initiate molecular excitation, ionization, and dissociation reactions at near-ambient gas temperatures. This unique characteristic has motivated extensive research into plasma-assisted CO_2 conversion over the past two decades[8].

Among various non-thermal plasma sources, dielectric barrier discharge (DBD) reactors have been widely investigated due to their operational stability, simplicity of design, and compatibility with atmospheric-pressure operation[9]. Early experimental studies by Eliasson and Kogelschatz demonstrated the potential of DBD plasmas for gas treatment and environmental applications[10], establishing a foundation for subsequent research on CO_2 conversion. Later works by Fridman, Nozaki, and Aerts et al[11]. highlighted the importance of electron-driven vibrational excitation and dissociation pathways in CO_2-containing plasmas. These studies showed that the addition of noble gases such as argon or helium can significantly enhance electron density and energy efficiency by lowering the breakdown voltage and stabilizing the discharge[12,13].

Recent research trends have focused on improving CO_2 conversion efficiency through reactor optimization, plasma-catalyst coupling, and advanced power modulation techniques. Numerical modeling has become an essential tool in this context[14], as demonstrated by the works of Hagelaar, Pancheshnyi[15], and Bogaerts, who developed fluid and hybrid plasma models capable of describing discharge dynamics, plasma chemistry, and transport phenomena. These models have provided valuable insights into the role of operating parameters such as applied voltage, excitation frequency, gas composition, pressure, and dielectric material properties[16,17].

Despite these advances, several challenges remain, including limited energy efficiency, complex plasma chemistry[18], and strong sensitivity of discharge behavior to operating conditions. In particular, the influence of dielectric properties and gas mixtures on the electrical and chemical performance of DBD reactors is not yet fully understood[19]. Therefore, further modeling and systematic parametric studies are required to bridge the gap between fundamental plasma physics and practical reactor design[20].

The objective of the work conducted in this thesis is to simulate a dielectric barrier discharge (DBD) at atmospheric pressure in CO_2/Ar gas mixtures for the purpose of understanding and enhancing CO_2 conversion. The thesis is structured as follows:

The first chapter provides a general overview of plasmas and electrical discharges, introducing fundamental plasma concepts, classification of discharge regimes, and voltage–current characteristics of gas discharges. Particular emphasis is placed on non-thermal plasmas and their advantages for gas treatment and environmental applications.

The second chapter is devoted to the fundamentals of dielectric barrier discharges. It reviews the historical development of DBDs, their operating principles, discharge regimes, reactor configurations, and the role of dielectric materials in stabilizing the discharge and preventing arc formation.

In the third chapter, the plasma modeling framework is presented. The governing equations, plasma chemistry, transport coefficients, boundary conditions, and numerical solution strategies are detailed. The computational approach adopted allows for the self-consistent simulation of electrical, kinetic, and chemical phenomena occurring in CO_2/Ar DBD systems.

The fourth chapter focuses on the modeling and electrical characterization of CO_2/Ar dielectric barrier discharges. Simulation results are analyzed and compared with experimental data to validate the model. The effects of key operating parameters, including applied voltage, excitation frequency, gas composition, pressure, and dielectric properties, are systematically investigated. The results demonstrate that argon addition significantly enhances electron density and CO production, while optimal operating conditions exist for maximizing CO_2 conversion efficiency.

Objectives

The main objective of this thesis is to investigate and optimize the behavior of non-thermal dielectric barrier discharge (DBD) plasmas for carbon dioxide (CO_2) treatment through numerical modeling and electrical characterization. In particular, this work aims to improve the understanding of plasma–gas interactions and the influence of operating conditions on discharge performance.

The specific objectives of this thesis are as follows:

- To provide a comprehensive theoretical background on plasmas, electrical discharges, and non-thermal plasma technologies, with emphasis on dielectric barrier discharges.
- To develop a numerical plasma model capable of describing the physical and electrical behavior of CO_2/Ar DBD discharges under atmospheric pressure conditions.
- To analyze the influence of key operating parameters, such as applied voltage, excitation frequency, gas composition, and dielectric properties, on discharge characteristics and plasma stability.
- To characterize the electrical behavior of the DBD reactor through voltage–current analysis and evaluation of discharge regimes.
- To assess the role of argon addition in enhancing plasma ignition, discharge uniformity, and energy transfer efficiency.
- To contribute to the optimization of DBD operating conditions for efficient CO_2 activation and potential conversion applications.

Graphical abstract

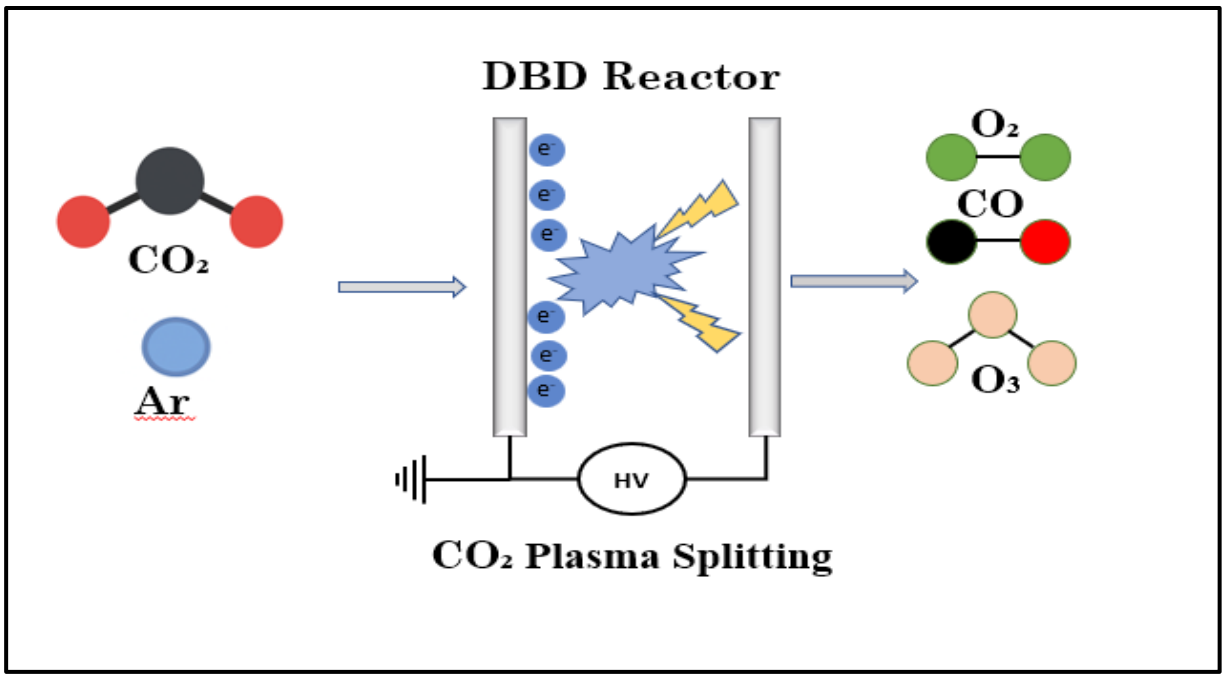

Chapter I:

General overview of plasmas and electrical discharges

I.1. Introduction

The steady rise in greenhouse gas pollution, especially carbon dioxide (CO_2),has become one of the most critical environmental challenges facing modern society[21]. Driven largely by man-made activities like burning fossil fuels and industrial operations, and energy production, the accumulation of CO_2 in the atmosphere has intensified global warming[22], climate change, and a wide range of environmental impacts. Addressing these challenges requires not only effective mitigation strategies but also innovative technologies capable of reducing emissions while enabling sustainable utilization of carbon resources.

Carbon capture and utilization (CCU) is a promising strategy to reduce CO_2 emissions by capturing and converting CO_2 from industrial exhausts into valuable goods including fuels, chemicals, and materials[23]. However, the efficiency of CCU technologies strongly depends on the performance of CO_2 capture, separation, and conversion processes. Conventional separation methods, including absorption, adsorption, and cryogenic techniques, are widely used but often suffer from high energy consumption, operational complexity, and environmental concerns[24].

In this context, plasma-based technologies have gained increasing attention as an alternative and complementary solution for the treatment of gaseous effluents. Plasmas, particularly cold or non-thermal plasmas, offer unique advantages due to their ability to generate highly energetic electrons while maintaining near-ambient gas temperatures. This non-equilibrium characteristic enables efficient gas activation, chemical conversion, and pollutant degradation without excessive thermal energy input.

This chapter provides a comprehensive overview of greenhouse gas emissions and their environmental consequences, followed by a detailed discussion of CO_2 capture and separation technologies. The fundamentals of plasma science, including plasma definitions, classifications, physical parameters, and voltage–current characteristics of gas discharges, are presented to establish the theoretical background. Special emphasis is placed on cold plasmas and non-thermal discharges, their operating regimes, and various plasma configurations such as glow discharge, plasma jets, corona discharge, gliding arc plasma, and dielectric barrier discharges. The chapter highlights the role of electric fields in gas ionization and underlines the importance of avoiding

arc formation in non-thermal plasma applications, particularly for CO_2 treatment and environmental protection.

I.2. Greenhouse gas emissions

The progressive increase in greenhouse gas (GHG) concentrations in the atmosphere has become a major global concern due to its direct impact on climate change[25], global warming, and environmental degradation. Infrared light from the Earth's surface is absorbed by greenhouse gases and then released again, producing the so-called greenhouse effect. Although the greenhouse effect is vital for sustaining Earth's livable temperature, the rapid enhancement caused by human activities leads to climate imbalance[26].

According to international climate assessments (IPCC, UNFCCC), global GHG emissions have risen steadily during the industrial revolution, mostly as a result of changes in land usage and the burning of fossil fuels. Carbon dioxide (CO_2) is still the most significant of all the greenhouse gases because its high concentration, long atmospheric lifetime, and central role in anthropogenic warming.

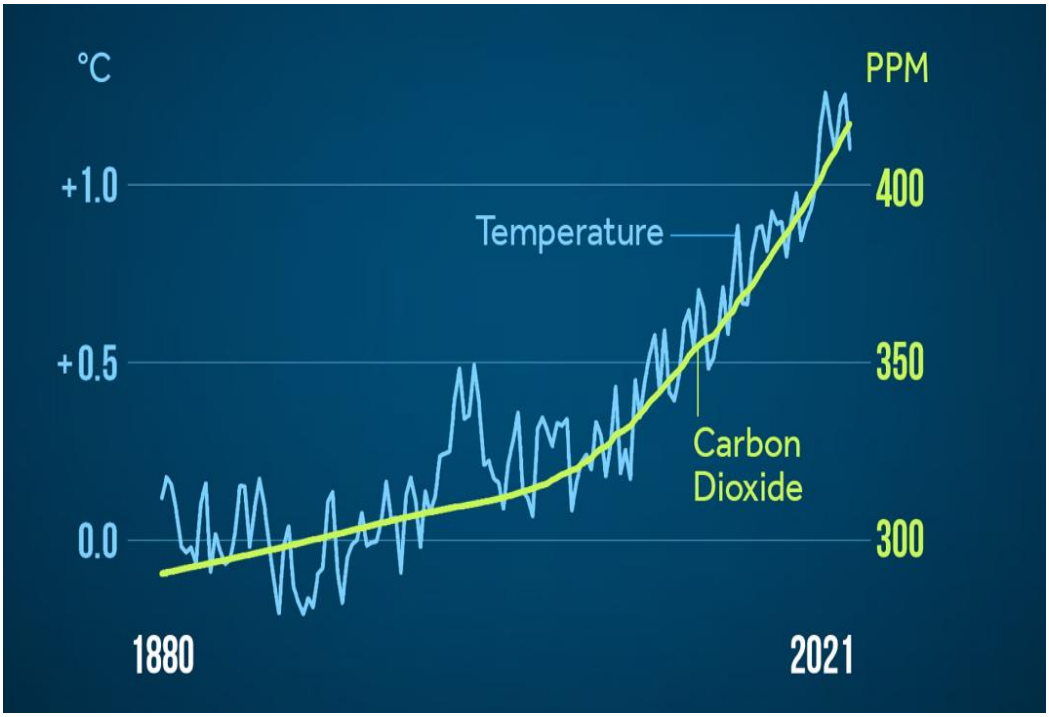

Figure I.1: Annual CO_2 peak and temperature[27].

I.2.1 Major greenhouse gases

Greenhouse gases include several classes of naturally occurring and human-emitted compounds:

- **Carbon dioxide (CO_2):** primarily produced by the combustion of fossil fuels such as coal, oil, and natural gas, this emission contributes to global warming. It constitutes seventy-five percent of total emissions. It can persist in the atmosphere for centuries,

inducing prolonged climate alterations.

- **Methane (CH_4):** Methane is another greenhouse gas emitted via operations such as oil and natural gas extraction, as well as cattle rearing through enteric fermentation. Methane, while remaining in the atmosphere for a limited duration, is more effective than CO_2 at capturing radiation. Methane possesses a Global Warming Potential that is 25 times greater than that of CO_2 over a century.
- **Nitrous oxide (N_2O):** mostly originates from the application of synthetic and organic fertilizers. It has a significantly greater warming potential than CO_2 and contributes to the depletion of the stratospheric ozone layer.
- **Fluorinated gases: (HFCs, PFCs, SF_6):** Man-made substances, released through various procedures and utilized in products such as refrigerants, solvents, and foam-blowing agents, possess remarkable potency in contributing to warming. They possess a potency thousands of times greater than CO_2 and persist in the atmosphere for thousands of years.

Each gas differs in atmospheric lifetime and radiative forcing, expressed as the Global Warming Potential (GWP). CO_2 serves as the reference gas (GWP = 1).

I.2.2 Anthropogenic sources of CO_2 emissions

Anthropogenic carbon dioxide (CO_2) emissions originate primarily from human activities associated with energy production, industrial processes, and land-use changes. The primary source of CO2 emissions worldwide is the burning of fossil fuels, such as coal, oil, and natural gas, for transportation, heating, and electricity generation.

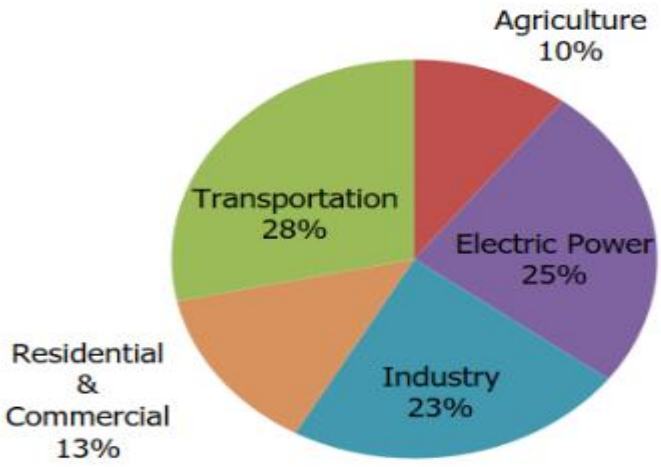

Figure I.2: Anthropogenic sources of CO_2 emissions[28].

Industrial activities, particularly cement production, iron and steel manufacturing, and chemical processing, contribute significantly through both fuel combustion and process-related

emissions. In addition, deforestation and land-use changes reduce the capacity of natural carbon sinks while releasing stored carbon into the atmosphere through biomass burning and soil degradation. Rapid urbanization, population growth, and increased energy demand have further intensified these emissions, making anthropogenic CO_2 a major driver of global climate change and environmental degradation.

I.3 Environmental impact of CO_2 emissions

Carbon dioxide (CO_2) is the most important long-lived anthropogenic greenhouse gas, and its continuous accumulation in the atmosphere has profound environmental consequences. Due to its ability to absorb infrared radiation, excess CO_2 intensifies the natural greenhouse effect, driving large-scale alterations in the Earth's climate system. The environmental impacts associated with elevated CO_2 concentrations are both global and long-lasting, making CO_2 mitigation one of the most urgent scientific and technological challenges[29].

I.3.1 Global warming and climate change

The increase in atmospheric CO_2 directly contributes to the positive radiative forcing responsible for global warming. Rising global temperatures have been linked to:

- Higher frequency and severity of heatwaves
- Shifts in climate patterns and precipitation
- Increased evaporation and drought conditions
- Intensification of cyclones and storms

Climate models consistently identify CO_2 as the dominant driver of present-day warming, owing to its atmospheric lifetime that spans decades to centuries.

I.3.2 Ocean acidification

Approximately one-quarter of anthropogenic CO_2 emissions are absorbed by the world's oceans. Dissolved CO_2 reacts with seawater to form carbonic acid, lowering the ocean's pH. This process leads to:

- Reduced availability of carbonate ions
- Threats to calcifying organisms (corals, shellfish, plankton)
- Disruption of marine food chains

- Decline in biodiversity and fisheries productivity

Ocean acidification is now recognized as one of the most rapid large-scale chemical changes in Earth's history.

I.3.3 Cryosphere melting and sea-level rise

Elevated CO_2 levels contribute to the warming of the Arctic and Antarctic regions, accelerating the melting of glaciers, ice sheets, and sea ice. This results in:

- Global sea-level rise through thermal expansion and melting
- Increased coastal flooding and erosion
- Loss of habitats for polar species
- Long-term changes in ocean circulation and climate regulation

These impacts pose significant risks to coastal populations and infrastructure worldwide.

I.3.4 Ecosystem degradation

The combined stressors associated with CO_2 emissions warming, altered precipitation, and ocean chemistry affect terrestrial and aquatic ecosystems. CO_2-driven environmental changes lead to:

- Increased public health risks (heat stress, vector-borne diseases)
- Increased risk of wildfires
- Decreased agricultural productivity in vulnerable regions
- Widespread loss of biodiversity

These consequences highlight the importance of developing sustainable CO_2 mitigation and conversion technologies.

I.4. Overview of CO_2 capture

CO_2 gas capturing is the initial and most energy-demanding phase in CCS and CCU systems; thus, the adoption of an effective capture method is crucial for the advancement of CCU technology. The capture method is most effective when executed at the source of emissions, such as flue gas from cement production or steelmaking, are promptly caught and separated on-site. Carbon dioxide extracted from the atmosphere necessitates separation and purification through a scrubbing procedure prior to its utilization in chemical processes[30].

The capture process can be categorized into three distinct types based on the technique of their application.

I.4.1 Post-combustion capture

The most well-known and extensively used CO_2 separation technique is post-combustion capture. This method extracts CO_2 from the flue gas that is created when fossil fuels are burned in gas turbines or traditional air-fired boilers. The flue gas typically contains CO_2 at low concentrations (3–15 vol%), mixed with N_2, O_2, water vapor, and trace impurities (SO_x, NO_x, particulates).

Chemical absorption using amine-based solvents (e.g., monoethanolamide) remains the dominant post-combustion technology due to its high selectivity and maturity. The process consists of absorbing CO_2 in a packed column, regenerating the solvent through stripping at elevated temperatures, and recycling it back into the absorber. Alternative approaches, such as adsorption, membrane separation, and carbonate looping, are under active development to reduce energy consumption and solvent degradation.

The main advantages of post-combustion capture include its compatibility with existing power plants (retrofitting) and well-established operating principles. However, its major limitations are the high energy penalty associated with solvent regeneration and the need for extensive gas pretreatment to remove contaminants that cause corrosion and solvent degradation[31,32].

I.4.2 Pre-combustion capture

Systems that rely on gasification, such integrated gasification combined cycle (IGCC) facilities, usually incorporate pre-combustion capture. In this configuration, a carbonaceous fuel (coal, biomass, or natural gas through reforming) is first converted into synthesis gas (syngas), a mixture of CO, H_2, CO_2, steam, and impurities. The CO is subsequently shifted to CO_2 via the water gas shift (WGS) reaction, generating a gas mixture rich in H_2 and CO_2.

Because CO_2 in pre-combustion systems is present at relatively high pressure and concentration, separation is more efficient and less energy intensive compared to post-combustion capture. Technologies typically employed include physical solvents (e.g., Selexol, Rectisol), adsorption processes , and high-temperature membranes.

Pre-combustion capture offers several benefits, including high CO_2 capture efficiency, lower separation costs, and the production of a valuable hydrogen-rich fuel suitable for low-emission power generation or industrial applications. Its main drawbacks are the complexity of gasification and reforming systems, high capital costs, and limited suitability for retrofitting existing power plants[33].

I.4.3 Oxy-fuel combustion

Oxy-fuel combustion includes burning fuel in a mixture of nearly pure oxygen and recycled flue gas instead of atmospheric air. Through the removal of nitrogen from the combustion operation, the resulting flue gas is composed mainly of CO_2 and H_2O, enabling straightforward CO_2 separation through simple condensation of water vapor.

The process requires an air separation unit (ASU) to generate oxygen with high purity (typically 95–99%), which is one of the major contributors to the overall energy consumption. Flue gas recirculation is employed to control flame temperature and maintain heat transfer characteristics similar to those of conventional combustion systems.

The key advantages of oxy-fuel combustion include high CO_2 concentration in the flue gas, the production of a relatively pure CO_2 stream (>95%), and the possibility of integrating the technology into both new installations and retrofitted boilers. However, the major limitation lies in the significant energy demand of the ASU, along with challenges related to material compatibility, corrosion, and the handling of impurities such as SO_x and NO_x.

Studies indicate that even in highly optimized CCS facilities using the most advanced solvents, The amount of energy needed for CO_2 capture still exceeds the energy required for CO_2 compression prior to storage . This highlights the importance of developing capture

technologies that minimize energy consumption. Among the available options, post-combustion capture remains the most mature and widely implemented approach in industrial settings. Although certain analyses suggest that pre-combustion and oxy-fuel systems can achieve the same electrical output with lower energy demand than post-combustion processes , these technologies require significant modifications to existing power plants, which substantially increases the associated capital investment[34].

I.5. Overview of CO_2 separation technologies

In most carbon capture systems, the CO_2 stream is not directly usable because it contains various impurities such as combustion by-products, inert nitrogen, or residual hydrocarbons. The choice of an appropriate separation method largely depends on the capture approach employed. Nevertheless, the majority of separation technologies are compatible with both post-combustion and pre-combustion capture processes. The following section provides an overview of several widely used CO_2 separation techniques.

I.5.1 Absorption

represents the most mature and extensively developed approach for post-combustion CO_2 capture. This process employs chemical solvents under atmospheric pressure and moderate operating temperatures, typically between 40 and 50 °C [35]. Solvents exhibiting high selectivity toward CO_2 are particularly advantageous, as they yield superior capture efficiencies and enable product purities exceeding 95% [36]. Despite its technological readiness, absorption-based capture is associated with several limitations. The process demands substantial energy input for CO_2 separation, with specific energy consumption commonly reported in the range of 0.5–0.8 MJ_e per kilogram of CO_2 captured [37], in addition to the considerable thermal energy required for solvent regeneration. Furthermore, when the inlet gas contains impurities such as sulfur dioxide or particulate matter, pre-treatment is essential to prevent accelerated solvent degradation and to preserve operational reliability.

I.5.2 Adsorption

Adsorption-based CO_2 capture technologies were first investigated in the mid-20th century, when Colburn and Dodge examined the use of alumina and silica for removing CO_2 from submarine atmospheres [38]. Since then, extensive research efforts have focused on identifying and optimizing sorbent materials capable of enhancing the efficiency and economic viability of

CO_2 capture processes [39]. The selection of an appropriate sorbent is a critical factor, as it directly influences process performance. Numerous studies have shown that inexpensive and readily available natural sorbents, such as calcium oxide (CaO), can provide satisfactory capture efficiencies; however, further investigation is required to address issues related to sorbent attrition, deactivation, and long-term stability [40]. Major challenges hindering large-scale industrial deployment include sorbent degradation, mechanical wear, and the influence of high operating temperatures. In applications involving CO_2 capture from biogas, additional complications arise, including difficulties associated with biomass handling and feeding, tar formation, and sorbent poisoning due to the presence of hydrogen sulfide (H_2S) in the feed gas.

I.5.3 Low-temperature

Low-temperature CO_2 separation has been extensively examined as an alternative capture technology. Berstad et al. [41] proposed a detailed process configuration in which the gas mixture is first thoroughly dried to prevent solid formation and subsequently compressed to approximately 100 bar before being cooled to −55 °C. Under these conditions, CO_2 condenses and can be separated from the remaining gas stream. Reported results indicate that CO_2 purities between 99.7 and 99.9 mol% are achievable with this method. Despite its effectiveness, the principal limitation

of cryogenic separation lies in its high energy demand. This requirement is mainly associated with the substantial compression work needed prior to cooling and the significant energy consumption of the refrigeration system required to maintain such low temperatures.

I.6 Categories of carbon capture and utilization products

After carbon capture, it is subsequently transformed into vital products. CCU products can be classified into three primary categories:

I.6.1 Fuels

To achieve climate objectives, it is essential to primarily substitute fossil fuel-based energy demand with renewable electricity. Nevertheless, certain sectors, including aviation, shipping, heavy transportation, and energy-intensive industries, face challenges in replacing hydrocarbons with electricity, either due to practical limitations or feasibility issues.

In these sectors, CCU fuels serve as drop-in solutions to mitigate emissions and transition from fossil resources. These are generated through the reaction of captured carbon with hydrogen derived from water electrolysis, utilizing renewable or low-carbon electricity[42]. CCU fuels can be stored, transported, and utilized directly or converted back into electricity. They are more convenient and cost-effective to store and transport than electricity and can be utilized within existing infrastructures in most instances. Additionally, they can be stored on a large scale for prolonged durations, facilitating the utilization of renewable energy in sectors that cannot directly employ it .

Existing technologies facilitate the production of CCU fuels. The inaugural flight utilizing CCU kerosene traversed Europe in 2021.

I.6.2 Chemicals

A significant portion of the chemical products integral to our contemporary daily existence, including plastics, packaging, furniture, clothing, pharmaceuticals, and food and feed, relies on carbon as a fundamental feedstock. Nonetheless, the manufacturing of these products entails extensive utilization of fossil carbon and considerable greenhouse gas emissions, with approximately 60 to 70% attributed to end-of-life emissions. CCU technologies facilitate the integration of renewable energy into the chemical sectors and enable the utilization of captured carbon as a replacement for fossil carbon, thereby fostering a circular carbon economy.

Technologies exist to transition to CO_2 and water as feedstock; however, scaling up necessitates substantial renewable energy resources. In the chemical sector, the effectiveness of climate change mitigation through carbon capture and utilization will largely hinge on the ability to replace

traditional products, commercialized products include cleaning agents, polymers, isolation materials, textiles, and more, all made using captured carbon as feedstock[43,44].

I.6.3 Materials

The construction and building industries are responsible for nearly one quarter of global CO_2 emissions. One promising mitigation strategy involves the permanent storage of CO_2 within solid materials through mineral carbonation, also referred to as mineralization. In nature, this process occurs over geological timescales, as illustrated by the slow formation of limestone over millions of years. Carbon capture and utilization (CCU) technologies replicate this natural mechanism in an accelerated manner by reacting CO_2 with calcium-rich materials to form calcium carbonate ($CaCO_3$). The resulting product can be used directly as a construction material, such as aggregates or bricks, or further processed for cement production. Various mineral waste streams, including steel slags, incineration residues, and construction and demolition waste, provide abundant feedstocks for carbonation reactions with captured CO_2. This approach supports a circular materials economy by reducing landfill disposal and limiting the extraction of virgin mineral resources from quarries. Today, bricks, tiles, pavements, components of buildings, and insulation materials are being produced through the process of CO_2 mineralization[45].

I.7 Treatment of gaseous effluents by plasma processes

Plasma-based technologies have emerged as an effective and versatile solution for the treatment of gaseous effluents, particularly those containing pollutants such as volatile organic compounds (VOCs), nitrogen oxides (NO_x), sulfur compounds, ozone-depleting substances, and greenhouse gases like CO_2. Unlike conventional thermal or catalytic methods, plasma processes operate under non-equilibrium conditions, enabling the generation of highly reactive species electrons, ions, radicals, excited molecules, and photons while maintaining the gas phase at near-ambient temperature. This unique characteristic makes plasma systems especially attractive for treating heat-sensitive pollutants and for applications where low energy consumption and rapid response times are required.

I.7.1 Definitions of Plasmas

The term plasma originates from the Greek word “πλάσμα”, meaning “formed” or “moldable matter,” referring to the creation of a deformable or adaptable entity [46]. The designation plasma was first used in physics by the American physicist and chemist Irving Langmuir in 1928 , during his investigations of oscillations in ionized gases. He introduced this term to describe an ionized gas contained within a discharge tube. Langmuir chose the name plasma by analogy to blood

plasma, because the transport of charged particles (electrons and ions) reminded him of the motion of blood cells within the plasma of the bloodstream.

A plasma is a state of matter composed of a mixture of electrons, ions, free radicals, and neutral species in both ground and excited states, as well as photons. On a macroscopic scale, it is electrically neutral. However, unlike ordinary gases which consist solely of electrically neutral particles plasma contains a significant number of charged particles. As a result, it exhibits electrical conductivity, and its constituents interact through a variety of electromagnetic processes.

These unique properties lead scientists to consider plasma as the fourth state of matter, following the three classical states solid, liquid, and gas when arranged along increasing temperature.

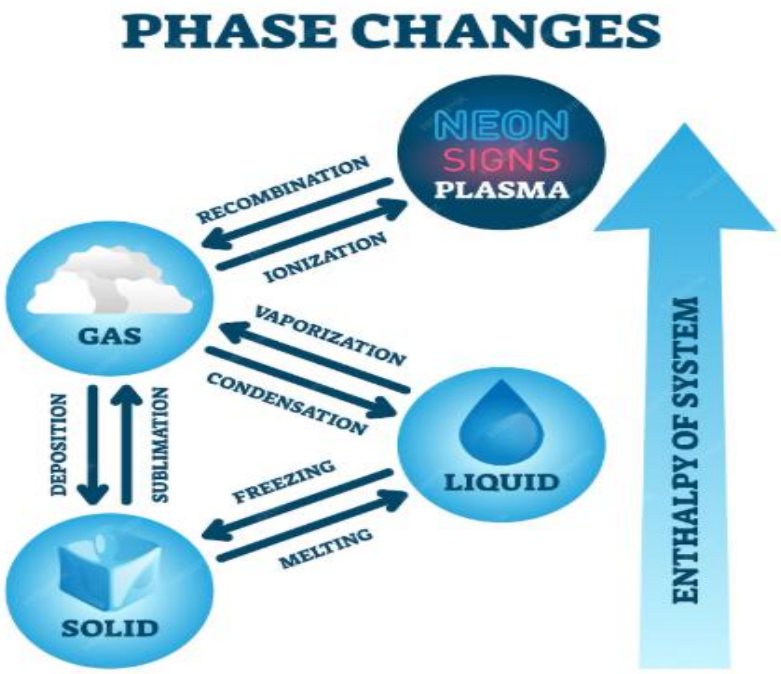

Figure I.3: The different states of matter with the main phase changes[47].

I.7.2 Characteristic quantities of plasmas and their classifications

Plasmas are generally more abundant in the universe; they represent more than 99% of matter, which exists in various forms. The unique characteristics of plasma have become vital for many everyday applications

Plasmas exhibit a wide range of physical behaviors governed by their charged particle dynamics, electromagnetic interactions, and thermodynamic state. To describe and classify plasmas, several characteristic quantities are commonly used. These parameters help determine how a plasma interacts with fields and matter, and they provide essential criteria for selecting appropriate modeling approaches and experimental conditions[48].

therefore, plasmas can be divided into two categories:

- **Natural plasmas**

It is very rare to find this type of plasma on the Earth's surface because they are represented by stars, interstellar media, the ionosphere, nebulae, quasars, pulsars, comet tails, solar winds, and also meteorological phenomena such as lightning and auroras, which correspond to light emissions from plasmas.

- **Industrial plasmas**

They are now present in various fields of application. This type of plasma is artificially produced in laboratories by applying an electric field to a neutral gas under certain pressures. The application of these plasmas has spread to various fields such as lighting (neon lamps), plasma screens, the materials industry (thin film production, surface treatment, and etching), as well as the medical field (UV lamp sterilizers, ionizers, etc.).

I.7.3 Physical parameters of plasmas

Not all plasmas have the same characteristics and they can therefore be classified

according to certain specific parameters. These parameters are essentially[49]:

a. Degree of Ionization

The degree of ionization represents the fraction of neutral particles that have been ionized in the plasma. It is defined as:

$$\alpha = \frac{n_i}{n_i + n_n} \tag{I.1}$$

where n_i and n_n are the ion and neutral number densities, respectively.

Plasmas can range from weakly ionized ($\alpha \langle 10^{-4}$) to fully ionized ($\alpha \approx 1$).

b. Plasma Density

The total electron density is a key indicator of plasma activity, typically ranging from 10^8 -10^{10} m^{-3} in low-temperature plasmas and up to 10^{25} m^{-3} in high-temperature fusion plasmas.

Electron density influences conductivity, reaction rates, and wave propagation.

c. Electron Temperature

The kinetic energy of electrons is described by the electron temperature .

In non-thermal plasmas, T_e lies in the range of 1–10 eV (10^4–10^5 K), while ions and neutrals remain much colder. Conversely, in thermal plasmas, all species share the same high temperature.

$$E_c = \frac{1}{2} m_e v^2 = \frac{3}{2} k_B T_e \tag{I.2}$$

d. Debye Length

The Debye length λ_D characterizes the length scale over which electric potentials are screened within a plasma:

$$\lambda_D = \sqrt{\frac{\varepsilon_0 k_B T_e}{n_e e^2}} \tag{I.3}$$

A necessary condition for a gas to behave as a plasma is that the characteristic system size L must satisfy:

$$L >> \lambda_D \tag{I.4}$$

This ensures collective electromagnetic behavior.

e. Plasma Frequency

The electron plasma frequency ω_{pe} defines the natural oscillation frequency of electrons in response to perturbations:

$$\omega_{pe} = \sqrt{\frac{n_e e^2}{\varepsilon_0 m_e}} \tag{I.5}$$

It provides insight into wave propagation and temporal response of the plasma.

f. Collision Frequency

The collision frequency between charged and neutral species determines whether the plasma is collisional or collisionless. In atmospheric-pressure plasmas such as dielectric barrier discharges, collisions are very frequent, leading to drift–diffusion dominated transport.

g. Mean Free Path

The mean free path λ is the average distance a particle travels between collisions. It is crucial in determining transport processes and discharge regime (Townsend, glow, arc, or streamer).

$$\lambda = \frac{1}{\pi (r_1 + r_2)^2 N} \tag{I.6}$$

I.7.4 Classification and Properties of Plasmas

Plasmas can be broadly classified according to their thermodynamic equilibrium and energy distribution among charged and neutral species. Depending on operating conditions such as temperature, pressure, and electron density, plasmas exhibit significantly different physical

properties and technological applications. The table below compares high-temperature plasmas, thermal plasmas, and non-thermal (cold) plasmas in terms of their plasma state, characteristic temperatures, electron densities, pressure ranges, typical examples, and major applications. This classification highlights the fundamental differences between equilibrium and non-equilibrium plasmas and explains why each type is suited to specific industrial, environmental, and energy-related processes. [50].

Table I.1: Comparison of physical properties and applications of different plasma types.

Parameter	**High temperature plasma**	**Thermal plasma**	**Non-thermal plasma**
Thermal equilibrium	Electron, ion, and gas temperatures are approximately equal $T_e \approx T_i \approx T_g$	Near thermal equilibrium between electrons, ions, and heavy species $T_e \approx T_i \approx T_g$	Strong thermal non-equilibrium, with electrons much hotter than heavy species $T_e \geq T_i \approx T_g$
Characteristic temperature	Extremely high temperatures, typically in the range of $T_p = 10^6 - 10^8 K$	Elevated temperatures, generally below $T_p \leq 2\times10^4 K$	low gas temperatures, usually between $T_p = 300 - 10^3 K$
Electron density	Very high electron densities, exceeding $n_e \geq 10^{20} m^{-3}$	Comparable high electron densities, on the order of $n_e \geq 10^{20} m^{-3}$	Much lower electron densities, around $n_e \approx 10^{10} m^{-3}$
Operating pressure	Can exist over a broad pressure range	Typically, close to atmospheric pressure $\approx 101 kPa$	Often operates at or above $10 kPa$
Examples	Fusion plasmas generated by high-energy lasers	Arc discharges and radio-frequency inductively coupled plasmas	Glow discharges, corona discharges, dielectric barrier discharges
Typical applications	Energy research and defense technologies	Waste treatment, ceramic processing, material cutting and welding	Environmental remediation, air purification, and surface or polymer modification

I.8. Voltage–current characteristics of gas discharges

The voltage–current (V–I) characteristics of gas discharges provide fundamental insight into the different discharge regimes that occur as the applied electric field and current are increased.

These characteristics describe the transition from weakly ionized conditions to fully developed plasmas and are essential for understanding and controlling non-thermal discharges.

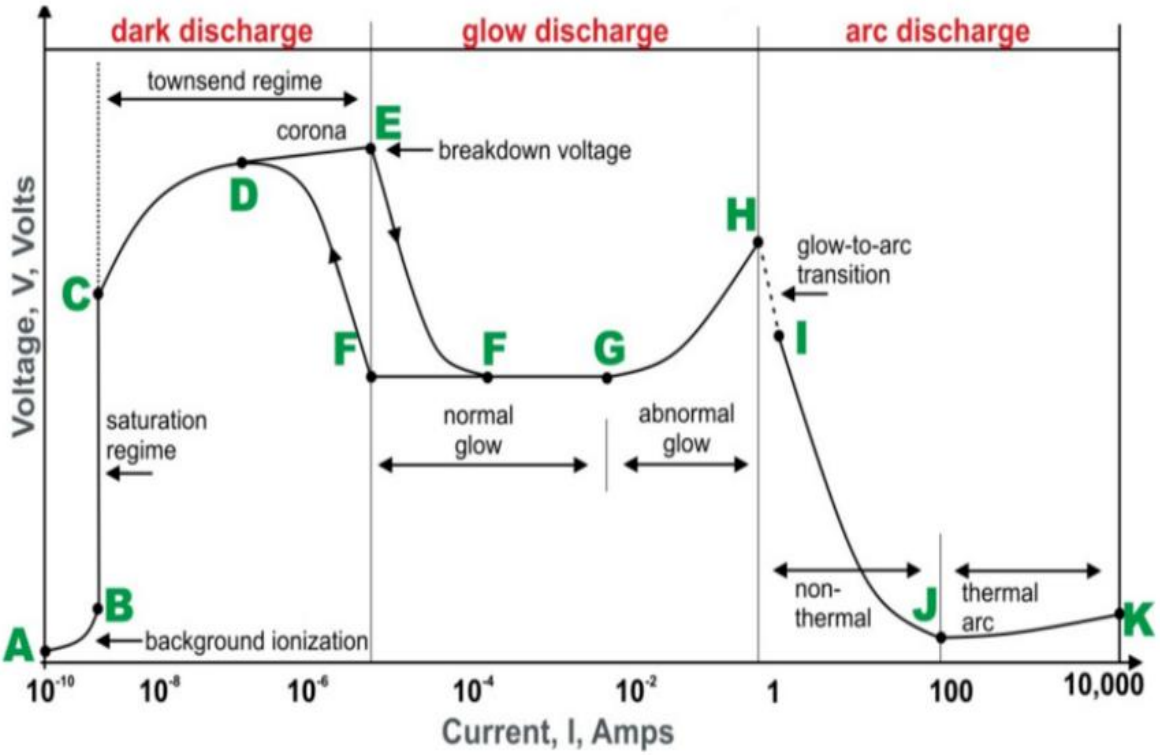

Figure I.4: Direct current (DC) discharge voltage-current characteristics.

A. Dark discharge

This discharge regime is referred to as *dark discharge* because it does not produce visible light detectable by the naked eye.

- **Background ionization:**

When the applied voltage V_{app} is set to a very low value slightly above 0 V, the anode collects free electrons naturally present in the gas. These electrons are mainly generated by external sources such as cosmic radiation. Under these conditions, a very weak current flows through the discharge gap, and its magnitude increases gradually as the applied voltage rises. This operating region corresponds to zone A–B of the static current–voltage characteristic shown in Figure I-4.

- **Saturation regime :**

As the applied voltage V_{app} is further increased, a point is reached where all the free electrons and ions produced by background ionization are fully collected by the anode and cathode, respectively. If the applied electric field (V_{app} / d) remains insufficient to ionize the gas, no additional charge carriers are created. Consequently, the discharge current becomes limited solely

by the rate of ionization caused by cosmic radiation. In this regime, the current reaches a constant value and remains independent of the applied voltage.

- **Townsend discharge:**

With a further increase in the applied electric field, electrons gain higher kinetic energy and undergo more energetic collisions with neutral gas molecules. When their energy exceeds the ionization threshold, these collisions generate additional electrons and positive ions. The newly created electrons are also accelerated by the electric field, leading to successive ionization events and resulting in an electron multiplication process known as an electron avalanche, as illustrated in Figure I-4. In this region (C–D), the discharge current increases exponentially with the applied voltage.

B. Glow discharge:

At the breakdown voltage, the ionization rate becomes sufficient to form a self-sustained plasma across the electrode gap.

- A sudden drop in voltage occurs due to increased conductivity.
- The discharge transitions from dark to luminous.
- This point marks the formation of a stable plasma column.

Breakdown depends strongly on gas type, pressure, and electrode spacing (Paschen's law).

- **Normal Glow Discharge:**

Once the breakdown voltage is reached at point E, electrical breakdown occurs, leading to a sudden transition from the dark discharge to the glow discharge regime. This transition is discontinuous and marked by a sharp increase in current accompanied by a significant drop in the inter-electrode voltage. As a result, the plasma becomes visibly luminous.

After reaching point F, the discharge enters the normal glow region. In this regime, the discharge voltage remains nearly constant over several orders of magnitude of increasing current. The cathode current density is essentially fixed and independent of the total discharge current. At low currents, the plasma occupies only a limited area of the cathode surface. As the current increases from F to G, the plasma spreads progressively across the cathode until the entire surface is uniformly covered at point G.

- **Abnormal Glow Discharge:**

Beyond point G, the discharge enters the abnormal glow regime. Since the cathode surface is already fully covered by plasma, any further increase in current requires a rise in the discharge

voltage to force the cathode current density above its natural value. Consequently, the voltage increases markedly with increasing current. This regime is typically associated with enhanced cathode heating and, at sufficiently high currents, can lead to thermionic emission from an incandescent cathode, as observed near point H.

When moving from point G toward lower currents (i.e., to the left on the current–voltage characteristic), a hysteresis behavior is observed. The glow discharge can be sustained at significantly lower currents and current densities than those required for its initial ignition at point F. The discharge remains in the luminous regime until point F′, where it transitions directly back to the Townsend discharge without passing again through the corona or pre-breakdown regimes.

C. Arc discharge

At point H, the electrodes become sufficiently heated for the cathode to emit electrons via thermionic emission. When the DC power supply possesses a low internal resistance, this enhanced electron emission triggers a glow-to-arc transition, corresponding to the transition from point H to I on the current–voltage characteristic.

Following this transition, the discharge enters a non-thermal arc regime (I–J). In this region, the discharge voltage decreases rapidly with increasing current due to the additional electron flux provided by thermionic emission. The presence of this strong electron source reduces the electric field required to sustain the discharge. Throughout the arc regime from I to K, the discharge exhibits a negative differential resistance, meaning that the voltage decreases as the current rises until reaching a minimum at point J. Beyond this point, the voltage begins to increase slowly as the current continues to grow.

As electron and heavy-particle heating intensifies, the discharge progressively approaches thermal equilibrium. This marks the transition into the thermal arc regime (J–K), where the plasma becomes fully thermalized and characterized by very high temperatures and current densities. At point K, the arc reaches a stable thermal equilibrium, dominated by intense Joule heating, strong electrode erosion, and highly conductive plasma conditions.

Table I.2: Characteristics of electrical discharge regimes in gases

Regime	Visibility	Voltage Trend	Current	Thermal State
Background ionization	No	Increases	Very low	Non-thermal
Townsend (dark)	No	Increases	Low	Non-thermal
Glow discharge	Yes	Nearly constant	Moderate	Non-thermal
Abnormal glow	Yes	Increases	High	Transitional
Arc discharge	Yes	Low	Very high	Thermal

I.8.1 Importance of avoiding arc formation in non-thermal plasmas

Avoiding arc formation is therefore a critical requirement in non-thermal plasma systems, such as dielectric barrier discharges. The use of current-limiting mechanisms, including dielectric barriers and pulsed or alternating voltage excitation, ensures that the discharge remains in the glow or filamentary regime. Maintaining operation below the arc transition is essential for preserving plasma stability, energy efficiency, and selectivity in plasma-assisted chemical processes.

I.8.2 Role of electric fields in gas ionization

Electric fields are a key part of the starting process. and sustainment of gas ionization and plasma formation. When a sufficiently strong electric field is applied across a gaseous medium, free electron originating from background ionization sources such as cosmic rays, natural radioactivity, or photoemission are accelerated toward the anode. As these electrons gain kinetic energy from the electric field, they collide with neutral gas molecules and atoms.

If the electron energy exceeds the ionization threshold of the gas, electron-impact ionization occurs, producing additional electrons and positive ions. This multiplication process leads to the formation of electron avalanches, which are the primary mechanism underlying the onset of electrical discharges. The efficiency of ionization strongly depends on the reduced electric field (E/N or E/p), which represents the ratio of the electric field strength to the gas number density or pressure. Higher reduced electric fields increase the mean electron energy and enhance ionization rates.

In addition to direct ionization, electric fields also promote excitation, dissociation, and attachment processes. Excited species can contribute indirectly to ionization through stepwise ionization and Penning ionization, while dissociation processes generate reactive radicals essential for plasma chemistry. At atmospheric pressure, strong electric fields are required to overcome frequent electron–neutral collisions, leading to highly non-equilibrium conditions where electrons are energetic while heavy species remain near ambient temperature.

Once ionization begins, the generated space charges modify the local electric field distribution, influencing discharge development and stability. This feedback mechanism is particularly important in streamer and dielectric barrier discharges, where localized field enhancement governs microdischarge formation. Therefore, precise control of the applied electric field is essential for achieving stable, efficient, and non-thermal plasma operation.

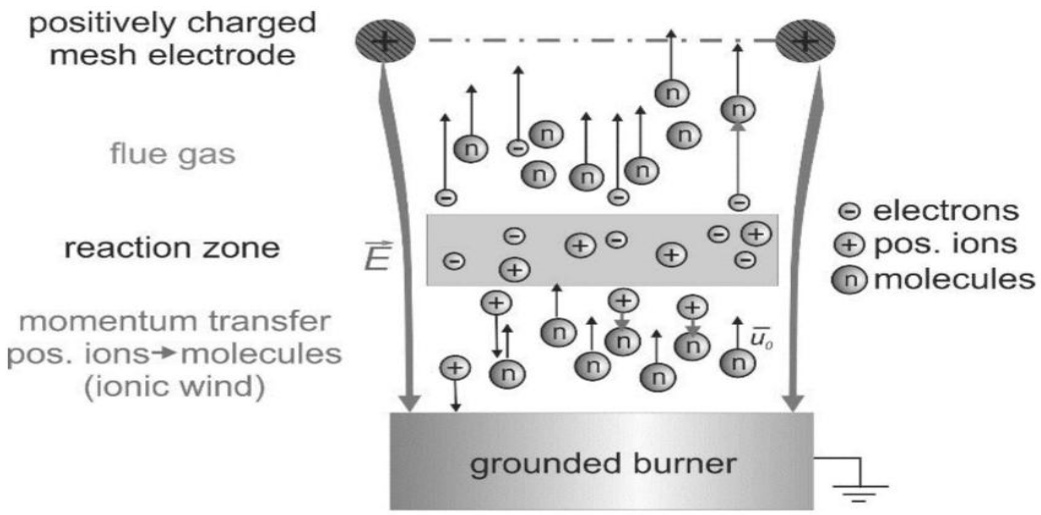

Figure I.5: Electric fields function in gas ionization.

I.9 Cold plasmas and non-thermal discharges

I.9.1 Definition of cold plasma

Cold plasmas, also referred to as non-thermal plasmas, are partially ionized gases in which the different plasma species are not in thermal equilibrium. In this type of discharge, electrons possess much higher kinetic energy than ions and neutral particles. As a result, the electron temperature can reach several electronvolts, while the gas temperature remains close to ambient or moderately elevated values. This strong thermal non-equilibrium distinguishes cold plasmas from thermal plasmas, where all species share approximately the same temperature.

Cold plasmas can be generated at low or atmospheric pressure using electric fields through various discharge configurations, such as glow discharges, dielectric barrier discharges (DBDs), corona discharges, and radio-frequency plasmas. Their ability to operate without significant gas heating makes them particularly attractive for applications involving temperature-sensitive materials and chemical processes.

I.9.2 Different types of cold plasma

Cold plasmas can operate under various discharge modes depending on the applied electric field, pressure, electrode configuration, and power supply. These modes differ in their spatial uniformity, temporal behavior, and energy distribution, which strongly influence plasma chemistry and applications.

I.9.2.1 glow discharge

Glow discharges can be classified into two main categories: atmospheric-pressure glow discharges and low-pressure glow discharges. Low-pressure systems are especially beneficial in food science applications because they allow processing at relatively low temperatures, thereby reducing the risk of degradation of heat-sensitive components. These systems operate under vacuum conditions generated by a vacuum pump and may use either ambient air or selected gases. The gas flow rate plays a significant role in determining the visual appearance of the plasma, particularly its color . Plasma generation in low-pressure glow discharges typically requires voltages above 100 V and operating pressures in the range of 1–1000 Pa Figure I.6. A major advantage of this configuration is its ability to treat large volumes or surface areas efficiently .

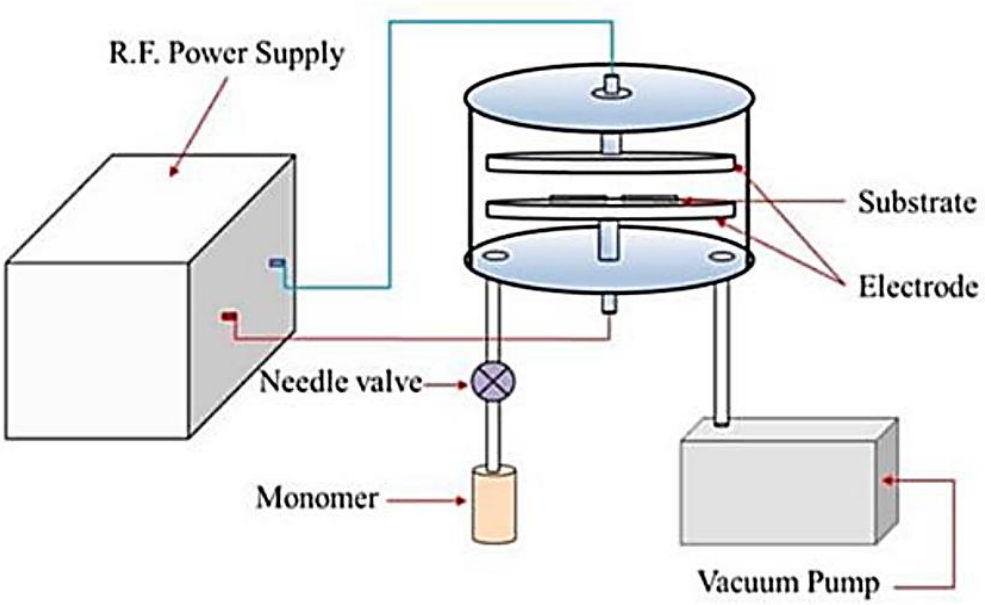

Figure I.6: Schematic of the glow discharge setup.

I.9.2.2 Plasma jet

A plasma jet is produced when an ionized gas stream flows between two electrodes and is expelled beyond the electrode region due to a high gas flow velocity. Unlike other plasma systems, this configuration allows the plasma to extend into open space, enabling applications outside a confined reactor Figure I. 7. This design offers enhanced control over plasma characteristics, including density, temperature, and chemical composition. Plasma jets are particularly well suited for applications requiring localized treatment, such as processing narrow or inaccessible regions. Despite their high precision, plasma jets have a relatively limited treatment area. Ongoing research focuses on expanding the effective treatment surface, and similar to other cold plasma technologies, plasma jets are well adapted for treating heat-sensitive materials.

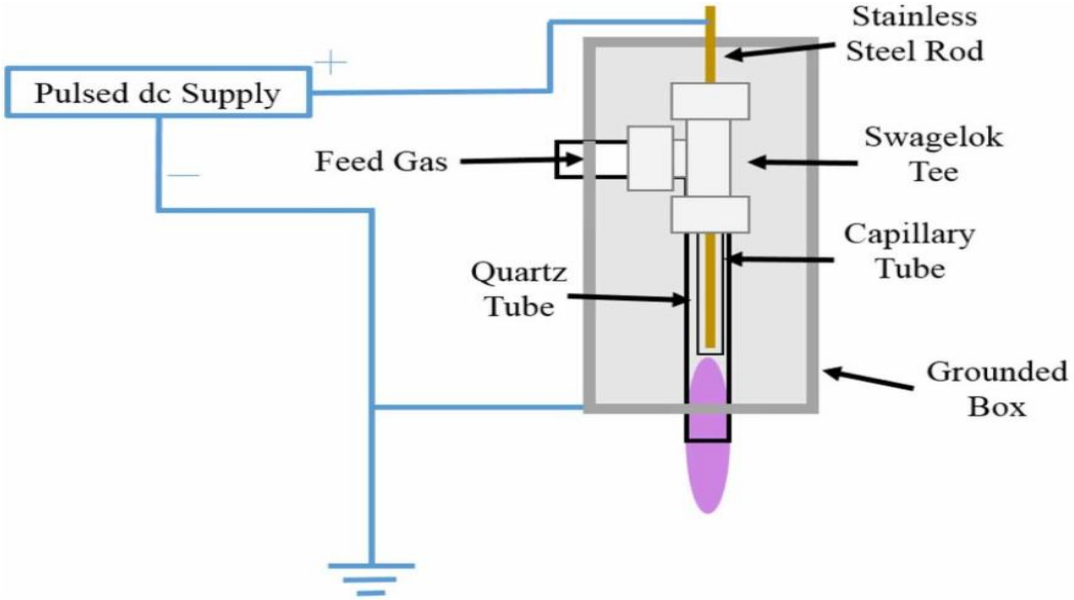

Figure I.7: Schematic of the Plasma jet setup.

I.9.2.3 Corona discharge

Corona discharges occur in strongly non-uniform electric fields, typically around sharp electrodes such as needles or wires Figure I.8. Ionization is localized near the high-field region, and the discharge remains non-thermal and spatially confined. Corona plasmas are commonly used in electrostatic precipitation, ozone generation, and pollution control.

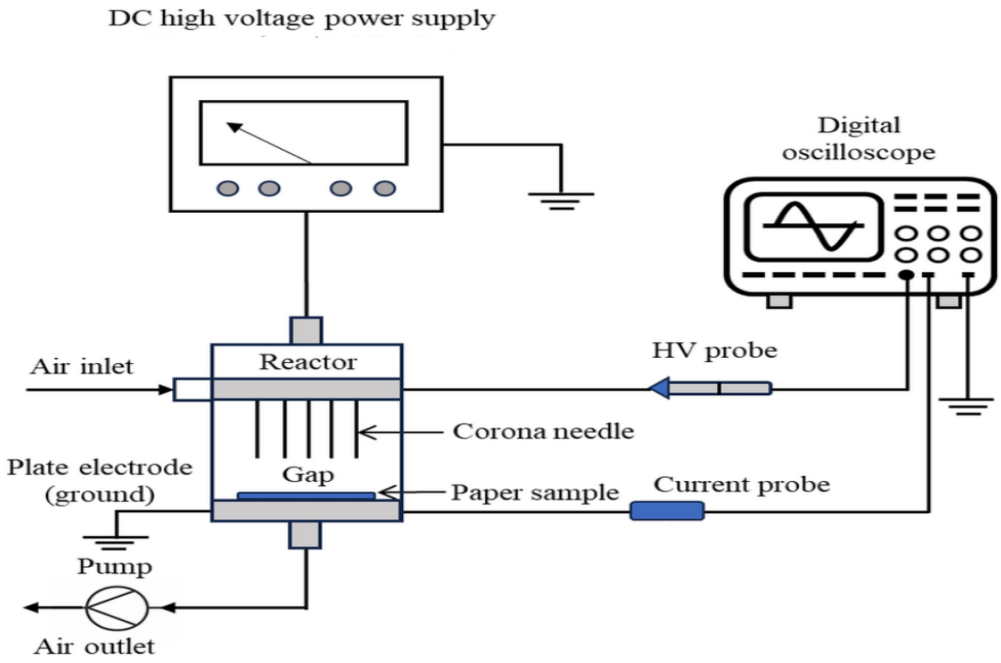

Figure I.8: Schematic of the Corona discharge setup.

I.9.2.4 Gliding arc plasma

Gliding arc plasma is generated when a gas stream flowing between two electrodes is exposed to a high applied voltage, resulting in a non-thermal plasma under atmospheric conditions Figure I.9 Compared with other cold plasma technologies, operation at atmospheric pressure is technically simpler and more suitable for industrial implementation. The gas flow rate is a key parameter in gliding arc systems, as it governs the plasma jet velocity and trajectory and strongly influences both the temperature and chemical composition of the plasma . By adjusting the gas flow, it is possible to either enhance the plasma intensity or achieve a more controlled discharge. Lower gas flow rates favor the formation of highly reactive and concentrated plasma, which is particularly effective for surface cleaning and modification processes. In contrast, higher flow rates are better suited for large-scale applications such as drying or bulk processing, where a more stable and less reactive plasma is desirable .

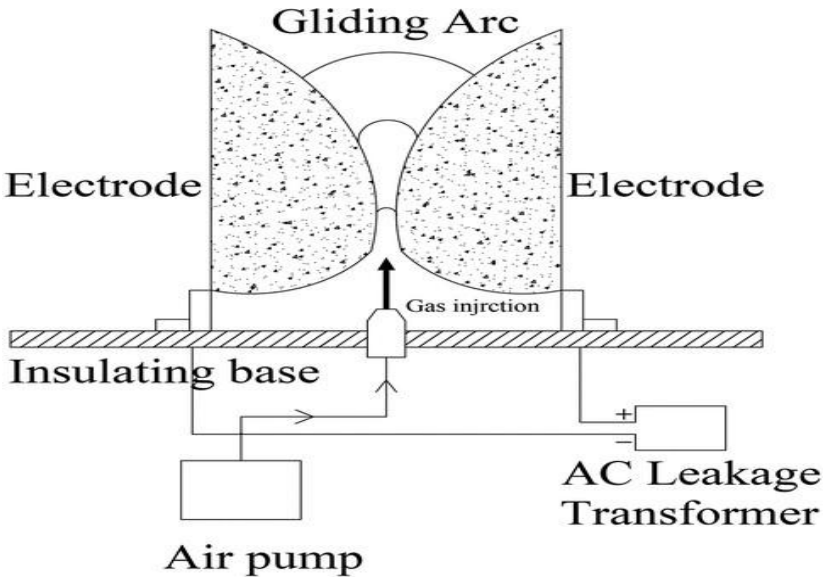

Figure I.9: Schematic of the Gliding arc plasma setup.

I.9.2.5 Dielectric barrier discharges plasma

Dielectric barrier discharges are generated between electrodes separated by one or more dielectric layers and powered by alternating or pulsed high voltage as shown in Figure I. 10. The dielectric barrier limits the current and prevents transition to arc formation. DBDs operate in filamentary or diffuse (homogeneous) modes and are particularly effective at atmospheric pressure. They are widely used for ozone production, CO_2 conversion, surface treatment, and plasma medicine.

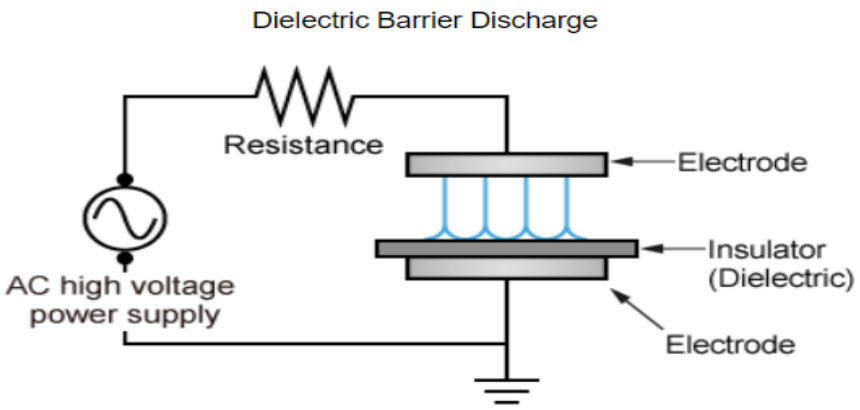

Figure I.10: Setting up a dielectric barrier discharges plasma.

I.9.3 Advantages of non-thermal plasmas

Non-thermal plasmas offer several significant advantages over thermal plasma systems. First, they enable high chemical reactivity at low temperatures, allowing efficient activation of stable molecules such as CO_2, N_2, and O_2 without excessive energy consumption. Second, the limited gas heating reduces thermal degradation of materials and minimizes energy losses associated with heating the entire gas volume.

Additionally, non-thermal plasmas can operate under atmospheric pressure and near-ambient conditions, eliminating the need for complex vacuum systems and facilitating their integration into industrial-scale processes. These advantages make non-thermal plasmas highly attractive for a wide range of applications, including environmental remediation, gas conversion, surface modification, and sustainable energy technologies.

Furthermore, non-thermal plasmas provide fast response times, easy controllability, and operation at atmospheric pressure, eliminating the need for complex vacuum systems. These characteristics make them well suited for continuous and scalable industrial processes. Furthermore, the presence of energetic electrons enhances reaction selectivity by favoring specific reaction pathways, which is particularly important in plasma-assisted chemical conversion and environmental applications, Table I. 3 show the essential uses for low-pressure and atmospheric non-thermal plasma.

Table I.3: Essential uses for low-pressure and atmospheric non-thermal plasma.

Plasma Pressure Regime	**Application Area**	**Typical Uses**
Atmospheric-pressure non-thermal plasma	Medical and biomedical	Sterilization, wound healing, dentistry, cancer treatment
	Environmental	Air purification, gas and liquid treatment
	Food and agriculture	Food decontamination, agricultural treatments
	Surface engineering	Surface modification, polymerization
	Industrial processing	Thin-film deposition, material functionalization
Low-pressure non-thermal plasma	Materials processing	Thin-film deposition, polymerization
	Microelectronics and fabrication	Etching, surface structuring
	Chemical processing	Gas and liquid treatment
	Surface engineering	Surface activation and modification

I.10 Conclusion

This chapter has presented a detailed overview of the fundamental aspects related to greenhouse gas emissions, with a particular focus on carbon dioxide and its detrimental environmental impacts. The mechanisms of CO_2 capture, separation, and utilization were discussed, highlighting both conventional technologies and emerging approaches aimed at reducing the carbon footprint of industrial activities.

Plasma-based processes were introduced as a powerful and versatile tool for the treatment of gaseous effluents. The fundamental principles of plasmas, including their characteristic parameters, classifications, and electrical behavior, were examined to provide a solid theoretical foundation. The voltage–current characteristics of gas discharges were analyzed, emphasizing the

different discharge regimes and the critical importance of preventing arc formation in non-thermal plasma systems to preserve energy efficiency and material integrity.

Furthermore, cold plasmas and non-thermal discharges were explored in detail, with particular attention given to their distinct types and configurations, such as glow discharge, plasma jets, corona discharge, gliding arc plasma, and dielectric barrier discharges. The advantages of non-thermal plasmas, including low operating temperatures, high chemical reactivity, and flexibility in atmospheric or low-pressure operation, make them especially attractive for CO_2 conversion and environmental applications.

Overall, this chapter establishes the scientific and technological background necessary for understanding plasma-assisted CO_2 treatment processes. It provides a conceptual framework that supports the subsequent chapters, where plasma reactor designs, modeling approaches, and experimental investigations of CO_2 conversion and utilization are addressed in greater detail.

References

[1] R. S. Nerem, 'Main Greenhouse Gases| Center for Climate and Energy Solutions', Proc. Natl. Acad. Sci, vol. 115, no. 9, pp. 2022–2025, 2017.

[2] M. Goel, M. Sudhakar, and R. V. Shahi, 'Carbon capture, storage and utilization: A possible climate change solution for energy industry'. CRC Press, 2019.

[3] International Energy Agency, 'CO2 Capture and Utilisation', Paris, 2022.

[4] H. Ritchie, M. Roser, and P. Rosado, 'CO_2 and greenhouse gas emissions', Our world in data, 2020.

[5] A. Bogaerts and E. C. Neyts, 'Plasma Technology: An Emerging Technology for Energy Storage', ACS Energy Letters. 2018. doi: 10.1021/acsenergylett.8b00184.

[6] W. J. Bond, G. F. Midgley, and F. I. Woodward, 'The importance of low atmospheric CO2and fire in promoting the spread of grasslands and savannas', Glob Chang Biol, vol. 9, No. 7, pp. 973–982, 2003.

[7] F. Schenuit et al., 'Carbon dioxide removal policy in the making: assessing developments in 9 OECD cases', Frontiers in Climate, vol. 3, p. 638805, 2021.

[8] A. Bogaerts and G. Centi, 'Plasma technology for CO2 conversion: a personal perspective on prospects and gaps', Front Energy Res, vol. 8, p. 111, 2020.

[9] Kogelschatz, U. (2003). Dielectric-barrier discharges: their history, discharge physics, and industrial applications. Plasma chemistry and plasma processing, 23(1), 1-46.

[10] Eliasson, B., & Kogelschatz, U. (2002). Modeling and applications of silent discharge plasmas. IEEE transactions on plasma science, 19(2), 309-323..

[11] Fridman, G., Friedman, G., Gutsol, A., Shekhter, A. B., Vasilets, V. N., & Fridman, A. (2008). Applied plasma medicine. Plasma processes and polymers, 5(6), 503-533.

[12] S. Alberici, P. Noothout, G. U. R. Mir, M. Stork, and F. Wiersma, 'Assessing the potential of CO2 utilisation in the UK', AssessingCO2_utilisationUK_ReportFinal_260517v2,1, pdf, 2017.

[13] P. Guning and C. Hills, 'Carbon negative: first commercial application of Accelerated Carbonation Technology', 2014.

[14] Bogaerts, A., & Centi, G. (2020). Plasma technology for CO2 conversion: a personal perspective on prospects and gaps. Frontiers in Energy Research, 8, 111.

[15] Hagelaar, G. J. M., & Pitchford, L. C. (2005). Solving the Boltzmann equation to obtain electron transport coefficients and rate coefficients for fluid models. Plasma sources science and technology, 14(4), 722.

[16] Suh, Y. K. (2012). Modeling and simulation of ion transport in dielectric liquids-Fundamentals and review. IEEE Transactions on Dielectrics and Electrical Insulation, 19(3), 831-848.

[17] Teyssedre, G., & Laurent, C. (2005). Charge transport modeling in insulating polymers: from molecular to macroscopic scale. IEEE Transactions on Dielectrics and Electrical Insulation, 12(5), 857-875.

[18] Sun, X., Bao, J., Li, K., Argyle, M. D., Tan, G., Adidharma, H., ... & Ning, P. (2021). Advance in using plasma technology for modification or fabrication of carbon-based materials and their applications in environmental, material, and energy fields. Advanced Functional Materials, 31(7), 2006287.

[19] Ahasan, M. R., Hossain, M. M., & Wang, R. (2025). Dielectric Barrier Discharge Reactors for Plasma-Assisted CO2 and CH4 Conversion: A Comprehensive Review of Reactor Design, Performance, and Future Prospects. Energy Technology, 13(4), 2401177.

[20] Neyts, E. C., & Bogaerts, A. (2014). Understanding plasma catalysis through modelling and simulation, a review. Journal of Physics D: Applied Physics, 47(22), 224010.

[21] Kabir, M., Habiba, U. E., Khan, W., Shah, A., Rahim, S., De los Rios-Escalante, P. R., ... & Shafiq, M. (2023). Climate change due to increasing concentration of carbon dioxide and its impacts on environment in 21st century; a mini review. Journal of King Saud University-Science, 35(5), 102693.

[22] Basu, P., Mandal, M., Jana, S., Biswas, A., & Ray, S. (2025). Impact of Anthropogenic Activities on Global Warming and Energy Demand. The Intersection of Global Energy Politics and Climate Change: A Comprehensive Analysis of Energy Markets and Economics, 63-81.

[23] Peres, C. B., Resende, P. M., Nunes, L. J., & Morais, L. C. D. (2022). Advances in carbon capture and use (CCU) technologies: a comprehensive review and CO2 mitigation potential analysis. Clean technologies, 4(4), 1193-1207.

[24] Song, C. (2006). Global challenges and strategies for control, conversion and utilization of CO2 for sustainable development involving energy, catalysis, adsorption and chemical processing. Catalysis today, 115(1-4), 2-32.

[25] Ramanathan, V., & Feng, Y. (2009). Air pollution, greenhouse gases and climate change: Global and regional perspectives. Atmospheric environment, 43(1), 37-50.

[26] Methane Concentration and Temperature & Carbon Dioxide: Methane data and CO2 data reported by NOAA's Earth System Research Laboratory Global Monitoring Division

[27] Kumar, A. (2018). Global warming, climate change and greenhouse gas mitigation. In Biofuels: greenhouse gas mitigation and global warming: next generation biofuels and role of biotechnology (pp. 1-16). New Delhi: Springer India.

[28] Koerner, B., & Klopatek, J. (2002). Anthropogenic and natural CO2 emission sources in an arid urban environment. Environmental Pollution, 116, S45-S51.

[29] Jamel, M., & Zhang, C. (2024). Green finance, financial technology, and environmental innovation impact on CO_2 emissions in developed countries. Journal of Energy and Environmental Policy Options, 7(3), 43-51.

[30] Zhou, Q., Koiwanit, J., Piewkhaow, L., Manuilova, A., Chan, C. W., Wilson, M., & Tontiwachwuthikul, P. (2014). A comparative of life cycle assessment of post-combustion, pre-combustion and oxy-fuel CO2 capture. Energy Procedia, 63, 7452-7458

[31] Kheirinik, M., Ahmed, S., & Rahmanian, N. (2021). Comparative techno-economic analysis of carbon capture processes: Pre-combustion, post-combustion, and oxy-fuel combustion operations. Sustainability, 13(24), 13567.

[32] Wang, M., Lawal, A., Stephenson, P., Sidders, J., & Ramshaw, C. (2011). Post-combustion CO2 capture with chemical absorption: A state-of-the-art review. Chemical engineering research and design, 89(9), 1609-1624.

[33] Rao, A. B., Rubin, E. S., & Berkenpas, M. B. (2004). An integrated modeling framework for carbon management technologies. Carnegie Mellon University (US).

[34] Castel, C., Bounaceur, R., & Favre, E. (2021). Membrane processes for direct carbon dioxide capture from air: possibilities and limitations. Frontiers in Chemical Engineering, 3, 668867.

[35] Raganati, F., & Ammendola, P. (2024). CO2 post-combustion capture: a critical review of current technologies and future directions. Energy & Fuels, 38(15), 13858-13905.

[36] Odunlami, O. A., Vershima, D. A., Oladimeji, T. E., Nkongho, S., Ogunlade, S. K., & Fakinle, B. S. (2022). Advanced techniques for the capturing and separation of CO2–a review. Results in Engineering, 15, 100512.

[37] Adams, D. (2010). Flue gas treatment for CO2 capture (pp. 1-61). London, UK: IEA Clean Coal Centre.

[38] Webley, P. A. (2014). Adsorption technology for CO2 separation and capture: a perspective. Adsorption, 20(2), 225-231.

[39] Do, H., Jung, J., Cho, M., & Lee, C. H. (2024). Adsorption equilibria and kinetics of CO2 and N2 on silica-alumina gels for reducing gas production by CO2 removal from iron flue gases. Journal of Environmental Chemical Engineering, 12(6), 114732.

[40] Berman, D., Guha, S., Lee, B., Elam, J. W., Darling, S. B., & Shevchenko, E. V. (2017). Sequential infiltration synthesis for the design of low refractive index surface coatings with controllable thickness. ACS nano, 11(3), 2521-2530.

[41] Berstad, D., Anantharaman, R., & Nekså, P. (2013). Low-temperature CO2 capture technologies–Applications and potential. International Journal of Refrigeration, 36(5), 1403-1416.

[42] Dermühl, S., & Riedel, U. (2023). A comparison of the most promising low-carbon hydrogen production technologies. Fuel, 340, 127478.

[43] Callegari, A., Bolognesi, S., Cecconet, D., & Capodaglio, A. G. (2020). Production technologies, current role, and future prospects of biofuels feedstocks: A state-of-the-art review. Critical Reviews in Environmental Science and Technology, 50(4), 384-436.

[44] Müller, L. J., Kätelhön, A., Bringezu, S., McCoy, S., Suh, S., Edwards, R., ... & Bardow, A. (2020). The carbon footprint of the carbon feedstock CO 2. Energy & Environmental Science, 13(9), 2979-2992.

[45] Sanna, A., Uibu, M., Caramanna, G., Kuusik, R., & Maroto-Valer, M. M. (2014). A review of mineral carbonation technologies to sequester CO 2. Chemical Society Reviews, 43(23), 8049-8080.

[46] Perucca, M. (2010). Introduction to plasma and plasma technology. Plasma Technology for Hyperfunctional Surfaces: Food, Biomedical, and Textile Applications, 1-32.

[47] Langmuir, I. (1964). Surface chemistry. Nobel Lectures. Chemistry 1922-1941, 287-325.

[48] LAHOUEL, M. H. A. (2021). Modélisation et simulation d'une décharge à barrière diélectriques dans un Mélange gazeux à la pression atmosphérique (Doctoral dissertation, Djilali BENYOUCEF/Hocine TEBANI). http://hdl.handle.net/123456789/1642

[49] Mohamed Chérif Bouzidi. " Étude d'une Décharge à Barrière Diélectrique (DBD) homogène dans l'azote à pression atmosphérique : Effet mémoire et Optimisation du transfert de

Puissance". Sciences de l'ingénieur [physics]. Institut National Polytechnique de Toulouse - INPT, 2013.

[50] Khunda, D. (2023). Design and operation of dielectric barrier discharge microreactor for CO_2 Utilization (Doctoral dissertation, University of Warwick).

Chapter II

Fundamentals of Dielectric Barrier Discharges

II.1 Introduction

Non-thermal plasmas have attracted increasing attention over the past decades due to their ability to generate highly reactive chemical species while maintaining low gas temperatures. Among the various non-thermal plasma sources, dielectric barrier discharges (DBDs) are particularly attractive because they can operate stably at atmospheric pressure, require relatively simple reactor configurations, and allow precise control of plasma characteristics. These features make DBDs well suited for a wide range of applications, including environmental remediation, gas conversion, surface modification, and biomedical treatments[1].

A defining feature of DBDs is the presence of at least one dielectric layer placed between the electrodes, which plays a crucial role in stabilizing the discharge and preventing the transition to thermal arc regimes. The dielectric barrier limits the discharge current through surface charge accumulation, leading to the formation of numerous short-lived micro-discharges or, under specific conditions, more homogeneous plasma structures. As a result, DBDs exhibit rich and complex electrical behavior, strongly influenced by operating parameters such as applied voltage, frequency, gas composition, pressure, and reactor geometry[2].

Understanding the physical mechanisms governing DBD operation is essential for optimizing their performance and ensuring efficient plasma–chemical processes. This chapter provides a comprehensive overview of the fundamental aspects of dielectric barrier discharges. It begins with a brief historical background and a discussion of the main reactor configurations currently used. The definition and operating principle of DBDs are then introduced, followed by a detailed description of gas breakdown phenomena, including Townsend and streamer mechanisms.

The chapter further examines the different operating regimes of DBDs, highlighting the filamentary, homogeneous, and multi-peak modes, which are critical for determining plasma uniformity and reactivity. Finally, major application areas of DBD technology are presented, with particular emphasis on environmental processes and carbon dioxide conversion. Overall, this chapter establishes the theoretical and conceptual framework necessary for understanding the experimental and numerical investigations discussed in the subsequent chapters.

II.2 Dielectric Barrier Discharges (DBD)

As the work developed within the framework of this thesis aims at the simulation and characterization of dielectric barrier discharges, we will attempt to present, in this section, the two main types of DBD plasmas considered in this study. We will present the different possible configurations and describe the principles and phenomena involved in the operation of this type of discharge[3].

II.2.1 History of the DBD

The dielectric barrier discharge (DBD) is one of the oldest and most extensively studied forms of non-thermal plasma. Its history dates back to the mid-19th century, when the German physicist Werner von Siemens first introduced the concept in 1857. Siemens demonstrated that placing a dielectric material between electrodes could prevent the transition to spark or arc breakdown, allowing the generation of a stable, diffuse discharge at atmospheric pressure. His original work was primarily motivated by the need to develop efficient ozone generators, which to this day are still based on DBD technology[4].

During the late 19th and early 20th centuries, research on DBDs was largely driven by industrial applications, particularly ozone production, surface treatment, and electrical insulation systems. The use of a dielectric barrier enabled operation at relatively high voltages while limiting current peaks, making it possible to sustain a cold, filamentary or diffuse plasma without overheating the gas.

A major milestone occurred in the early 20th century with the development of silent discharges, a term historically used to describe DBDs because the dielectric layer suppressed the audible noise typical of arc discharges. This led to wider adoption in ozonizers and various industrial plasma reactors.

In the second half of the 20th century, advancements in high-voltage electronics and diagnostics enabled better control and characterization of DBDs. Researchers began exploring their potential in surface engineering, polymer modification, plasma display panels, and chemical processing.

The term dielectric barrier discharges encompass all discharge configurations in which a current flow between two metal electrodes separated by a gas and one or more layers of dielectric. With planar configurations (with one or two dielectrics in different locations) or cylindrical configurations and a surface configuration where one of the electrodes is encapsulated in the dielectric; discharges are classified into three main families, namely: volumetric plasma discharge (VD-DBD), surface plasma discharge (SV-DBD), and coplanar plasma discharge.

As part of this thesis, we have particularly focused on: volumetric dielectric barrier discharges and surface dielectric barrier discharges.

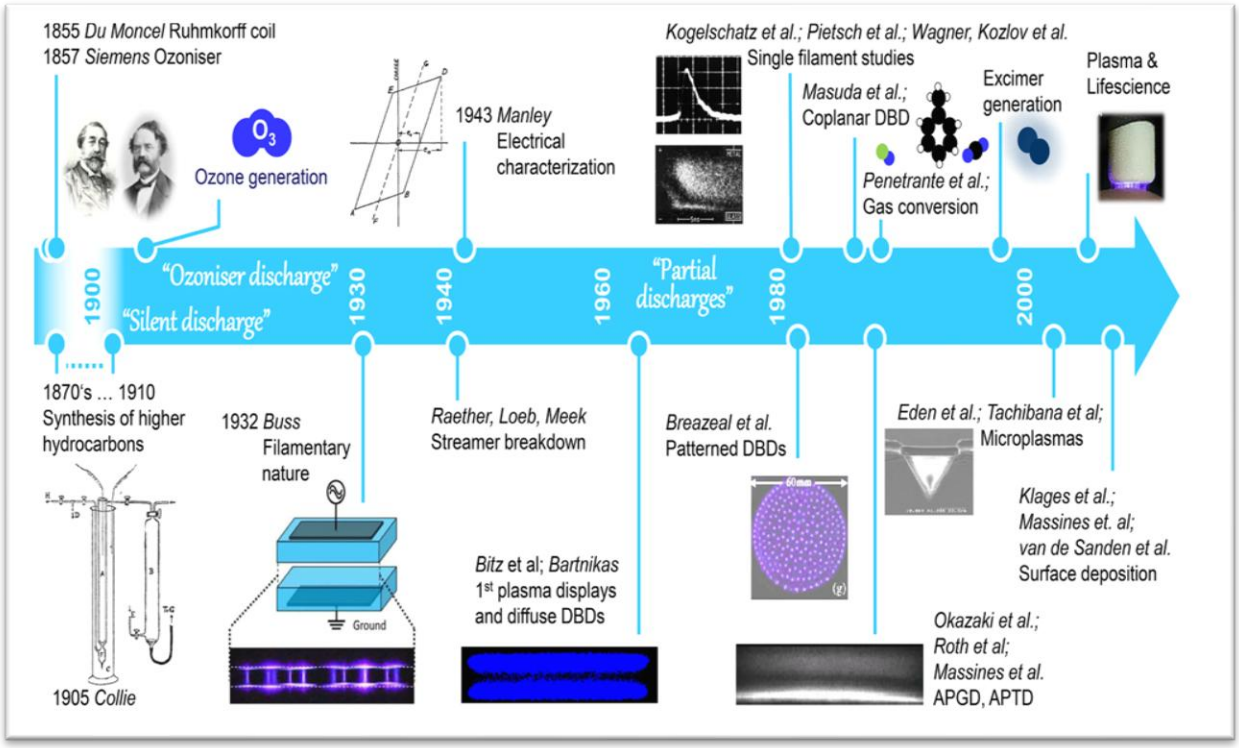

Figure II.1: Selected milestones of research on DBD[5].

II.2.2 Current configurations of DBDs

Cold plasmas are commonly generated using electric fields, and to ensure discharge stability while preserving thermal non-equilibrium and preventing the transition to an arc, careful control of the reactor geometry is essential. The geometry of the discharge reactor plays a crucial role in defining the electric field distribution and, consequently, in governing the initiation and development of microdischarges within the inter-electrode gap. Dielectric barrier discharges can be implemented in a variety of geometric configurations, each offering distinct discharge characteristics and operational advantages [6].

Figure II. 2 (a) illustrates the main configurations of dielectric barrier discharge (DBD) reactors commonly employed in plasma-based applications. The planar reactor geometry is shown in both two-sided and one-sided configurations, where the discharge gap is formed between a high-voltage electrode and a grounded electrode separated by one or two dielectric barriers. The two-sided configuration provides a more uniform electric field distribution across the discharge gap, whereas the one-sided configuration offers a simpler design and easier implementation in practical systems. The cylindrical reactor configuration, presented in Figure II. 2 (b), consists of a coaxial geometry in which the high-voltage electrode is surrounded by a dielectric barrier and enclosed by a grounded outer electrode, making it particularly suitable for continuous gas treatment and enhanced discharge stability. Figure II. 2 (c) shows surface and coplanar discharge configurations, where the plasma develops along the dielectric surface rather than across the gas gap; these

configurations are especially advantageous for surface modification, ozone generation, and localized plasma activation. A comparative summary of these DBD reactor configurations, including their operating characteristics, advantages, and typical applications, is provided in Table II. 1, The table compares the main DBD configurations and shows that reactor geometry strongly affects discharge behavior and performance. Planar DBD are simple and relatively uniform, making them suitable for diagnostics and modeling, but they suffer from limited gas residence time and scaling issues. Coaxial DBD provide stable filamentary discharges and efficient gas–plasma interaction, offering good scalability for industrial use, although they are more complex and less uniform. Surface (coplanar) DBD generate plasma confined to the dielectric surface with low power consumption and compact design, but their small plasma volume limits their effectiveness for bulk gas treatment [7].

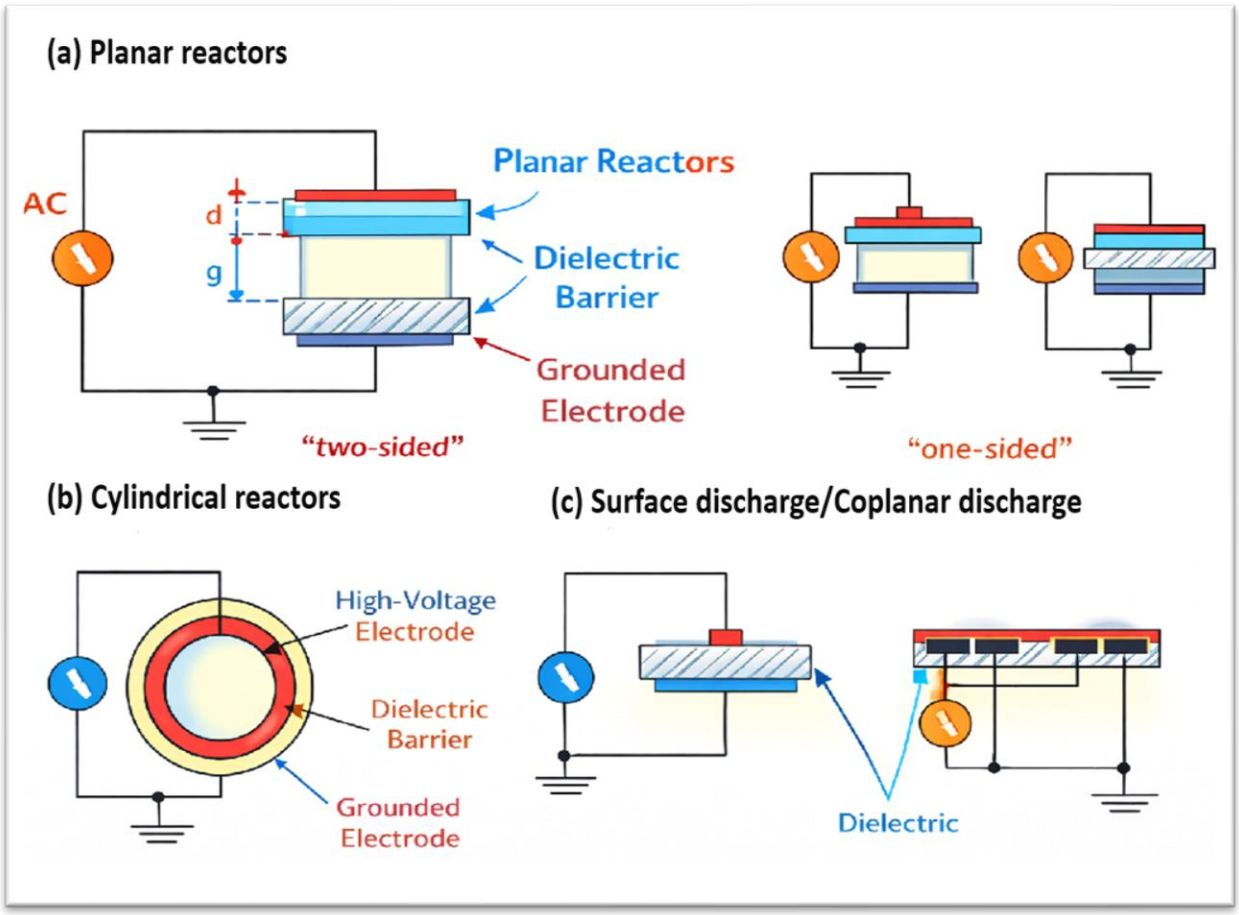

Figure II.2: The different configurations of a volumetric DBD discharge[8].

Table II.1: Comparison of common dielectric barrier discharge (DBD) reactor configurations.

DBD	**Geometry / Structure**	**Discharge Characteristics**	**Advantages**	**Limitations**
Planar DBD	Parallel plate electrodes separated by one or two dielectric barriers; flat geometry	Filamentary or diffuse discharge depending on gas and operating conditions; relatively uniform electric field (especially in two-sided configuration)	Simple design; good plasma uniformity; easy diagnostics and modeling (1D/2D); suitable for atmospheric pressure operation	Limited gas residence time; edge effects; scaling to large areas may be challenging
Cylindrical DBD	Coaxial configuration with central high-voltage electrode, dielectric barrier, and outer grounded electrode	Stable filamentary discharge; strong radial electric field; efficient gas–plasma interaction	High discharge stability; suitable for continuous gas flow; good scalability for industrial systems	More complex fabrication; less uniform field compared to planar geometry
Surface / Coplanar DBD	Electrodes embedded or placed on the same side of the dielectric; plasma develops along dielectric surface	Surface-confined discharge; strong local electric fields; non-uniform plasma distribution	No direct electrode exposure to gas; low power consumption; compact design	Limited plasma volume; less effective for bulk gas conversion

II.2.3 Definition and operating principle of the dielectric barrier discharge

A dielectric barrier discharge (DBD) is generated between two electrodes, at least one of which is covered by a dielectric material (such as glass, quartz, or alumina), and operated under an alternating high-voltage excitation. The presence of the dielectric layer is the key feature that distinguishes DBDs from conventional electrical discharges and governs their operating mechanism[9].

When an AC voltage is applied across the electrodes, an electric field develops in the gas gap. As the applied voltage increases and exceeds the breakdown threshold of the gas, electrons are accelerated and initiate ionization through electron–neutral collisions, leading to the formation of localized microdischarges (filaments) or a diffuse discharge, depending on operating conditions (pressure, gas composition, gap distance, and voltage waveform).

During the positive half-cycle of the applied voltage (Figures II. 3 a and b), electrons drift toward the anode while positive ions move toward the cathode. Charged particles accumulate on the surface of the dielectric barrier, forming surface charges. This charge deposition locally reduces the electric field in the gas gap, thereby rapidly quenching the microdischarge and preventing the transition to a thermal arc.

In the negative half-cycle (Figure II. 3c), the polarity of the applied voltage reverses. The previously deposited surface charges enhance or oppose the applied electric field, facilitating the ignition of new microdischarges at different locations. This repetitive charging and discharging process leads to a sequence of short-lived current pulses synchronized with the AC voltage.

From an electrical point of view (Figure II. 3 d), the DBD can be represented by an equivalent circuit consisting of the gas gap, modeled as a nonlinear resistor in parallel with a capacitance, and the dielectric barrier, represented by a capacitor. The applied voltage is divided between the gas voltage and the dielectric voltage. The capacitive nature of the dielectric explains the characteristic phase shift between the applied voltage and the discharge current.

Overall, the dielectric barrier limits the discharge current, ensures non-thermal plasma operation at atmospheric pressure, and enables stable, repetitive breakdown events. These properties make DBDs particularly suitable for applications such as ozone generation, surface treatment, gas conversion, and CO_2 splitting, where high electron energies are required while maintaining a low gas temperature[10].

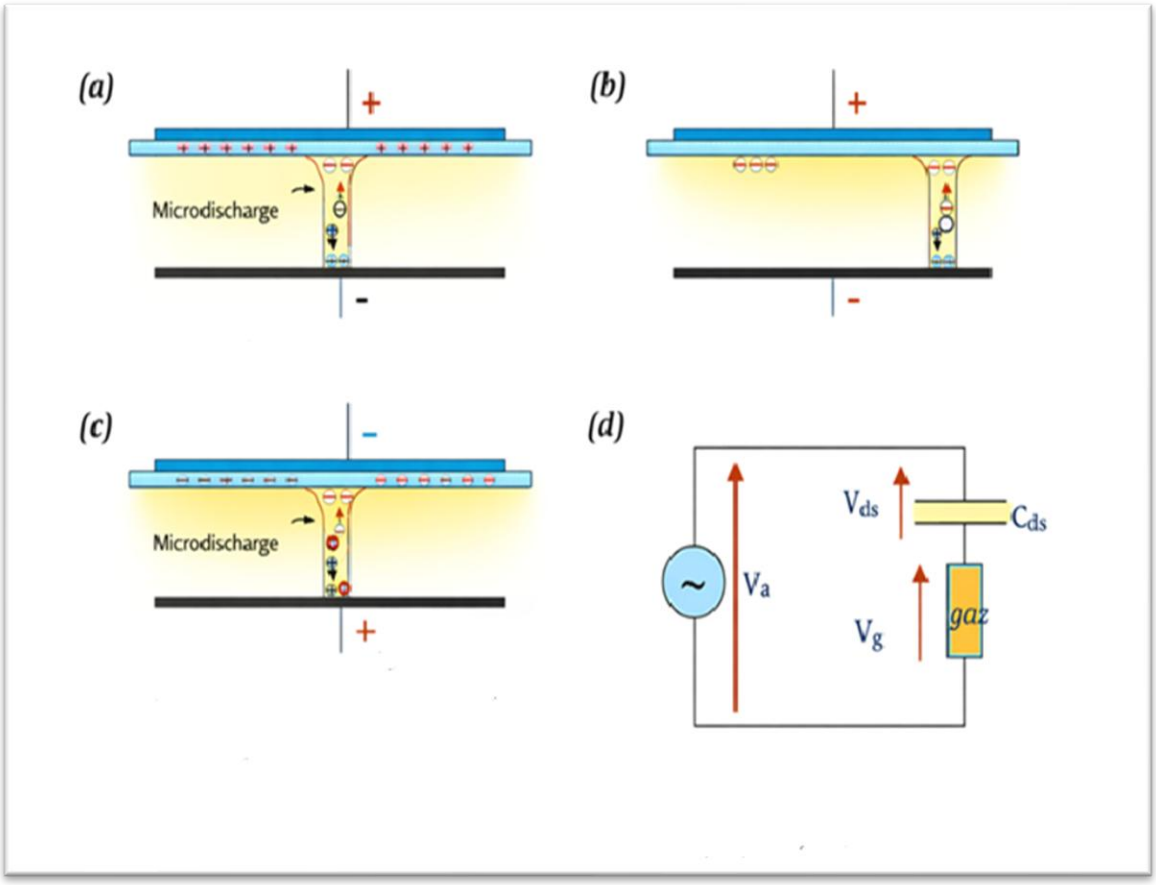

Figure II.3: Operating principle of a Dielectric Barrier Discharge (DBD)[11].

II.3 Characteristic of Breakdown in Gasses

Electrical breakdowns, detectable by the spark or discharge generated, transpire when the electric field above the necessary threshold for discharge start. The mechanisms of breakdown in gases are mostly the avalanche mechanism and the Streamer mechanism[12].

II.3.1 Electronic avalanche (Townsend discharge)

If we consider a gas contained between two electrodes, there may exist in this gas, in the absence of any applied electric field, a certain number of charges created by natural mechanisms, such as ultraviolet radiation or radioactivity, or by artificial mechanisms, for example by ultraviolet bombardment to extract electrons. -If an electric field is applied, the electrons are sufficiently accelerated by the field to produce other electrons thru collisions, which in turn acquire enough energy from the electric field to ionize other atoms, and so on, and the number of free electrons will continue to increase as they continue to move under the action of the electric field. It is this phenomenon that causes an exponential increase in the electronic charge density as one moves away from the electrode. The breakdown therefore occurs due to the avalanche phenomenon, as shown in figure (I.2)[13].

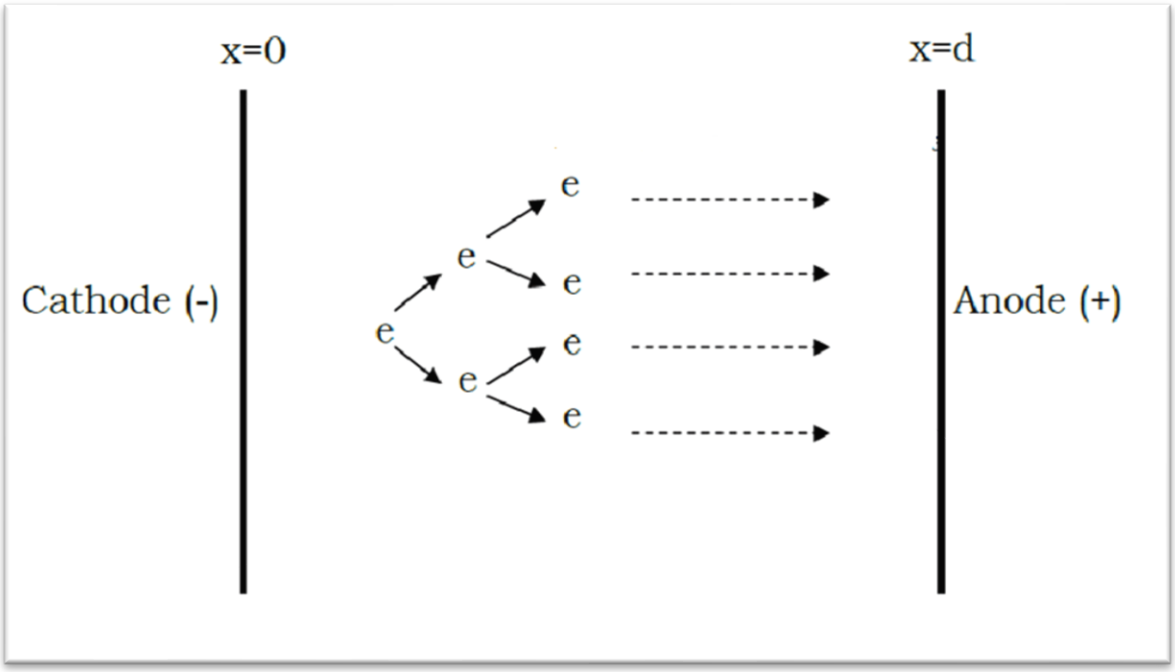

Figure II.4: Electronic avalanche.

This avalanche can be studied quantitatively based on the knowledge of the Townsend ionization coefficient. α [14], represents the number of electrons (or positive ions) created by an electron per unit length along a line of force of the applied field. An exploitable empirical expression considers that the thermal energy of the electrons is acquired

by the work of the electric field over a distance on the order of the mean free path. However, the latter is inversely proportional to the pressure. So, by introducing the constants A and B determined experimentally, we have:

$$V_b = \frac{Bpd}{\ln(Apd) - \ln(\ln(1+1/\gamma))} \qquad \text{(II. 1)}$$

With:

d:the inter-electrode distance [cm].

p: the gas pressure expressed in Torr.

A and B: Are two constants that depend on the gas. They are expressed respectively in [$Torr^{-1}.cm^{-1}$] and [$V.Torr^{-1}.cm^{-1}$].

γ: is the second Townsend coefficient that depends on the nature of the electrodes.

The values A and B are determined experimentally for each gas Table II.2 and they are considered constant over a reduced field domain E/p .

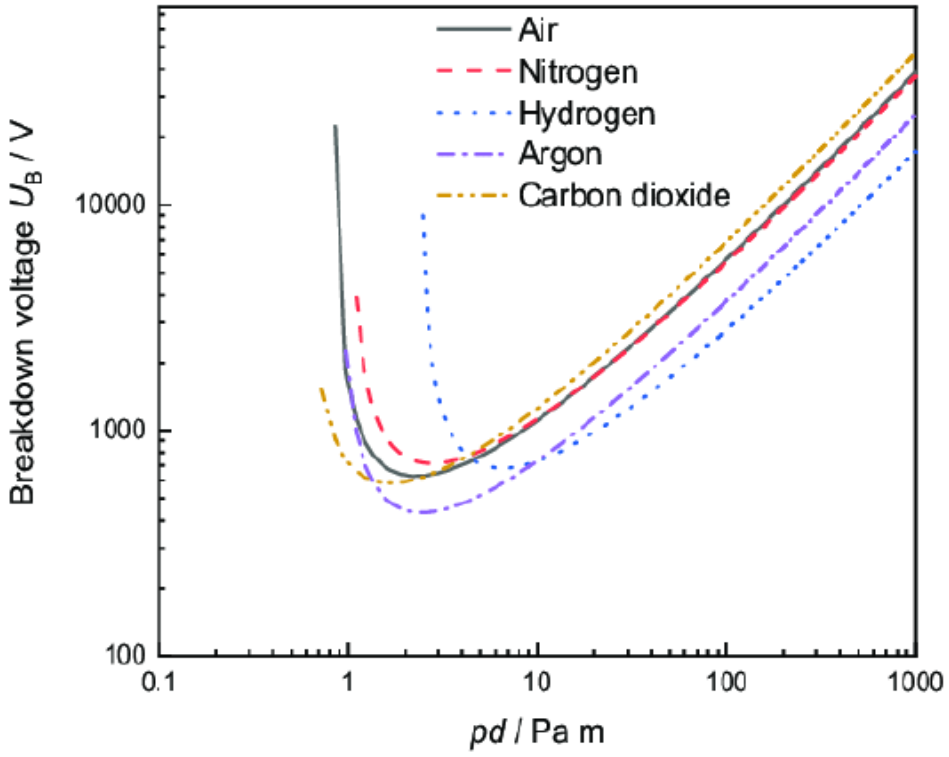

Figure II.5: Paschen curve for different gasses.

For a constant temperature, Figure II. 5presents the Paschen curves for different gasses such as Ar, He, N_2, H_2, CO_2, and Air. The plot of the breakdown voltage is given as a function of the product of gas pressure x inter-electrode distance (p x d).

Several tracing modes exist in the field of cold plasma. The most common ones are the Townsend breakdown, the streamer-type breakdown, and the spark-type breakdown. The nature of these breakdowns is conditioned by the values of the product p x d. Thus, if:

- p x d is less than a few tens of Torr.cm, the breakdown is usually of the Townsend type, which leads to a homogeneous discharge of large radius.
- p x d is higher, the breakdown is normally of the streamer type, which leads to a discharge of small radius, very energetic and non-homogeneous.
  In what follows, we will describe these two types of breakdowns because they are the ones that will occur in the discharges studied in this work.

Whatever the type of breakdown, the electron avalanche is the origin of any breakdown process (called the primary process); the initiation of this process is conditioned by two important parameters: the first is the presence of free electrons in the interelectrode space, these electrons are seed electrons the second is a positive effective ionization coefficient αeff; the latter is given by the expression:

Table II.2: The values of constants A and B for different gasses and the ranges of E/p where the formula is valid [15,16]

Gaz	**Paschen constant A ($Torr^{-1}.cm^{-1}$)**	**Paschen constant B ($V.Torr^{-1}.cm^{-1}$)**	**Valid reduced field range E/p ($V.Torr^{-1}.cm^{-1}$)**
Air	15	365	100-800
Mercury vapor (Hg)	20	370	200-600
Argon (Ar)	14	180	100-600
Carbon dioxide (CO_2)	20	466	500-1000
Hydrogen (H_2)	5	130	150-600
Xenon (Xe)	26	350	200-800
Nitrogen (N_2)	12	342	100-600
Water vapor (H_2O)	13	290	150-1000
Neon (Ne)	4	100	100-400
Krypton (Kr)	17	240	100-1000
Hydrogen chloride (HCl)	25	380	200-1000
Helium (He)	3	34	20-150

$$\alpha_{eff} = \alpha - a \qquad \text{(II. 2)}$$

Where α and a are respectively, the first Townsend ionization coefficient and the attachment coefficient [28]. This condition can be met if the reduced electric field E/N is sufficiently high to compensate for the low value of the mean free path of the electrons.

II.3.2 Townsend breakdown mechanism

At the beginning of the twentieth century, Townsend developed a theory that describes the breakdown process of a discharge at a pressure p, between two flat and parallel electrodes, separated by a distance d [29]. This theory provides an accurate description of this process for a set of conditions in which the product p x d is limited to a range of approximately 0.1-100 Pa.m (0.075-75 Torr.cm), the latter being based on secondary electron emission at the cathode under the effect of ion bombardment and metastable excited states.

By applying a voltage V between two flat electrodes at a distance d, a homogeneous electric field E0 of the form E0 = V/d will form; seed electrons produced in a gas by an external source will cause an avalanche of electrons toward the anode. The number of electrons produced by this

seed electron as it moves from the cathode to the anode is represented by $e^{\alpha.d}$. The Townsend relation is written. [17]

$$I = I_0 e^{\alpha.d} \tag{II.3}$$

Where:

I : is the current (A).

I_0 : is the current due to primary electrons (A).

α : is the first Townsend coefficient (m^{-1}) .

d : is the inter-electrode distance.

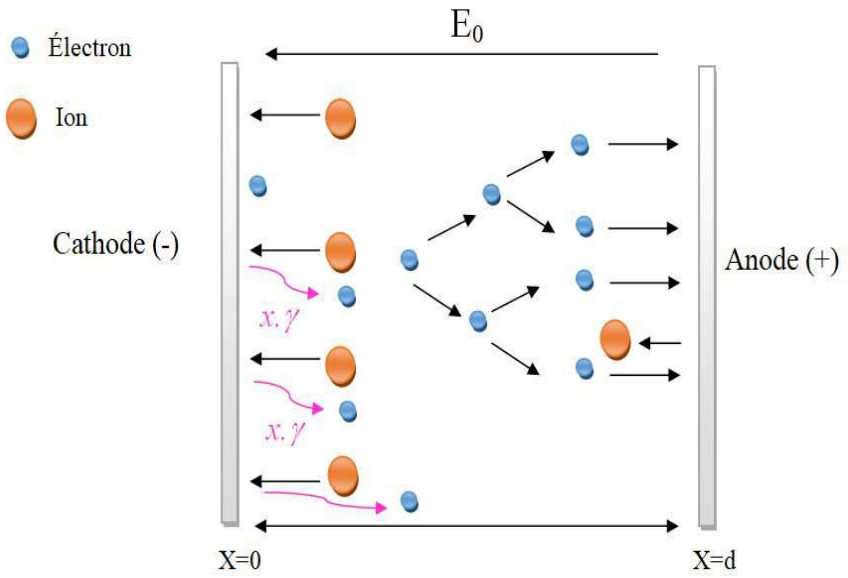

Figure II.6: The principle of the Townsend breakdown mechanism.

The transition of electrons from the cathode to the anode generates secondary electrons, leading to the creation of positively charged ions. These ions bombard the cathode with their kinetic energy and strip off secondary electrons (each ion hitting the cathode releases γ electrons) as illustrated in figure II. 6. This phenomenon is called the secondary emission effect, which depends on the nature of the electrode and the gas. The probability of producing secondary electrons in this way is reflected by the introduction of a second Townsend coefficient. Townsend was able to establish the condition for the appearance of an autonomous disruptive discharge (breakdown) in a gas expressed by:

$$\gamma(e^{\alpha.d} - 1) = 1 \tag{II.4}$$

For a new avalanche to occur, the positive ions formed in the primary electronic avalanche must extract at least one electron from the cathode. We say that the discharge is non-sustained if equation II.5 remains less than 1.

$$\gamma(e^{\alpha.d} - 1) \geq 1 \tag{II.5}$$

II.3.3 Streamer breakdown mechanism

As we presented earlier, the Townsend-type breakdown is obtained at low pressure and for a product p x d less than a few tens of Torr.cm. On the other hand, for high pressure, including atmospheric pressure; Leob [18], developed another mechanism called the "streamer mechanism." The latter cannot be described by the classical Townsend theory. When the product (p x d) is greater than 1000 Torr.cm, the streamer-type breakdown is observed. This type of breakdown is based on the formation of a secondary electron in the gas and the buildup of a significant space charge.

Its mechanism presents several stages of formation, citing (Figure II.7).

- The primary avalanche and the creation of a space charge.
- The creation of a secondary avalanche.
- The propagation of the streamer.
- The Formation of the Filament Channel.

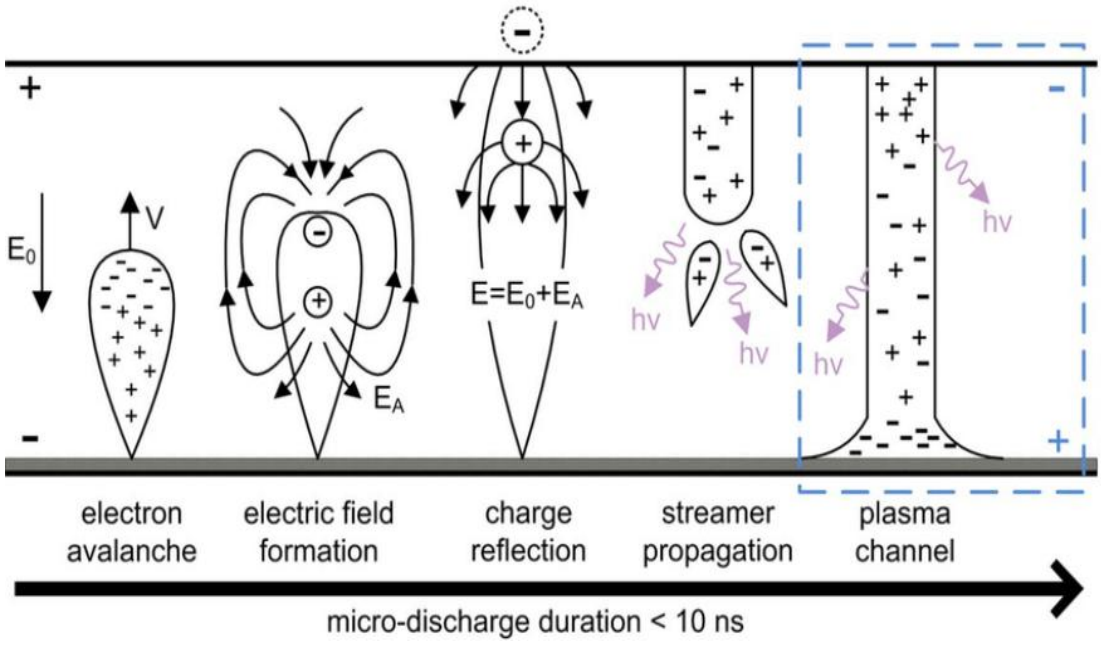

Figure II.7: The streamer-type breakdown mechanism; the primary electron avalanche; streamer propagation; filament establishment.

II.4 The different operating modes of a DBD

In this section, we present the main characteristics of dielectric barrier discharge regimes based on the type of gas breakdown. For a DBD discharge, we can distinguish two main families of

breakdown, according to their mechanisms: filamentary discharges "streamer breakdown" and homogeneous discharges "Townsend breakdown," but there is also a third type of discharge that derives from the homogeneous discharge. This is the multi-peak discharge. These different regimes are influenced by several parameters, such as pressure, frequency, applied voltage, inter-electrode distance, and the nature of the gas[19].

II.4.1 The filamentary regime of a DBD

The filamentary regime is the most characteristic operating mode of dielectric barrier discharges, especially at atmospheric pressure. In this regime, the discharge does not form a uniform plasma across the entire electrode gap. Instead, it consists of many short-lived, highly localized microdischarges, commonly referred to as filaments or microchannels.

These filaments appear as bright, needle-like plasma channels that form randomly in space and time during each half-cycle of the applied AC voltage. Their initiation is driven by strong local electric field enhancements which cause rapid electron avalanches. Once formed, a filament undergoes a very fast ionization process, typically lasting only a few nanoseconds, during which the local electron density can reach values as high as 10^{14}-10^{16} cm^3. Because the current is confined to these very small conductive channels, the instantaneous current in a filament can be quite high, even though the overall discharge power remains moderate[20].

A key feature of the filamentary regime is the presence of dielectric barriers, which prevent the transition to a thermal arc. When a filament strikes the dielectric surface, charges accumulate on the barrier, rapidly reducing the local electric field and extinguishing the microdischarge. This charge deposition mechanism ensures that filaments remain transient and self-limiting, preventing the formation of a continuous arc and maintaining the non-thermal character of the discharge.

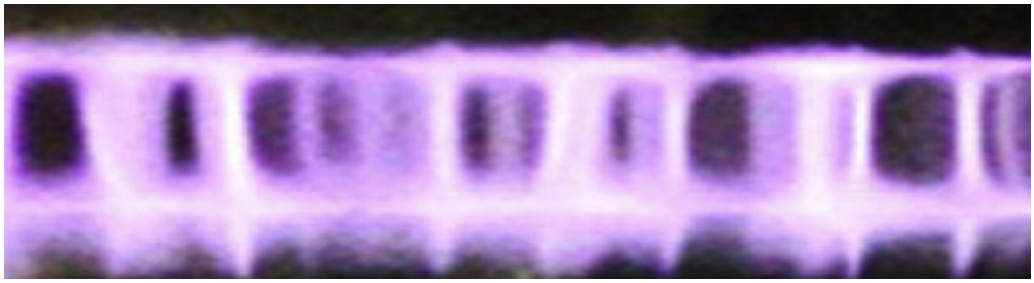

Figure II.8: filamentary DBD .

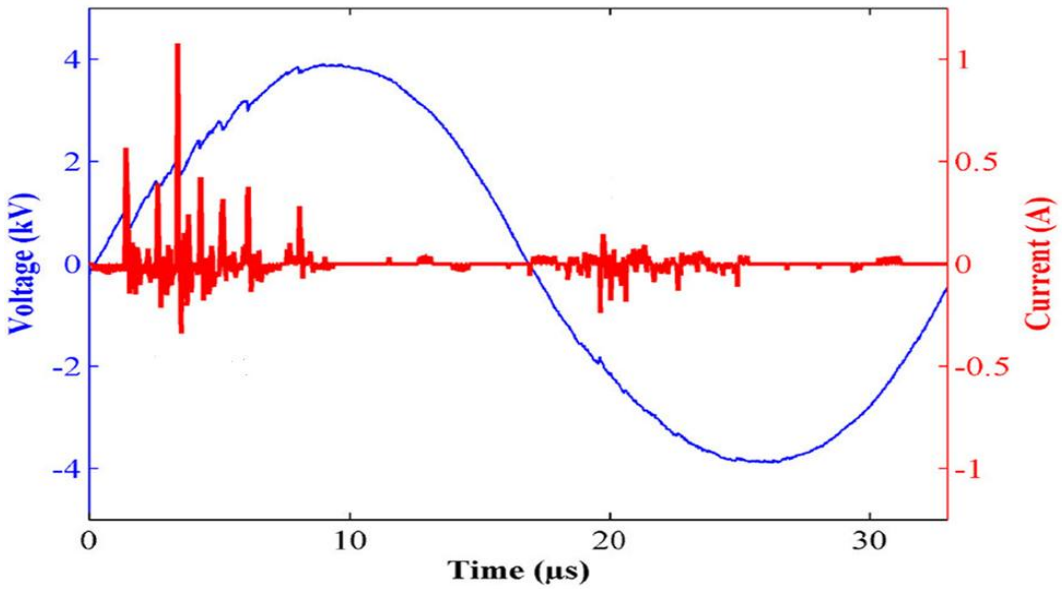

Figure II. 9: Measurement with an oscilloscope of the applied voltage and current of a filamentary DBD discharge.

The filamentary regime is advantageous for processes requiring high local electron energy, intense electric fields, or strong chemical reactivity, such as pollutant degradation, ozone generation, and CO_2 conversion. However, because filaments are spatially and temporally nonuniform, this regime can be more difficult to model and control. The spatial inhomogeneity may also lead to uneven treatment of surfaces or gas volumes if not properly optimized.

The current-time electrical response of a filamentary discharge is characterized by several current peaks, for each half period, of very short duration (on the order of a few nanoseconds (ns)) and an amplitude of a few milliamperes (mA) per square centimeter[21].

II.4.2 The homogeneous regime of a DBD

The homogeneous regime, also called the diffuse regime, refers to an operating mode of dielectric barrier discharges in which the plasma appears uniform, smooth, and evenly distributed across the electrode surface. Unlike the filamentary regime characterized by numerous short-lived microdischarges the homogeneous regime is defined by the absence of discrete filaments. Instead, the discharge behaves like a continuous glow covering the entire gap.

This regime typically occurs under specific conditions where the formation of localized microchannels is suppressed. Such conditions include higher gas pressures, appropriate gas mixtures (e.g., He, He/CO_2, or He/O_2), lower applied voltages, and short electrode gaps. Helium, in particular, plays a key role because of its high ionization cross section and efficient Penning ionization processes, which encourage a uniform spread of energy deposition[22].

In the homogeneous regime, the electric field distribution remains relatively uniform across the gas gap. As a result, charge carriers are generated more evenly and do not accumulate locally to trigger strong filamentary avalanches. The electron density is moderate and distributed over a larger volume, leading to a smooth current waveform and lower instantaneous power density compared to filamentary discharges. This uniform behavior is beneficial for applications requiring controlled surface treatment, uniform chemical activation, and gentle plasma chemistry, since it avoids localized overheating or material damage.

Despite its apparent simplicity, achieving and maintaining a homogeneous regime can be challenging. Minor impurities, local field enhancements, or excessive voltage can destabilize the uniform discharge and lead to filament formation. Thus, careful control of gas composition, pressure, and the external electrical circuit is essential. The homogeneous regime provides a stable and predictable plasma environment, making it valuable for plasma-assisted chemistry, thin-film deposition, and biomedical applications where uniformity and low thermal impact are required[23].

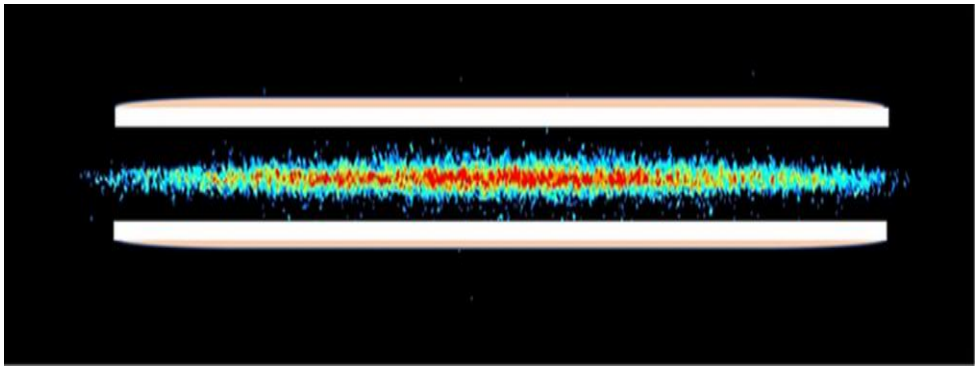

Figure. II.10: homogeneous DBD

From an electrical perspective, the luminous regime is defined by a single current peak for every half-period Figure II.10, which is equivalent to the creation of a single discharge channel that covers the electrodes' whole surface. A single current peak for every half-period of the applied voltage is another characteristic of the Townsend-type regime, which is similarly characterized by the same observation Figure II. 11. The length of the current peak that emerges at each half-period distinguishes the two forms of discharge. It is on the order of a few microseconds (μs) in the luminous regime and on the order of a few tens of microseconds in the Townsend regime, which is longer than the luminescent regime.

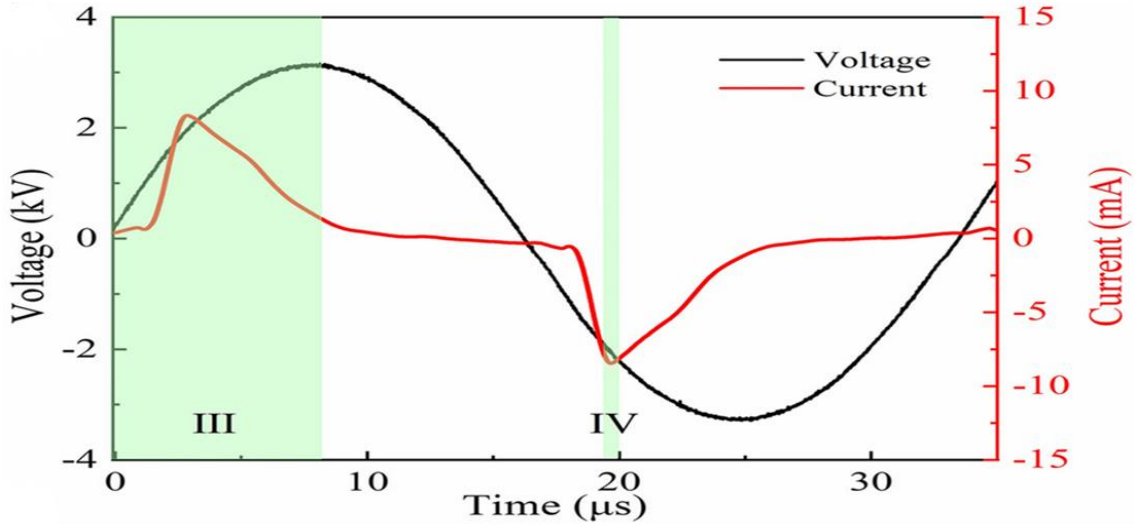

Figure II. 11:Measurement with the oscilloscope of the voltage and current of a homogeneous DBD discharge in CO_2.

II.4.3 The multi-peak regime of a DBD

The multi-peak regime refers to an operational mode where multiple current pulses occur within a single half-cycle of the applied AC voltage[24]. Instead of a single filamentary event per half-period, several distinct microdischarges appear sequentially as the voltage continues to increase after the first breakdown event as shown in Figure. II.12.

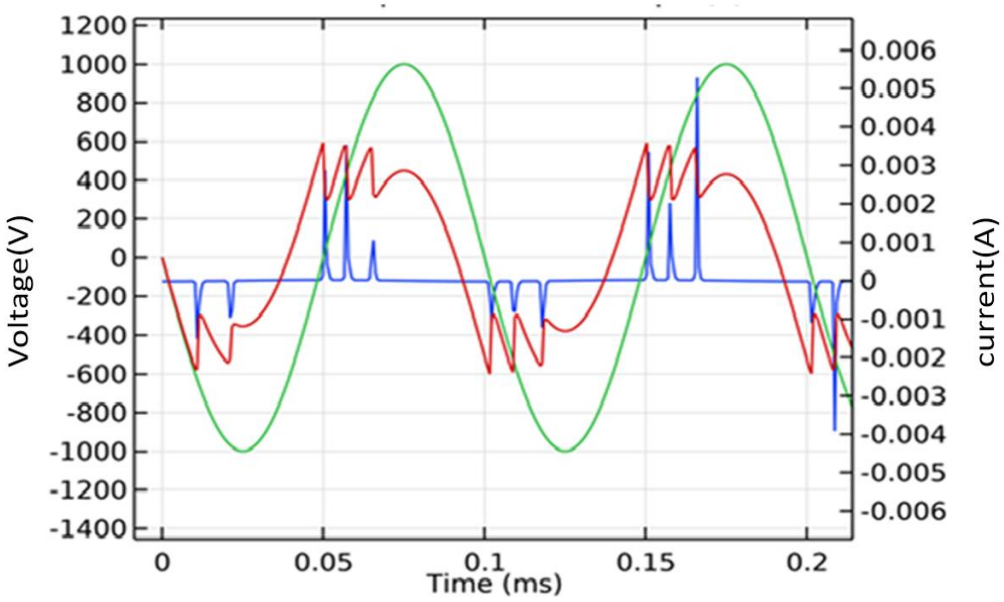

Figure. II. 12: Electrical characteristic of a multi-peak regime.

This regime arises due to the dynamic charging and discharging of the dielectric barrier:

A first microdischarge ignites when the local field exceeds the breakdown threshold.

The deposited surface charge lowers the local electric field, momentarily extinguishing the discharge[25].

As the applied voltage continues increasing, the field rises again in another region.

A second (or third) microdischarge forms at a new location.

This produces a series of current peaks within one half cycle, observable clearly in electrical measurements.

II.5 DBD Applications

Dielectric Barrier Discharge (DBD) plasmas have attracted significant interest over the past decades due to their ability to generate non-thermal plasma at atmospheric pressure while maintaining relatively low gas temperatures. This unique feature allows DBD systems to initiate energetic electron-driven chemical reactions without excessive thermal heating, making them highly versatile for a wide range of industrial, environmental, and biomedical applications. The presence of dielectric layers limits the discharge current and prevents arc formation, enabling stable operation under various conditions[26,27].

II.5.1 Environmental Applications

One of the most important application fields of DBDs is environmental protection, particularly in the treatment of gaseous effluents. DBD reactors are widely used for:

- Removal of volatile organic compounds (VOCs)
- Decomposition of toxic gases (NO_x, SO_2, H_2S)
- Ozone generation for air and water purification

The high-energy electrons produced in DBDs efficiently generate reactive species such as O, OH, O_3, and N radicals, which oxidize or decompose harmful pollutants into less toxic compounds. Due to their ability to operate at atmospheric pressure, DBD systems are especially suitable for exhaust gas treatment.

II.5.2 Carbon dioxide conversion and utilization

DBDs are increasingly investigated for CO_2 conversion and utilization, addressing both environmental and energy challenges. In DBD plasma, CO_2 molecules can be activated through electron impact excitation, vibrational pumping, and dissociation, leading to products such as CO, O_2, and syngas when combined with other reactants (e.g., H_2 or CH_4).

This non-thermal approach enables CO_2 conversion at relatively low bulk temperatures, offering a promising alternative to conventional thermochemical processes[28].

II.5.3 Surface treatment and material processing

DBD plasmas are extensively used for surface modification of polymers, textiles, metals, and glass. Typical applications include:

- Surface activation to improve adhesion and wettability
- Cleaning and removal of organic contaminants
- Functionalization by introducing polar surface groups

The homogeneous or filamentary plasma generated by DBDs allows precise surface treatment without damaging heat-sensitive materials, making this technique attractive for industrial manufacturing.

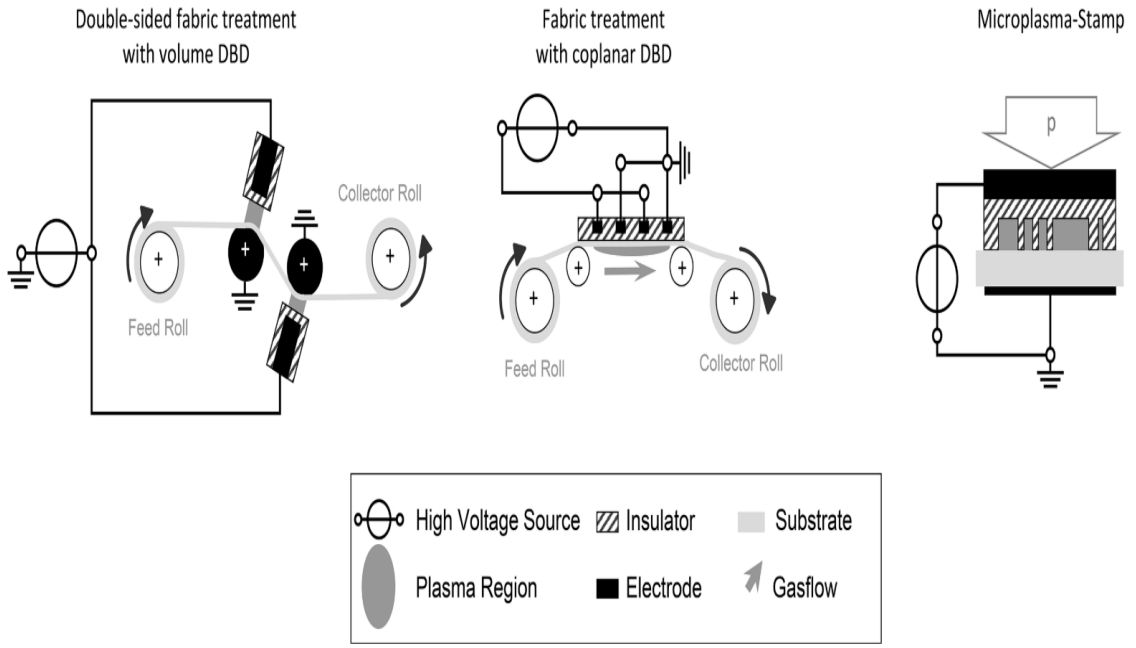

Figure. II.13: DBD-based surface treatment: micro plasma-stamp (right), coplanar DBD (center), and double-sided fabric treatment (left).

II.5.4 Plasma medicine and biotechnology

In recent years, DBDs have found applications in plasma medicine, where cold atmospheric plasmas are used for:

- Sterilization and disinfection

- Wound healing
- Inactivation of bacteria and viruses

The low gas temperature and controlled generation of reactive oxygen and nitrogen species (RONS) enable safe interaction with biological tissues, opening new possibilities in healthcare[29].

II.5.5 Ozone generation

DBDs are the most widely used technology for industrial ozone production. Ozone generated in DBD reactors is employed in water treatment, food processing, and chemical synthesis, splitting O_2 molecules into atoms that then recombine to form ozone O_3. DBD reactors, featuring electrodes separated by a dielectric (insulating) layer, allow for controlled microdischarges. The efficiency, scalability, and reliability of DBD-based ozone generators make them a mature and well-established application[30].

II.6 Conclusion

This chapter provides an overview of electrical discharges and non-thermal (cold) plasmas operating out of thermodynamic equilibrium, with a particular emphasis on their differences from thermal plasmas. A classification of the main types of electrical discharges is presented in the form of a flow chart. Special attention is given to the physical mechanisms governing low-pressure discharges, such as Townsend discharges, and atmospheric-pressure discharges, notably streamer-type discharges, based on their current–voltage breakdown characteristics. In addition, an overview of various cold plasma reactors is provided to characterize these non-equilibrium discharges and to highlight their fields of application.

Furthermore, the present section provides an overview of electrical discharges and non-thermal (cold) plasmas operating out of thermodynamic equilibrium, with a particular emphasis on their differences from thermal plasmas. A classification of the main types of electrical discharges is presented in the form of a flow chart. Special attention is given to the physical mechanisms governing low-pressure discharges, such as Townsend discharges, and atmospheric-pressure discharges, notably streamer-type discharges, based on their current–voltage breakdown characteristics. In addition, an overview of various cold plasma reactors is provided to characterize these non-equilibrium discharges and to highlight their fields of application.

Finally, this chapter includes the concept of dielectric barrier discharge (DBD) is introduced, together with the key physical elements that define its operation. The general principles of DBDs, their typical configurations, and their wide range of industrial applications are discussed. In line

with the objectives of this thesis, particular emphasis is placed on the fundamental operating principles of ozone generators, accompanied by a non-exhaustive review of their main applications.

References

[1] He, Y., Sang, W., Lu, W., Zhang, W., Zhan, C., & Jia, D. (2022). Recent advances of emerging organic pollutants degradation in environment by non-thermal plasma technology: A Review. Water, 14(9), 1351.

[2] Chenoui, M., Tebani, H., & Benyoucef, D. (2025). Kinetic Simulation of CO_2 Conversion in Dielectric Barrier Discharges. Physics of Semiconductor Devices & Renewable Energies Journal, 2(01).

[3] Massines, F., Ghérardi, N., Naudé, N., & Ségur, P. (2009). Recent advances in the understanding of homogeneous dielectric barrier discharges. The European Physical Journal-Applied Physics, 47(2), 22805.

[4] Sobel, A. (1991). Plasma displays. IEEE Transactions on plasma science, 19(6), 1032-1047.

[5] Brandenburg, R., Becker, K. H., & Weltmann, K. D. (2023). Barrier discharges in science and technology since 2003: a tribute and update. Plasma Chemistry and Plasma Processing, 43(6), 1303-1334.

[6] Palma, V., Cortese, M., Renda, S., Ruocco, C., Martino, M., & Meloni, E. (2020). A review about the recent advances in selected nonthermal plasma assisted solid–gas phase chemical processes. Nanomaterials, 10(8), 1596.

[7] Khoja, A. H., Tahir, M., & Amin, N. A. S. (2017). Dry reforming of methane using different dielectric materials and DBD plasma reactor configurations. Energy Conversion and Management, 144, 262-274.

[8] Mei, D., Duan, G., Fu, J., Liu, S., Zhou, R., Zhou, R., ... & Ostrikov, K. K. (2021). CO_2 reforming of CH4 in single and double dielectric barrier discharge reactors: Comparison of discharge characteristics and product distribution. Journal of CO_2 utilization, 53, 101703.

[9] Kogelschatz, U., Eliasson, B., & Egli, W. (1997). Dielectric-barrier discharges. Principle and applications. Le Journal de Physique IV, 7(C4), C4-47.

[10] Kelber, J. A. (2003). Study of Interactions Between Diffusion Barrier Layers and Low-k Dielectric Materials for Copper/low-k Integration (Doctoral dissertation, University of North Texas).

[11] Hao, L., Khan, M. I., Lei, Y., Zhou, S., & Fan, B. (2025). Interfacial electro-hydrodynamics inspired micro/nano-fluidic energy conversion: from mechanism to applications. Lab on a Chip, 25(17), 4161-4220.

[12] Cookson, A. H. (1981). Review of high-voltage gas breakdown and insulators in compressed gas. IEE Proceedings A (Physical Science, Measurement and Instrumentation, 128(4), 303-312.

[13] Abdel-Salam, M. (2018). Electrical breakdown of gases. In High-Voltage Engineering (pp. 115-148). CRC Press.

[14] Llewellyn-Jones, F. (1981). The development of theories of the electrical breakdown of gases. In Electrical Breakdown and Discharges in Gases: Part A Fundamental Processes and Breakdown (pp. 1-71). Boston, MA: Springer US.

[15] Shock, E. L., Oelkers, E. H., Johnson, J. W., Sverjensky, D. A., & Helgeson, H. C. (1992). Calculation of the thermodynamic properties of aqueous species at high pressures and temperatures. Effective electrostatic radii, dissociation constants and standard partial molal properties to 1000 C and 5 kbar. Journal of the Chemical Society, Faraday Transactions, 88(6), 803-826

[16] Husain, E., & Nema, R. S. (2007). Analysis of Paschen curves for air, N_2 and SF_6 using the Townsend breakdown equation. IEEE transactions on electrical insulation, (4), 350-353.

[17] Tirumala, R., & Go, D. B. (2010). An analytical formulation for the modified Paschen's curve. Applied physics letters, 97(15).

[18] Loeb, L. B. (1948). Statistical factors in spark discharge mechanisms. Reviews of Modern Physics, 20(1), 151.

[19] Valdivia-Barrientos, R., Pacheco-Sotelo, J., Pacheco-Pacheco, M., Benítez-Read, J. S., & López-Callejas, R. (2006). Analysis and electrical modelling of a cylindrical DBD configuration at different operating frequencies. Plasma sources science and technology, 15(2), 237.

[20] Abdollahzadeh, M., Pascoa, J. C., & Oliveira, P. J. (2018). Comparison of DBD plasma actuators flow control authority in different modes of actuation. Aerospace science and technology, 78, 183-196.

[21] Belov, I., Paulussen, S., & Bogaerts, A. (2016). Appearance of a conductive carbonaceous coating in a CO2 dielectric barrier discharge and its influence on the electrical properties and the conversion efficiency. Plasma Sources Science and Technology, 25(1), 015023.

[22] Massines, F., Ghérardi, N., Naudé, N., & Ségur, P. (2009). Recent advances in the understanding of homogeneous dielectric barrier discharges. The European Physical Journal-Applied Physics, 47(2), 22805.

[23] Lu, X., Fang, Z., Dai, D., Shao, T., Liu, F., Zhang, C., ... & Jiang, C. (2023). On the chronological understanding of the homogeneous dielectric barrier discharge. High Voltage, 8(6), 1132-1150.

[24] Chen, B., Tan, Z., & Song, X. (2012). Study on multi-peak behavior of pulsed dielectric barrier discharges in atmospheric-pressure helium. Vacuum, 86(12), 1992-1997.

[25] Pellerin-Boudriau, V., Montpetit, F., Profili, J., & Stafford, L. Optical emission spectroscopy of single-peak, multi-peak, and nanosecond repetitively pulsed dielectric barrier discharges in He.

[26] Subedi, D. P., Joshi, U. M., & Wong, C. S. (2017). Dielectric barrier discharge (DBD) plasmas and their applications. In Plasma science and technology for emerging economies: an AAAPT experience (pp. 693-737). Singapore: Springer Singapore.

[27] Xu, X. (2001). Dielectric barrier discharge—properties and applications. Thin solid films, 390(1-2), 237-242

[28] Yousaf, M., Zaman, M., Mahmood, A., Imran, M., Elkamel, A., Rizwan, M., ... & Riaz, F. (2022). Carbon dioxide utilization: A critical review from multiscale perspective. Energy Science & Engineering, 10(12), 4890-4923.

[29] Kuchenbecker, M., Bibinov, N., Kaemlimg, A., Wandke, D., Awakowicz, P., & Viöl, W. (2009). Characterization of DBD plasma source for biomedical applications. Journal of Physics D: Applied Physics, 42(4), 045212

[30] Lahouel, M. H. A., Benyoucef, D., & Gadoum, A. (2023). One Dimensional Modeling Of Dielectric Barrier Discharge in Pure Oxygen at Atmospheric Pressure Using Comsol Multiphysics. arXiv preprint arXiv:2302.13813.

Chapter III

Plasma Model Parameters and Computational Approach

III.1 Introduction

Numerical modeling plays a central role in the study and understanding of plasma discharges, particularly when experimental investigations are limited by technical, financial, or diagnostic constraints. Plasma systems often involve a complex interplay between charged and neutral species, electromagnetic fields, chemical reactions, and energy transport. Capturing these phenomena experimentally with high temporal and spatial resolution is challenging; therefore, computational models provide an essential complementary tool for investigating plasma behavior under controlled conditions[1].

The numerical modeling of a plasma discharge consists of formulating a set of mathematical equations that describe the evolution of the plasma's physical variables such as particle densities, electric fields, temperatures, and velocities within a defined domain. These equations are derived from fundamental conservation laws, kinetic theory, and electromagnetic field theory. Depending on the level of detail required, different modeling approaches can be adopted, ranging from kinetic models, such as solutions of the Boltzmann equation, to fluid models based on moment equations or drift–diffusion approximations[2].

For dielectric barrier discharges (DBDs) at atmospheric pressure, fluid models are widely used due to their efficiency and ability to capture the essential physics of non-equilibrium plasmas. In such models, the first three moments of the Boltzmann equation are typically employed: particle continuity, momentum transport, and energy conservation. These moment equations are coupled with Poisson's equation, which determines the spatial distribution of the electric field generated by space charges. The resulting system of partial differential equations is solved numerically to predict key discharge characteristics, such as electron density, electric field profiles, current evolution, and power deposition.

Boundary conditions constitute an essential part of the modeling framework, as they define how the plasma interacts with its surrounding environment, including electrodes, dielectric surfaces, and open boundaries. Proper specification of boundary conditions ensures numerical stability and physical accuracy of the solution.

Overall, numerical modeling provides valuable insights into plasma ignition, propagation, mode transitions, and chemical conversion processes. It allows researchers to explore parameter regimes that are difficult to access experimentally, optimize reactor designs, and guide the development of plasma-assisted technologies, including CO_2 conversion, pollutant removal, ozone generation, and surface treatment.

III.2 Numerical modeling of a plasma discharge

III.2.1 Types of plasma models

The physical description of a plasma discharge relies on mathematical models that capture the behavior of charged and neutral species under the influence of electromagnetic fields. Depending on the level of detail required and the computational resources available, three principal categories of plasma models are commonly used: kinetic models, fluid models, and hybrid models. Each approach is based on specific assumptions and offers different advantages in terms of accuracy and computational efficiency.

III.2.1.1 Kinetic models

The kinetic model is the most accurate method for simulating the evolution of particles in a plasma discharge, but it is also the most challenging to use when dealing with complex geometries. We employ the kinetic description, in which the velocity variable is represented by the distribution function f = f (t, x,v), which describes plasma particles. Because it incorporates information about the particle velocity distribution, the distribution function has more information than fluid quantities[3].

- **Electron energy distribution function**

In this section, we discuss the electron energy distribution function (EEDF), which plays a very important role in plasma modeling. Several approaches can be used to describe the EEDF, such as the Maxwellian distribution, the Druyvesteyn distribution, or the solution obtained from the Boltzmann equation[4].

a. Maxwellian-shaped distribution

This distribution is used when the electron collision frequency is independent of velocity and when the electrons are in thermodynamic equilibrium with one another. In this case, electron–electron collisions lead to a Maxwellian-shaped distribution, while inelastic collisions between electrons and heavy particles cause the EEDF to decrease at higher electron energies. This distribution function is generally the solution of the Boltzmann equation in the absence of any external forces [5].

For a Maxwellian (Maxwell–Boltzmann) distribution at a temperature T, the expression of the function f is written in the form:

$$\mathrm{f}(E) = n_\alpha \frac{2}{(K_B.T_\alpha)^{3/2}} \sqrt{\frac{E}{\pi}} \exp(-\frac{E}{K_B.T_\alpha}) \qquad \text{(III.1)}$$

With:

n_α : is the density of species α .

T_α : is the temperature of species α .

K_B : is the Boltzmann constant.

E : is the energy.

From this function(III.1) , we can deduce

Particle density:

$$n = \int \mathrm{f}(E)dE \tag{III.2}$$

Its average speed:

$$\bar{v} = \frac{1}{n}\int V.f(E)dE = \sqrt{\frac{8K_BT}{\pi m}} \tag{III.3}$$

Its average energy:

$$\bar{E} = \frac{1}{n}\int \frac{1}{2}mv^2.f(E)dE = \frac{3}{2}K_BT \tag{III.4}$$

The shape of this distribution for a different species is illustrated in Figure III-1.

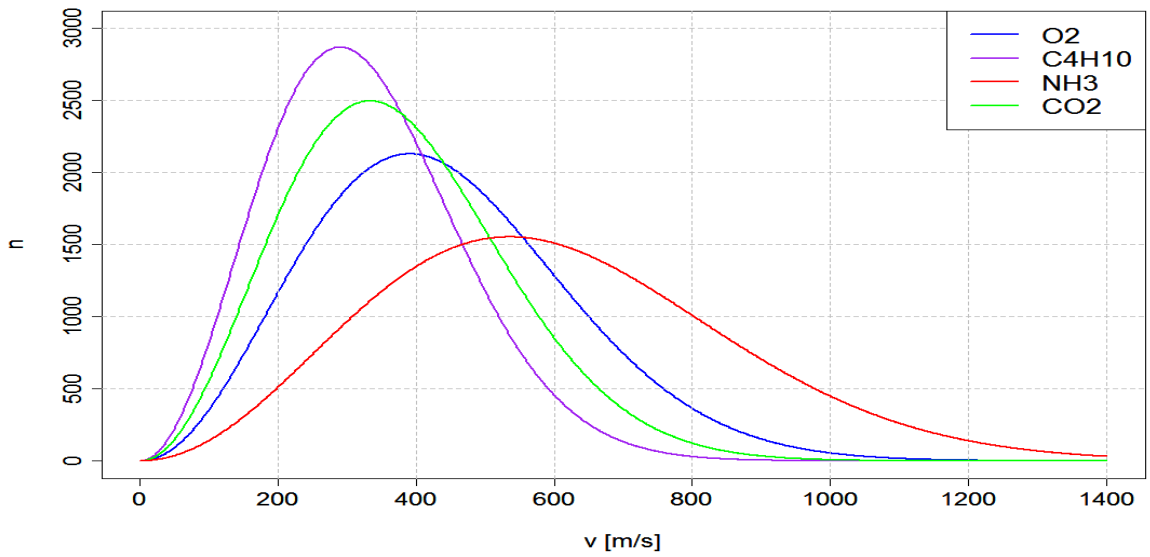

Figure III.1: Maxwell-Boltzmann speed distributions for a different species

The modeling findings are influenced by the FDEE selection, and as correct modeling of plasma discharges is crucial, it is essential to select the FDEE that most closely matches the state of the discharge under study. The estimated FDEEs are in agreement with a Maxwellian distribution (Maxwell-Boltzmann) in a wide range of plasma discharges.

b. Druyvesteyn distribution

The Druyvesteyn distribution is another commonly used form of the electron energy distribution function, particularly in plasmas where the electron collision frequency depends on velocity and elastic collisions with heavy species dominate. Unlike the Maxwellian distribution, which predicts a relatively high population of energetic electrons, the Druyvesteyn distribution exhibits a more rapid decrease at high energies. This results in a lower probability of finding electrons in the high-energy tail of the distribution[6].

Figure III. 2 shown a comparison between Druyvesteyn and Maxwell's electron energy distributions. The average electron energy for each distribution is shown by the numbers.

This distribution is generally obtained as a solution of the Boltzmann equation under the assumption of dominant elastic scattering and weak inelastic processes. For isotropic electrons, the Druyvesteyn distribution can be expressed as:

$$f_D(v) = \frac{1.04\sqrt{\pi}}{2}\left(\frac{m_e}{2\pi k_B T_e}\right)^{3/2} \exp\left(-0.55\left(\frac{m_e v^2}{2k_B T_e}\right)^2\right) \qquad \text{(III.5)}$$

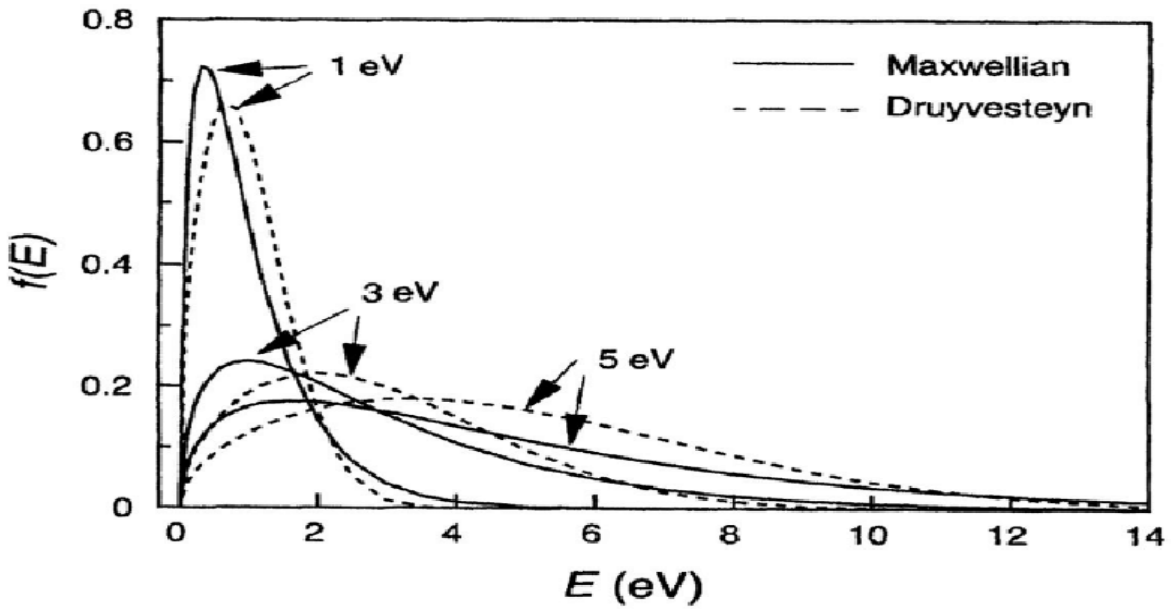

Figure III.2: Druyvesteyn and Maxwell's electron energy distributions. The average electron energy for each distribution is shown by the numbers.

III.2.1.2 Particle-in-Cell Monte Carlo collision models

This model allows us to solve the Boltzmann equation indirectly by simulating the trajectories of a determined number of species present in plasmas. This model is also known as the PIC-MCC (Particle In Cell- Monte-Carlo Collision) method , where PIC particle models involve evolving

particles (for example, electrons and ions) under the action of the electric field and determining their trajectories in space, while the MCC method consists of treating collisions. The particles present in the plasma are treated individually at each moment.
The integration of the equations of motion between two collisions determines the influence of the electric field. These equations are treated statistically by drawing random numbers whose probability densities depend on the cross-sections (so that we can determine the instant, the nature of the collisions, the trajectory of the particle after collisions).
As this type of plasma is weakly collisional, this model remains better suited for simulating low-pressure plasmas. The only drawback is related to the computation time, which is very long compared to other methods[7].

III.2.1.3 Fluid models

Fluid models offer a macroscopic description of plasma by using moment equations derived from the Boltzmann equation. Instead of resolving individual particle motions, fluid models track bulk quantities such as density, mean velocity, and temperature. The most common equations include:

- Continuity equations for species densities
- Momentum conservation equations
- Energy conservation equations
- Poisson's equation for the electric potential

At atmospheric pressure, where collisions dominate, the fluid approximation becomes particularly effective. The drift–diffusion approximation, a simplified form of the fluid model, is widely used for dielectric barrier discharges (DBDs). Fluid models are computationally efficient and capable of reproducing key plasma features such as ionization waves, streamer propagation, and discharge current–voltage behavior. Their main limitation is the assumption of local or quasi local equilibrium, which may not be valid in very fast transient or strongly non-uniform regions.

III.2.1.4 Hybrid models

Hybrid models combine the strengths of kinetic and fluid approaches to achieve both accuracy and computational feasibility. Typically, electrons whose distribution can be highly non-Maxwellian are treated kinetically, while ions and neutrals are described with fluid equations. This approach provides a more accurate representation of electron dynamics in regions such as sheaths,

ionization fronts, or microdischarge filaments, without the full computational burden of a fully kinetic model.

Hybrid models are particularly effective for:

- Capturing non-equilibrium electron behavior
- Resolving localized high-field regions
- Modeling transient discharges or streamer initiation
- Simulating plasmas with wide time- and length-scale separations

These models are increasingly used in atmospheric-pressure plasma research, including CO_2 conversion, because they balance fidelity and efficiency while providing access to detailed physical insights.

III.3 Description of the fluid approach

The fluid model is based on the transport equations for particles. They are obtained by taking the first three moments of the Boltzmann equation coupled to the Poisson equation which corresponds to the characteristic physical quantities of the plasma such as the charge density, momentum, kinetic pressure, and flow of thermal energy[8].

III.3.1 Boltzmann equation

To describe the transport properties of charged particles present in the discharge and under an electric field, the energy distribution function of electrons can be described by the following Boltzmann equation[9].

$$\frac{\partial f}{\partial t} + V \cdot \frac{\partial f}{\partial r} + \frac{F}{m} \cdot \frac{\partial f}{\partial V} = \left(\frac{\partial f}{\partial t}\right)_{collision} \tag{III.6}$$

With :

$$F = q(E + V \times B) \tag{III.7}$$

This equation consists of four terms:

$\frac{\partial f}{\partial t}$: Represents the evolution of the distribution function over time.

$V \cdot \frac{\partial f}{\partial r}$: Represents the spatial diffusion term of the particles.

$\frac{F}{m}\cdot\frac{\partial f}{\partial V}$: Represents the variations in particle velocity under the action of external forces.

$(\frac{\partial f}{\partial t})_{collision}$: Gives the variation of the distribution function under the effect of collisions with neutrals, that is, the redistribution of particles (electrons or ions) under the effect of collisions.

III.3.2 Continuity equation

This equation is also called the charge conservation equation, it represents the first moment of the Boltzmann equation that describes the transport of particles (electrons, ions, and neutrals), their flux under the influence of the electric field and collisions [10]. It is written in the form:

For the electrons: $$\frac{\partial n_e}{\partial t}+\vec{\nabla}\cdot(\vec{\Gamma}_e)=S_e \quad \text{(III.8)}$$

For the ions: $$\frac{\partial n_i}{\partial t}+\vec{\nabla}\cdot(\vec{\Gamma}_i)=S_i \quad \text{(III.9)}$$

For the metastable: $$\frac{\partial n_*}{\partial t}+\vec{\nabla}\cdot(\vec{\Gamma}_*)=S_* \quad \text{(III.10)}$$

The indices e, i, and * denote electrons, positive ions, and excited atoms. n and Γ represent the density and flux of particles (e, i, and *), respectively. S denotes the source term for particles (e, i, and *) due to various reactions in which the species are created or lost.

Generally, the source term for electrons is written

$$S_e=n_e(\nu_i-\nu_a)+n_n\nu_{\det}-r_e n_e n_p \quad \text{(III.11)}$$

ν_i , ν_a , and $\nu_{\det}$, the average frequencies of ionization, attachment, and detachment, respectively. r_e represents the recombination coefficient and n_n the density of negative ions. However, when dealing with an electropositive gas, where the attachment process does not occur, equation (III.11) becomes:

$$S_e=n_e\nu_i-r_e n_e n_p \quad \text{(III.12)}$$

In the general case, the source term for a particle p is determined by the reactions that occur in the discharge. The latter is expressed as follows [55]:

$$S_p = \sum_r C_{p,r} R_r = \sum_r [C_{p,r} k_r \prod_j n_j] \quad \text{(III.13)}$$

Were

r: the index of a reaction of production or destruction of the particle p

$C_{p,r}$: is the number of particles of species p created in a reaction of type r, which can be positive or negative.

R_r: the reaction rate which is proportional to the densities of the particles involved in these reactions.

For two-body reactions:

$$R_r = k_r . n_{1r} . n_{2r} \quad \text{(III.14)}$$

For three-body reactions:

$$R_r = k_r . n_{1r} . n_{2r} . n_{3r} \quad \text{(III.15)}$$

With k_r is the reaction rate coefficient. The rate coefficients are evaluated from cross-section data available on the LXCAT database using the following integral expression.

$$k_k = \gamma \int_0^\infty \varepsilon \sigma_k(\varepsilon) f(\varepsilon) d\varepsilon \quad \text{(III.16)}$$

Where (f) the electron energy distribution function (EEDF) and (σ) collision cross section (m^2) with

$$\gamma = \sqrt{\frac{2q}{m_e}} \quad \text{(III.17)}$$

With q represents the electron charge (C), and (m_e) corresponds to the electron mass (Kg).

III.3.3 Transfer of momentum equation

The equation of momentum for all species is expressed by the drift-diffusion approximation[11].

$$\vec{\Gamma}_e = -n_e \mu_e \vec{E} - \vec{\nabla}(n_e D_e) \quad \text{(III.18)}$$

$$\vec{\Gamma}_p = -n_p \mu_p \vec{E} - \vec{\nabla}(n_p D_p) \quad \text{(III.19)}$$

For metastable, we only consider the diffusion term.

$$\vec{\Gamma}_* = -\vec{\nabla}(n_* D_*) \quad \text{(III.20)}$$

Where E is the electric field, μ_k and D_k denote the mobility and diffusion coefficient of the charged species. These two coefficients are related by the Einstein relation:

$$\frac{D_k}{\mu_k} = \frac{K_B T_k}{q} = \frac{2}{3}\frac{\xi_k}{q} \tag{III.21}$$

With ξ_k the average energy, given by the relation

$$\xi_k = \frac{3}{2} K_B T_e \tag{III.22}$$

III.3.4 Equation for energy

It represents the third moment of the Boltzmann equation. In this simulation, the energy balance is only resolved for the electrons[12]:

$$\frac{\partial n_\varepsilon}{\partial t} + \vec{\nabla}.(\vec{\Gamma}_\varepsilon) + \vec{E}.\vec{\Gamma}_e = S_\varepsilon \tag{III.23}$$

$$\vec{\Gamma}_\varepsilon = -n_e \mu_\varepsilon \vec{E} - \vec{\nabla}(n_\varepsilon D_\varepsilon) \tag{III.24}$$

$$n_\varepsilon = n_e \varepsilon \tag{III.25}$$

With

n_ε; the energy density $\vec{\Gamma}_\varepsilon$; the average energy flow, Te; the electron temperature,

S_ε; the source term. μ_ε and D_ε represent mobility and diffusion coefficient for flow of energy, respectively.

III.3.5 Poisson equation

The coupling of the Boltzmann equation with the Poisson equation is necessary for describe the discharge because this equation gives the variations of the electric field as a function of the space charge[13].

The Poisson equation is written:

$$\Delta V = \frac{q}{\varepsilon_0}(n_e - n_i) \tag{III.26}$$

Where:

$$\vec{E} = -\nabla V \tag{III.27}$$

Strong coupling exists in the system of partial differential equations III.26. Adequate boundary conditions are necessary for its resolution.

III.3.6 Boundary conditions

When the discharge is created, there is production of electrical charges (electrons and ions) in the inter-electrode space with the creation of an electric field. Electrons being the most energetic and fastest particles in the discharge[14], the conditions on their evolution at the boundaries of the discharge space are represented by:

- The flow of electrons toward the electrodes and the walls of the reactor, which is represented by the expression:

$$-n.\Gamma_e = \frac{1}{2}V_{e,th}n_e - \sum_p \gamma_p.(\Gamma_p.n) \tag{III.28}$$

$$V_{e,th} = \sqrt{\frac{8K_BT_e}{\pi.m_e}} \tag{III.29}$$

With γ_p the secondary emission coefficient of electrons by the electrodes, n is the unit vector normal to the wall, $V_{e,th}$ represents the thermal velocity of the electrons, K_B the Boltzmann constant, and m_e the mass of the electron.

- The energy flux of electrons toward the electrodes and the reactor walls is given by:

$$-n.\Gamma_\varepsilon = \frac{5}{6}V_{e,th}n_e\varepsilon - \sum_p \varepsilon_p\gamma_p.(\Gamma_p.n) \tag{III.30}$$

- Accumulation of surface charges:

$$-\nabla\varepsilon_0\varepsilon_r.\nabla V = \rho \tag{III.31}$$

ρ represents the charge density, which is the amount of electric charge per unit volume in a given space, ε_0 represent permittivity of free space and ε_r permittivity of material dielectric

$$\rho = q\left(\sum_{k=1}^{N} Z_k n_k - n_e\right) \tag{III.32}$$

with Z_k is the electric charge, q is the absolute value of electronic charge.

III.3.7 Electric potential

In a dielectric barrier discharge (DBD), the electric potential plays a fundamental role in initiating, sustaining, and controlling the discharge. A DBD typically consists of two electrodes

separated by a gas gap, with at least one electrode covered by a dielectric layer. When an alternating high voltage is applied, a time-dependent electric potential is established across both the dielectric barrier and the gas gap[15].

DBDs operate at relatively high voltages, typically in the range of several kilovolts to tens of kilovolts**,** depending on gas composition, pressure, gap distance, and dielectric properties.

The applied voltage $V_{app}(t)$ is shared between the gas gap and the dielectric barrier according to their capacitances:

$$V_{app}(t) = V_{gap}(t) + V_{diel}(t) \tag{III.33}$$

The driven electrode receives an electric potential

$$V_{app}(t) = V_0 \sin(2.\pi.f.t) \tag{III.34}$$

III.3.8 Equivalent electrical circuit model

In order to study the electrical characteristics (discharge current, gas voltage, I(V) characteristic, and Lissajous curve) of a DBD plasma discharge, obtained thru simulation, it is possible to use certain methods applicable to the electrical characteristics of experimental DBD discharges. Thus, the application of these methods stems from the consideration of the equivalent electrical circuit of the DBD plasma reactor illustrated in Figure III. 3, for a configuration with a single dielectric.

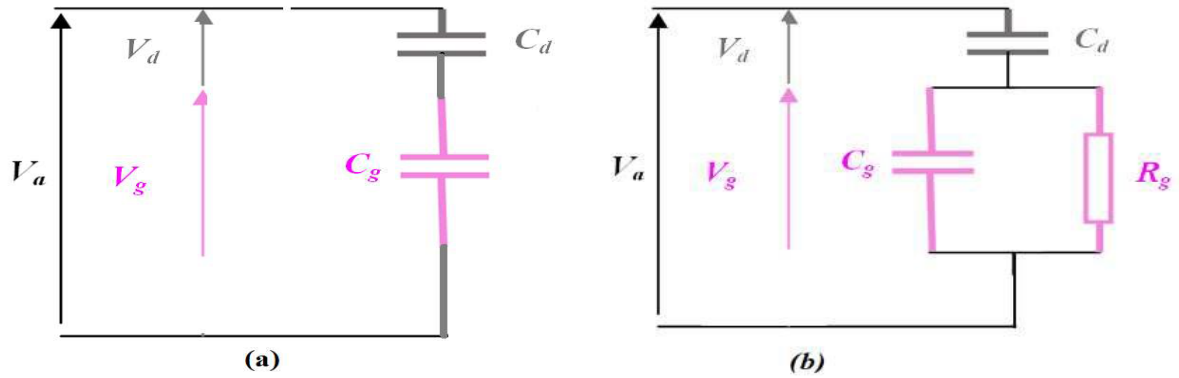

Figure III. 3: (a) Equivalent circuit of the DBD discharge without the presence of plasma, (b) Equivalent circuit of the DBD discharge with the presence of plasma.

Figure III. 3 (a) shows the equivalent diagram before the creation of the plasma discharge, with the aim of calculating the total capacitance of the DBD reactor, which is the sum of the two capacitors: that of the dielectric (Cd) and that of the gas (Cg).

$$C_d = \varepsilon_0 \varepsilon_{diel} \frac{S_{diel}}{d_{diel}} \quad \text{(III.35)}$$

$$C_g = \varepsilon_0 \varepsilon_{gaz} \frac{S_{electrode}}{d_{electrode}} \quad \text{(III.36)}$$

$$\frac{1}{C_{DBD}} = \frac{1}{C_d} + \frac{1}{C_g} \quad \text{(III.37)}$$

ε_{diel} and ε_{gaz} represent the relative permittivity of the dielectric and the gas, respectively. S_{diel} and S_{diel} represent the surface area, d_{diel} and $d_{electrode}$ denote the thickness of the dielectric and the inter-electrode distance, respectively.

III.3.9 Description of the particles present in plasma

A plasma is a partially or fully ionized gas composed of a variety of charged and neutral particles that interact through electromagnetic forces and collisions. The behavior and properties of a plasma are determined by the nature, density, and energy distribution of these particles[16,17].

a. Electrons

Electrons are the lightest and most mobile charged particles in a plasma. Due to their low mass, they respond rapidly to applied electric fields and are primarily responsible for energy transfer within the plasma. Electrons play a key role in excitation, ionization, dissociation, and attachment processes. In non-thermal plasmas, such as dielectric barrier discharges, electrons can reach high energies while the gas remains near ambient temperature.

b. Positive ions

Positive ions are formed through electron-impact ionization of neutral atoms or molecules. They are much heavier than electrons and therefore move more slowly. Positive ions contribute to charge neutrality, momentum transfer, and ion–surface interactions, particularly near electrodes and dielectric surfaces.

c. Negative ions

Negative ions are produced mainly by electron attachment processes, especially in electronegative gases such as oxygen or carbon dioxide. They influence plasma conductivity,

electric field distribution, and recombination processes. Negative ions are particularly important in atmospheric-pressure and non-thermal plasmas.

d. Neutral atoms and molecules

Neutral species constitute the majority of particles in most plasmas. Although electrically neutral, they play a central role in plasma chemistry through collisions with electrons and ions. Excited neutrals can store energy and participate in secondary reactions, while ground-state neutrals act as collision partners.

e. Excited species (metastables)

Excited atoms and molecules, including metastable states, possess higher internal energy and long lifetimes. These species significantly enhance plasma reactivity by enabling energy-efficient chemical pathways, such as stepwise ionization and dissociation.

f. Photons

Photons are emitted during radiative de-excitation of excited species. Although massless, photons contribute to plasma diagnostics and can induce photoionization or photodissociation processes, particularly in streamer and atmospheric-pressure discharges.

III.3.10 Characterization of reaction types for different species in plasma

Plasma is a reactive medium in which a wide variety of physical and chemical reactions occur due to interactions between electrons, ions, neutral species, excited states, and photons. These reactions govern plasma kinetics, energy transfer, and chemical conversion processes[18,19].

a. Elastic collisions

Elastic collisions occur when particles interact without a change in their internal energy states.

- Only momentum and kinetic energy are exchanged.
- Typically involve electron–neutral or ion–neutral collisions
- Do not lead to excitation or ionization
- Play an important role in electron energy redistribution and gas heating

b. Inelastic collisions

In inelastic collisions, part of the kinetic energy is converted into internal energy of the particles.

- **Excitation**

An electron collides with a neutral atom or molecule and raises it to an excited state:

$$e^- + A \rightarrow e^- + A^* \qquad \text{(III.38)}$$

Excited species can later emit photons or participate in further reactions.

- **Ionization**

Ionization occurs when an electron has sufficient energy to remove an electron from a neutral species:

$$e^- + A \rightarrow 2e^- + A^+ \quad \text{(III.39)}$$

This process increases plasma density and electrical conductivity.

- **Dissociation**

Molecular species can be broken into fragments by electron impact:

$$e^- + AB \rightarrow e^- + A + B \quad \text{(III.40)}$$

Dissociation is particularly important in molecular plasmas such as CO_2, O_2, and N_2.

c. Attachment reactions

In electronegative gases, free electrons may attach to neutral molecules to form negative ions:

$$e^- + A \rightarrow A^- \quad \text{(III.41)}$$

These reactions reduce electron density and influence plasma conductivity and stability.

d. Recombination reactions

Recombination processes involve the neutralization of charged particles.

- **Electron–ion recombination**:

$$e^- + A^+ \rightarrow A \quad \text{(III.42)}$$

- **Ion–ion recombination**:

$$A^+ + B^- \rightarrow A + B \quad \text{(III.43)}$$

Recombination reduces plasma density and releases energy, often in the form of heat or radiation.

e. Charge Exchange Reactions

Charge exchange occurs when an ion transfers its charge to a neutral species:

$$A^+ + B \rightarrow A + B^+ \quad \text{(III.44)}$$

These reactions affect ion composition and energy distribution, especially at atmospheric pressure.

f. Metastable-Induced Reactions

Excited or metastable species can initiate reactions without the need for high-energy electrons:

$$A^* + B \rightarrow C + D \quad \text{(III.45)}$$

Such reactions enhance plasma chemistry efficiency and are important in non-thermal plasmas.

g. Radiative Processes

Excited species may return to lower energy states by emitting photons:

$$A^* \rightarrow A + h\nu \tag{III.47}$$

Radiative processes are essential for plasma diagnostics and energy balance.

III.3.11 Ion mobilities

The standard formula for calculating ion mobility using polarizability is based on the Langevin polarization capture theory [20]

$$K = 13.88 \times \sqrt{\frac{1}{\alpha \times \mu}} \tag{III.48}$$

Where K ion mobility ($cm^2/V.s$) and α polarizability of neutral gas ($Å^3$) μ reduced mass of the ion-neutral pair (u)

$$\mu = \frac{M_{ion} \times M_{neutral}}{M_{ion} + M_{neutral}} \tag{III.49}$$

$$\frac{1}{\mu_{mix}} = \frac{\eta_1}{\mu_1} + \frac{\eta_2}{\mu_2} \tag{III.50}$$

η_1 and η_2 represent the molar fractions of gases 1 and 2, while μ_1 and μ_2 denote their respective ion mobilities.

III.4 Geometry of the model and simulation parameters

III.4.1 Geometry applied in the simulation

The geometry was developed using a one-dimensional approach following the framework described in Ref. [21], as shown in Figure III. 4 One-dimensional representations of the DBD reactor geometry, showing the powered and grounded electrodes, the discharge gap (1 mm), and two quartz dielectric layers with a thickness of 0.7 mm each. The dielectric barriers limit the discharge current and ensure non-thermal plasma operation by preventing the transition to an arc.

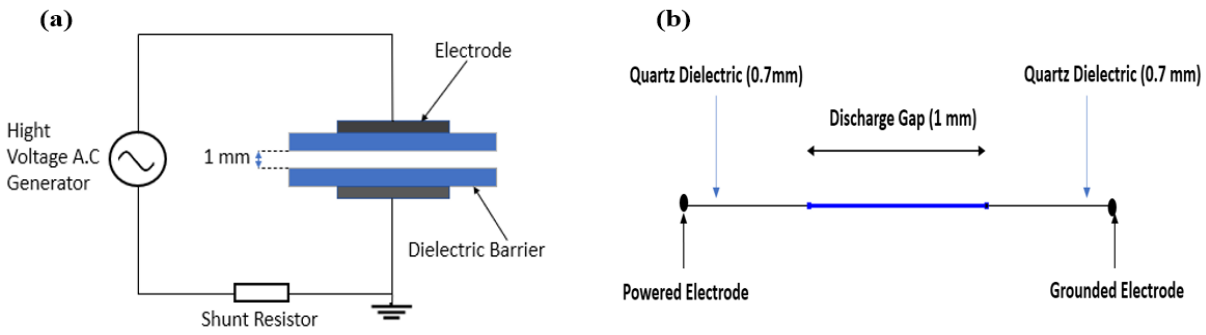

Figure III. 4: (a) Schematic of the DBD setup
(b) One-dimensional geometry applied in the simulation.

III.4.2 Methods of resolution and digital simulation software

The simulation of a physical model that contains several differential equations requires knowledge of the different resolution methods necessary to conduct a study. It involves discretizing the computational domain and making approximations to solve these partial differential equations.

III.4.2.1 The finite element method

The finite element method (FEM) is a numerical technique for solving complex partial differential equations (PDE) that arise in the modeling of plasma discharges, fluid dynamics, electromagnetics, and heat transfer. FEM is particularly suited to problems involving complex geometries, strongly coupled Multiphysics phenomena, and highly localized gradients conditions typically encountered in dielectric barrier discharge (DBD) plasmas at atmospheric pressure[22].

In plasma modeling, the governing equations (e.g., Poisson's equation, continuity equations, drift–diffusion equations, energy balance equations) are often nonlinear, coupled, and require fine spatial resolution in regions such as the sheath and ionization zones. FEM provides a stable and flexible framework for discretizing these equations and computing approximate solutions with controlled accuracy.

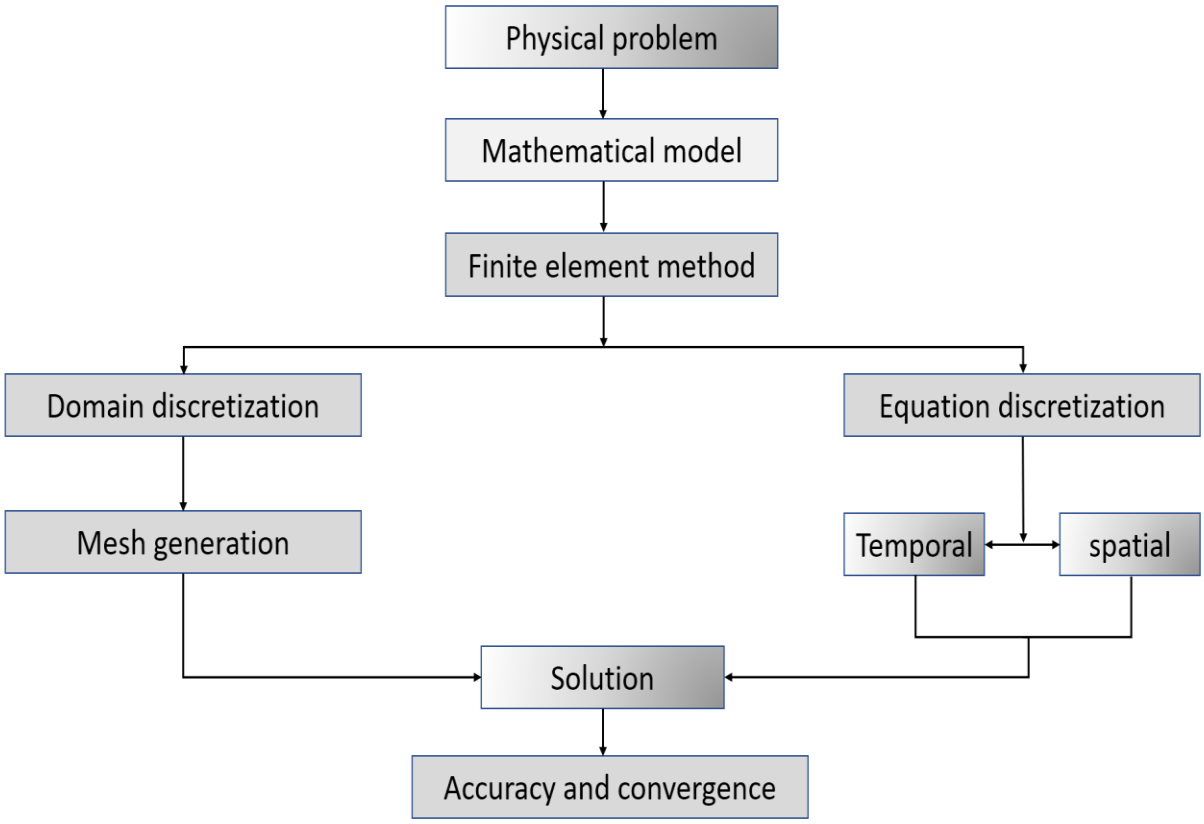

Figure III. 5: Schematic diagram of finite element method.

III.4.2.2 Diagram of numerical calculation by COMSOL multi-physics

The modeling procedure begins with the definition of the reactor geometry, which includes the inter-electrode gap, electrode configuration, and dielectric barrier dimensions. This step is followed by the specification of the physical, electrical, and material parameters, such as gas composition and properties, dielectric permittivity and thickness, applied voltage waveform, excitation frequency, and operating pressure. These parameters define the operating conditions of the dielectric barrier discharge and strongly influence the discharge dynamics.

Subsequently, the governing equations and associated boundary conditions are formulated using a fluid plasma description. This framework typically includes Poisson's equation for calculating the electric potential and electric field distribution, as well as continuity equations for electrons, ions, and neutral species to describe particle transport, generation, and loss mechanisms. Transport coefficients and reaction rate constants are introduced based on electron energy distribution functions and plasma chemistry models. Appropriate boundary conditions are imposed at electrodes and dielectric surfaces to account for charge accumulation, secondary electron emission, and particle fluxes.

After defining the physics of the problem, the computational domain is discretized through mesh generation, with particular attention given to regions exhibiting strong electric field gradients, such as near electrodes and dielectric interfaces. A time-dependent simulation is then carried out, often combined with a parametric sweep over selected operating parameters, to capture the transient and periodic behavior of the discharge over one or more voltage cycles.

Throughout the simulation process, numerical convergence is carefully monitored at each time step. If convergence is not achieved, adjustments are made to solver settings, time-step size, or mesh resolution. Once stable and convergent solutions are obtained, the validated model is employed for performance optimization, detailed data extraction, and systematic analysis of electrical and plasma characteristics. Finally, the numerical results are validated by comparison with theoretical predictions and available experimental data, ensuring the reliability and physical consistency of the modeling approach. [23].

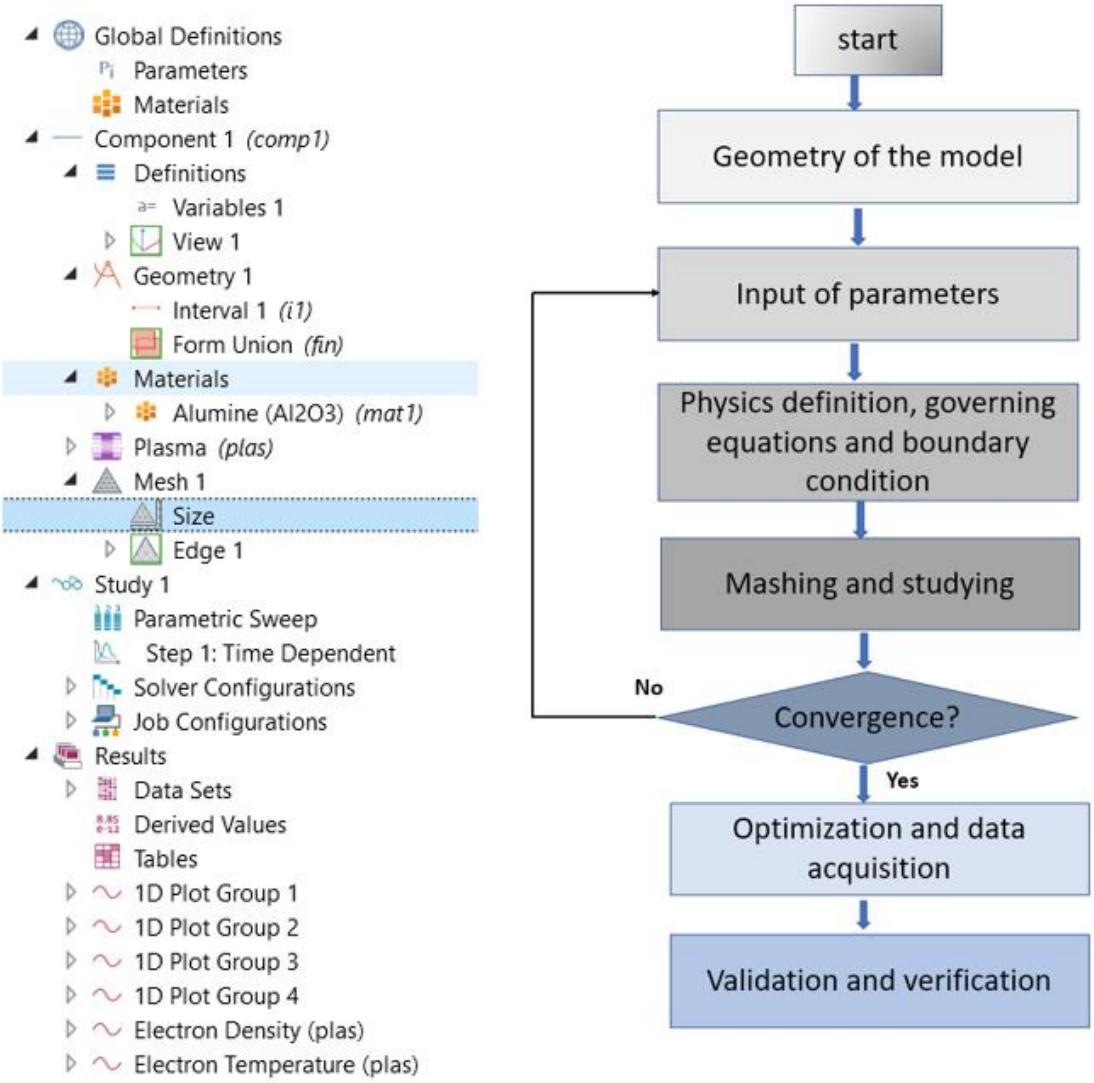

Figure III. 6: flowchart of calculation in COMSOL Multi-physics.

III.5 Conclusion

In this chapter, the fundamental elements required for modeling a dielectric barrier discharge (DBD) have been presented, including the plasma species involved during the discharge and the different types of collisions occurring between them. The mathematical formulation of an atmospheric pressure DBD controlled by dielectric barriers has then been introduced, together with the governing equations derived from this model. The procedure used to calculate the electrical characteristics of the discharge has also been described.

The proposed model is based on the solution of the Boltzmann equation. The governing equations are discretized using a widely adopted numerical approach, namely the finite difference method. This method was selected for its simplicity and effectiveness, as it relies on the discretization of the equations and the convergence of the resulting numerical scheme. Finally, the transport coefficients, as well as the initial and boundary conditions required for the simulations, are defined.

References

[1] Jayaraman, B., & Shyy, W. (2008). Modeling of dielectric barrier discharge-induced fluid dynamics and heat transfer. Progress in Aerospace Sciences, 44(3), 139-191.

[2] Szabo, J. J. (2001). Fully kinetic numerical modeling of a plasma thruster (Doctoral dissertation, Massachusetts Institute of Technology).

[3] Xu, S. Y., Cai, J. S., & Li, J. (2016). Modeling and simulation of plasma gas flow driven by a single nanosecond-pulsed dielectric barrier discharge. Physics of Plasmas, 23(10)..

[4] Carman, R. J., & Mildren, R. P. (2000). Electron energy distribution functions for modelling the plasmakinetics in dielectric barrier discharges. Journal of Physics D: Applied Physics, 33(19), L99 .

[5] Rao, M. V. V. S., Van Brunt, R. J., & Olthoff, J. K. (1999). Kinetic-energy distributions of positive and negative ions in Townsend discharges in oxygen. Physical Review E, 59(4), 4565.

[6] Li, M., Dew, S. K., & Brett, M. J. (1999). Effects of electron distribution functions on the floating potential of particles in the plasma: thin plasma sheaths. Journal of Physics D: Applied Physics, 32(16), 2056.

[7] Erden, E., & Rafatov, I. (2014). Particle in cell/Monte Carlo collision method for simulation of RF glow discharges: Effect of super particle weighting. Contributions to Plasma Physics, 54(7), 626-634.

[8] Warsi, Z. U. (2005). Fluid dynamics: theoretical and computational approaches. CRC press.

[9] Grad, H. (1963). Asymptotic theory of the Boltzmann equation. The physics of Fluids, 6(2), 147-181.

[10] Nedjar, Y. M. A., Mostefaoui, M., & Benyoucef, D. (2025). One-dimensional fluid modeling of methane dissociation in dielectric barrier discharge: Impact of voltage and dielectric constant. Plasma Physics and Technology, 12(1), 10-15.

[11] Benyoucef, D., & Yousfi, M. (2015). Particle modelling of magnetically confined oxygen plasma in low pressure radio frequency discharge. Physics of Plasmas, 22(1).

[12] Labdouni, N., Benyoucef, D., & Tebani, H. (2026). Cold Plasma Modeling for Air Pollution Control: NOx Removal in Dielectric Barrier Discharge Reactors. Bulletin of Chemical Reaction Engineering & Catalysis, 14.

[13] Lahouel, M. H. A., Benyoucef, D., & Tebani, H. (2019, February). Monte Carlo Simulation of Electron Transport Coefficients in Oxygen, Nitrogen, and Air. In International Conference on Plasma and Energy Materials ICPEM2019.

[14] LAHOUEL, M. H. A. (2021). Modélisation et simulation d'une décharge à barrière diélectriques dans un Mélange gazeux à la pression atmosphérique (Doctoral dissertation, Djilali BENYOUCEF/Hocine TEBANI).

[15] Chenoui.M. Tebani, H., & Benyoucef, D Zero-dimensional Modeling of Dielectric Barrier Discharge in Pure Carbon Dioxide, The 3rd edition of the international conference on materials science and engineering and their impact on the environment, Djilali Lyabes University of Sidi-Bel-Abbes, 29-30-May 2024.

[16] Dawson, J. M. (1983). Particle simulation of plasmas. Reviews of modern physics, 55(2), 403.

[17] Brown, L. S., Preston, D. L., & Singleton Jr, R. L. (2005). Charged particle motion in a highly ionized plasma. Physics Reports, 410(4), 237-333.

[18] Kee, R. J., Rupley, F. M., Meeks, E., & Miller, J. A. (1996). CHEMKIN-III: A FORTRAN chemical kinetics package for the analysis of gas-phase chemical and plasma kinetics (No. SAND-96-8216). Sandia National Lab.(SNL-CA), Livermore, CA (United States).

[19] Wende, K., von Woedtke, T., Weltmann, K. D., & Bekeschus, S. (2018). Chemistry and biochemistry of cold physical plasma derived reactive species in liquids. Biological Chemistry, 400(1), 19-38.

[20] Cortez, A. (2020). A Practical Approach to Ion Mobility. New Horizons in Time Projection Cambers, Santiago de Compostela (Spain).

[21] Bajon, C., Dap, S., Belinger, A., Guaitella, O., Hoder, T., & Naudé, N. (2023). Homogeneous dielectric barrier discharge in CO2. Plasma Sources Science and Technology, 32(4), 045012.

[22] Shiraiwa, S., Meneghini, O., Parker, R., Bonoli, P., Garrett, M., Kaufman, M. C., ... & Wukitch, S. (2010). Plasma wave simulation based on a versatile finite element method solver. Physics of Plasmas, 17(5).

[23] Abreha, B. G., Mahanta, P., & Trivedi, G. (2019, April). Numerical modeling and simulation of thermal energy storage for solar cooking using Comsol multiphysics software. In AIP Conference Proceedings (Vol. 2091, No. 1, p. 020004). AIP Publishing LLC.

Chapter IV

Modeling and Electrical Characterization of CO_2/Ar Dielectric Barrier Discharges

IV.1 Introduction

Numerical modeling plays a central role in the study and understanding of plasma discharges, particularly when experimental investigations are limited by technical, financial, or diagnostic constraints. Plasma systems often involve a complex interplay between charged and neutral species, electromagnetic fields, chemical reactions, and energy transport. Capturing these phenomena experimentally with high temporal and spatial resolution is challenging; therefore, computational models provide an essential complementary tool for investigating plasma behavior under controlled conditions.

The numerical modeling of a plasma discharge consists of formulating a set of mathematical equations that describe the evolution of the plasma's physical variables such as particle densities, electric fields, temperatures, and velocities within a defined domain. These equations are derived from fundamental conservation laws, kinetic theory, and electromagnetic field theory. Depending on the level of detail required, different modeling approaches can be adopted, ranging from kinetic models, such as solutions of the Boltzmann equation, to fluid models based on moment equations or drift diffusion approximations[1].

For dielectric barrier discharges (DBDs) at atmospheric pressure, fluid models are widely used due to their efficiency and ability to capture the essential physics of non-equilibrium plasmas. In such models, the first three moments of the Boltzmann equation are typically employed: particle continuity, momentum transport, and energy conservation. These moment equations are coupled with Poisson's equation, which determines the spatial distribution of the electric field generated by space charges. The resulting system of partial differential equations is solved numerically to predict key discharge characteristics, such as electron density, electric field profiles, current evolution, and power deposition[2].

Boundary conditions constitute an essential part of the modeling framework, as they define how the plasma interacts with its surrounding environment, including electrodes, dielectric surfaces, and open boundaries. Proper specification of boundary conditions ensures numerical stability and physical accuracy of the solution[3].

Overall, numerical modeling provides valuable insights into plasma ignition, propagation, mode transitions, and chemical conversion processes. It allows researchers to explore parameter regimes that are difficult to access experimentally, optimize reactor designs, and guide the

development of plasma-assisted technologies, including CO_2 conversion, pollutant removal, ozone generation, and surface treatment.

IV.2. Basic data of charged particles in carbon dioxide

IV.2.1 Plasma electrical properties

An analysis of Dielectric Barrier Discharge behavior in pure CO_2 under atmospheric conditions was conducted using the experimental configuration described in [4], enabling comparison and validation of the current simulation model. This examination focused on a 1D geometry consisting of two parallel plates and encompassed a broad spectrum of discharge parameters and operating environments pertinent to atmospheric pressure plasmas, as detailed in Table IV.1.

Table IV.1 Discharge parameters considered in this study

Parameters	**Value**
Maximum applied voltage	6,8,9 (Kv)
Frequency	2,3,4 (KHz)
Resistance	1 (kΩ)
Pressure	500, 760, 1000 (Torr)
Discharge gap	1 (mm)
Electrode area	9 (cm^3)
Preionization density	10^6 (m^3)
Thickness of dielectric	0.7 (mm)
Relative permittivity of dielectric	4.2 ,8.2 ,9.1 ,12
Molar mass CO_2 ,Ar respectively	0.04401, 0.04 (Kg/mol)
Polarizability CO_2 ,Ar respectively	2.91 ,1.64 ($Å^3$)
Gas temperature	300 (K)
Gas mixture content CO_2/Ar with Ar percentage	90, 75 ,50 ,25 ,10 (%)

IV.2.2 Cross section electron- carbon dioxide/Argon

The modeling of an electrical discharge in the gas mixture (CO_2/Ar) primarily requires knowledge of the electron-atom or molecule collision cross-section relative to the two constituents of the gas mixture.

Each inelastic process is associated with an effective cross-section. These inelastic processes are determined by the nature of the particles as well as that of the gas. This quantity is defined as the ratio of the number of incident particles that can undergo the reaction to the product of the number of target particles by the thickness of the plasma slice traversed. The effective cross-

section depends on the energy of the incident particles as well as the nature of the particles involved. It is possible to experimentally obtain these quantities. The range of error remains quite high, and it is often preferable to seek a quantity that allows us to have a macroscopic description of the reaction. These quantities are the reaction rates[5].

This figure shows the energy-dependent electron impact cross sections for various collision processes between electrons and CO_2 molecules, taken from the Phelps database. The cross sections are plotted as a function of electron energy over a wide range, from few eV to several keV, on a logarithmic scale.

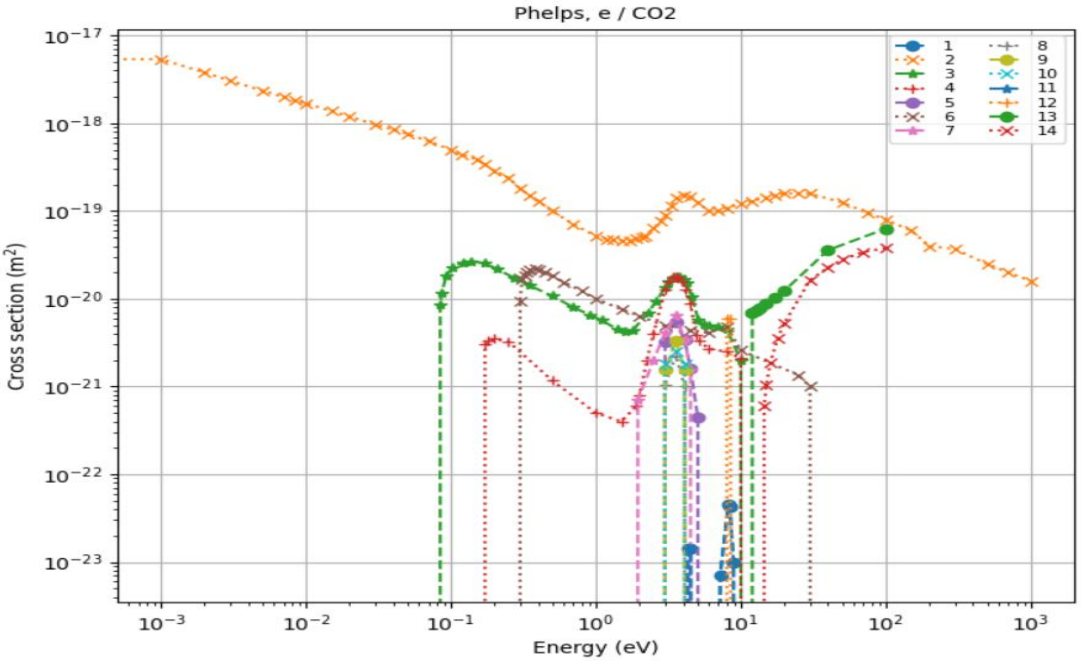

Figure IV.1: Cross sections for electrons interacting with CO_2 [Phelps, 2014].

At low electron energies (below a few eV), vibrational excitation processes dominate, characterized by relatively high cross sections. These reactions play a crucial role in non-thermal plasmas, as they allow efficient energy transfer from electrons to molecular vibrational modes without significant gas heating. As the electron energy increases, electronic excitation and dissociation processes become more significant, with cross sections peaking in the intermediate energy range.

At higher energies (typically above 10–15 eV), ionization processes appear and their cross sections increase, contributing to the generation of charged species and sustaining the plasma discharge. The coexistence of multiple reaction channels highlights the strong dependence of plasma chemistry on the electron energy distribution function (EEDF)[6].

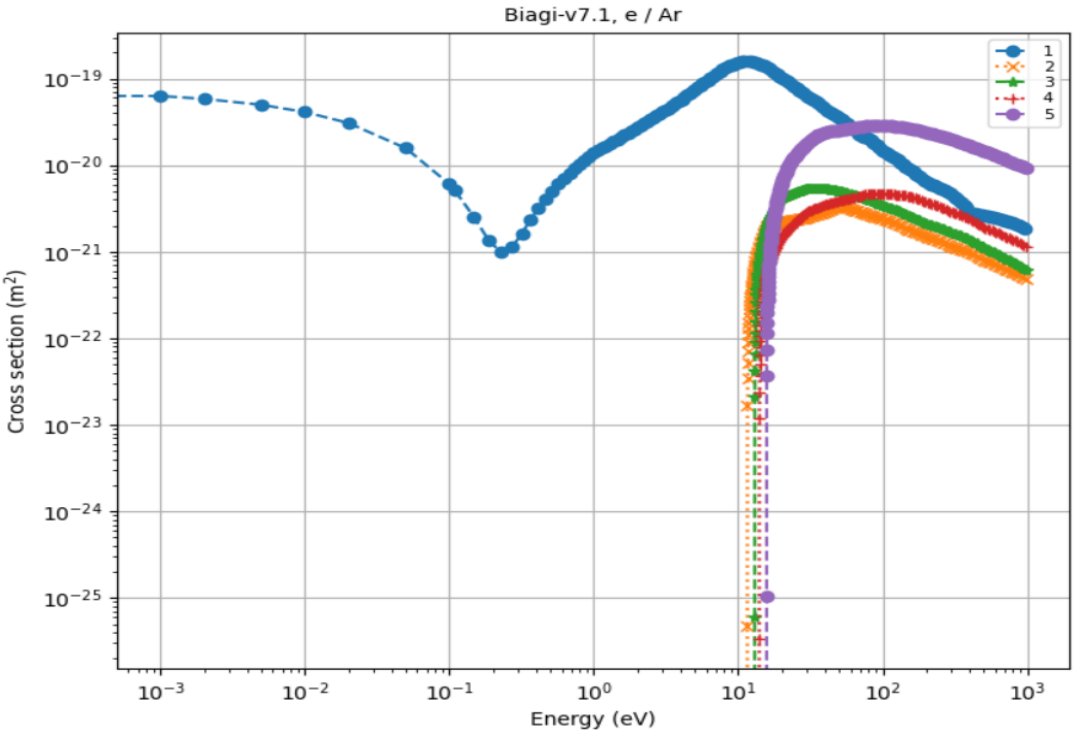

Figure IV.2: Cross sections for electrons interacting with Ar [Biagi].

This figure presents the energy-dependent electron impact cross sections for various collision processes between electrons and argon atoms, extracted from the Biagi v7.1 database. The cross sections are plotted versus electron energy on a logarithmic scale, covering the range from sub-eV energies to several keV.

At low electron energies (below 1 eV), elastic collisions dominate, with relatively high cross sections that strongly influence electron momentum transfer and transport properties. In the intermediate energy range, excitation processes become significant, corresponding to the

excitation of argon electronic states. These processes contribute to energy loss mechanisms and play an important role in sustaining non-thermal plasmas.

At higher electron energies (typically above 10–15 eV), ionization cross sections increase sharply, leading to the production of argon ions and secondary electrons. This process is essential for plasma maintenance and the development of electron avalanches in gas discharges.

IV.2.3 Validation of electron-neutral cross sections by transport parameters

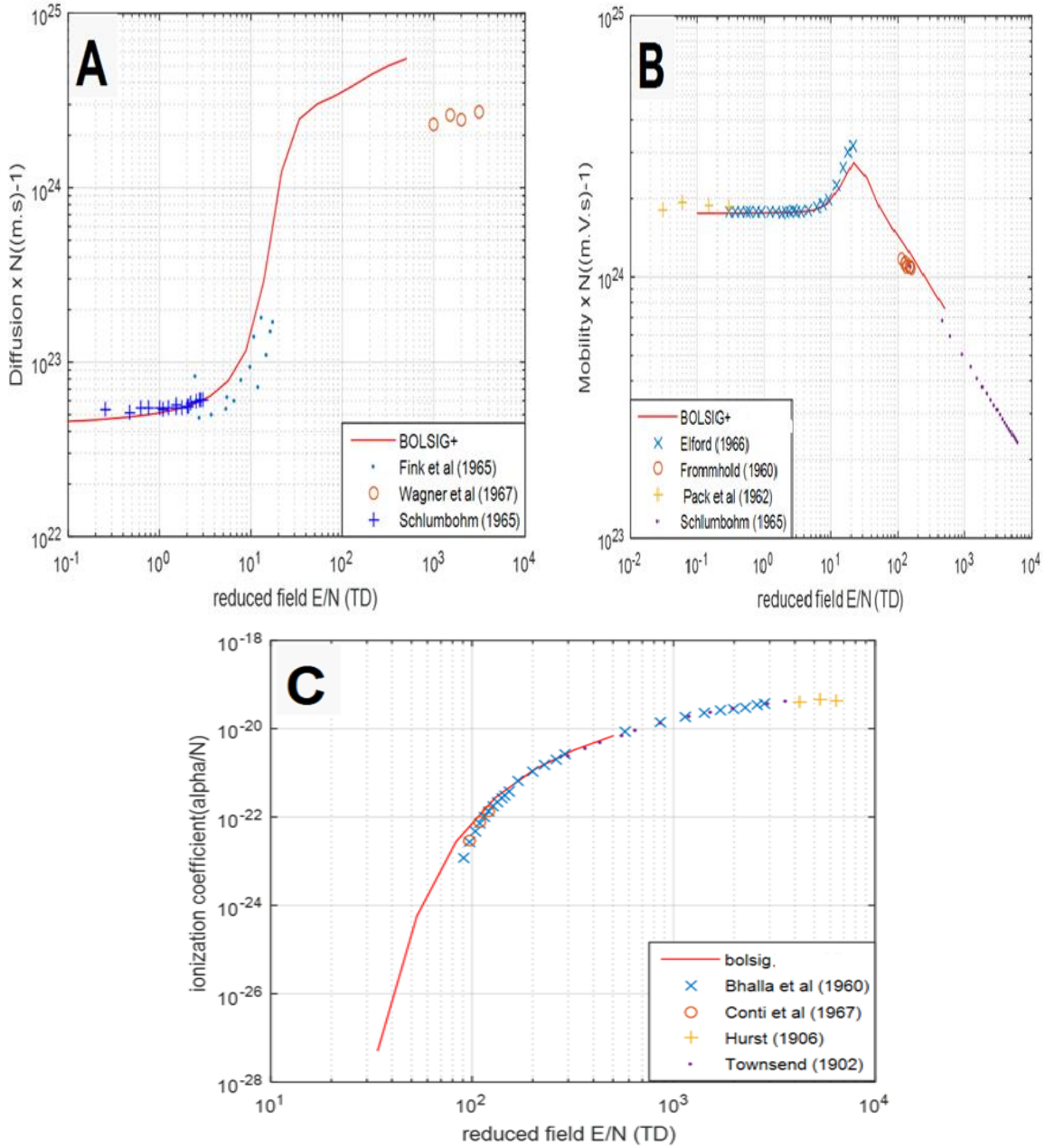

Figure IV.3: Comparison between the calculated and the measured transport coefficients of the electrons in CO_2 (A: Mobility, B: Diffusion, C: ionization coefficient)

Figure IV.3 illustrates the impact of the reduced electric field (E/N) on electron transport and reaction coefficients, using data from the BOLSIG+ Boltzmann solver alongside experimental literature.

(A) The electron diffusion coefficient (D×N) shows a strong increase with E/N, confirming enhanced electron energy transfer, with predictions aligning well with experimental results in lower fields;

(B) Electron mobility (μ×N) reveals a non-monotonic trend, peaking at intermediate E/N values due to shifts in collision mechanisms and electron energy distribution;

(C) The normalized ionization coefficient (α/N) rises sharply with E/N, indicating the growth of electron-impact ionization, The numerical results are consistent with experimental datasets reported in the literature.

Overall, the figure underscores the significant influence of the reduced electric field on electron transport properties, critical for accurately modeling dielectric barrier discharges and predicting plasma behavior.

IV.3 plasma chemistry

The plasma chemistry incorporated in the model, which includes a comprehensive array of 108 reactions involving 19 species as outlined in Table IV.2, addresses the principal electron–molecule, ion–molecule, and neutral–neutral interactions that regulate CO_2 conversion in dielectric barrier discharges. Specifically, electron impact reactions, including ionization, excitation, and dissociation of CO_2 and Ar, are detailed in Table IV.3, as they represent the principal mechanism for producing reactive species[7].

Table IV.2: Species in CO_2/Ar model

Neutral	Negative ions	Positive ions	Exited species
C, O, CO_2, O_2, O_3, CO, C_2O	e^-, O^-, O_2^-, O_3^-, CO_3^-, CO_4^-	CO_2^+, O^+, O_2^+, Ar^+, Ar_2^+	Ars

Table IV.3: Reactions explored in the model and their rate coefficients in (m^6/s) and (m^3/s) for three-body and tow-body respectively, CO_2(X,v=1-16) refers to the first 16 vibrationally excited states of CO_2.

N°	Reaction	Reaction rate	References
Elastic and Ionization electron impact reactions			
X1	$e^- + CO_2 \rightarrow CO + O^-$	Cross section	[8]
X2	$e^- + CO_2 \rightarrow e^- + CO_2$(X,v=1-16)	Cross section	[8]
X3	$e^- + CO_2 \rightarrow 2e^- + CO_2^+$	Cross section	[8]
X4	$e^- + CO_2 \rightarrow e^- + CO + O$	Cross section	[8]
X5	$e^- + CO \rightarrow e^- + CO$	Cross section	[8]
X6	$e^- + O_3 \rightarrow e^- + O_3$	Cross section	[8]
X7	$e^- + O_2 \rightarrow e^- + O_2$	Cross section	[8]
X8	$e^- + O \rightarrow e^- + O$	Cross section	[8]
X9	$e^- + Ar \rightarrow Ar + e^-$	Cross section	[8]
X10	$e^- + Ar \rightarrow Ars + e^-$	Cross section	[8]
X11	$e^- + Ar \rightarrow Ar^+ + 2e^-$	Cross section	[8]
X12	$e^- + Ars \rightarrow Ar^+ + 2e^-$	Cross section	[8]

X13	$e^- + Ars \rightarrow Ar + e^-$	Cross section	[8]
Electron–Atom or Molecule interactions			
E1	$e^- + Ar + Ar^+ \rightarrow Ar + Ar$	1.0×10^{-36}	[8,10]
E2	$e^- + CO_2^+ \rightarrow CO + O$	$2.0\times10^{-11}/(\sqrt{Te}\times T_g)$	[8,9]
E3	$e^- + CO_2^+ \rightarrow C + O_2$	$3.94\times10^{-13}\times T_e^{-0.4}$	[9]
E4	$e^- + O_2 \rightarrow 2e^- + O_2^+$	1.8×10^{-17}	[10]
Ion-Ion and Ion-Neutral reactions			
I1	$Ars + Ar \rightarrow Ar + Ar$	3.0×10^{-21}	[9]
I2	$Ars + Ars \rightarrow e^- + Ar^+ + Ar$	$1.625\times10^{-16}/\sqrt{T_g}$	[9]
I3	$2Ar + Ar^+ \rightarrow Ar_2^+ + Ar$	2.5×10^{-43}	[10]
I4	$Ar_2^+ + Ar \rightarrow Ar^+ + 2Ar$	2.496×10^{-36}	[10]
I5	$Ar^+ + CO_2 \rightarrow Ar + CO_2^+$	7.6×10^{-16}	[9]
I6	$Ar + CO_2 \rightarrow CO + O + Ar$	$1.27\times10^{-44}/(T_g/300)\times\exp(-170/T_g)$	[9,10]
I7	$O_2^- + Ar \rightarrow e^- + O_2 + Ar$	$2.7\times10^{-16}\sqrt{(T_g/300)}\times\exp(-5590/T_g)$	[9]
I8	$O_2^- + O_2^+ \rightarrow O + O + O_2$	4.2×10^{-13}	[8,10]
I9	$O_2^- + CO_2^+ \rightarrow CO + O_2 + O$	6.0×10^{-13}	[10]
I10	$O^- + CO \rightarrow CO_2 + e$	5.5×10^{-16}	[9]
I11	$O^- + O_2 \rightarrow O_3 + e$	1.0×10^{-18}	[9]
I12	$O^- + O_3 \rightarrow O_2 + O_2 + e$	3.0×10^{-16}	[9]
I13	$O^- + CO_2 + CO_2 \rightarrow CO_3^- + CO_2$	9.0×10^{-35}	[9,10]
I14	$Ar^+ + CO \rightarrow CO^+ + Ar$	9.0×10^{-17}	[11]
I15	$Ar^+ + O \rightarrow O^+ + Ar$	0.64×10^{-17}	[11]
I16	$Ar^+ + O_2 \rightarrow O_2^+ + Ar$	4.6×10^{-17}	[11]
I17	$Ar_2^+ + CO_2 \rightarrow CO_2^+ + 2Ar$	1.1×10^{-15}	[11]
I18	$Ar_2^+ + CO \rightarrow CO^+ + 2Ar$	8.5×10^{-16}	[11]
I19	$Ar_2^+ + O_2 \rightarrow O_2^+ + 2Ar$	1.2×10^{-16}	[11]
I20	$O_2^- + O_2^+ \rightarrow O_2 + O_2$	2.0×10^{-13}	[8,10]
I21	$O_2^- + O_3 \rightarrow O_2 + O_3^-$	4.0×10^{-16}	[8,10]
I22	$O^+ + CO_2 \rightarrow O_2^+ + CO$	9.4×10^{-16}	[8,10]
I23	$O^+ + CO_2 \rightarrow CO_2^+ + O$	4.5×10^{-16}	[8,10]
I24	$CO_2^+ + O \rightarrow O^+ + CO_2$	9.62×10^{-17}	[8,10]
I25	$CO_2^+ + O_2 \rightarrow O_2^+ + CO_2$	5.3×10^{-17}	[8,10]
I26	$O_3^- + O \rightarrow O_2 + O_2^-$	1.0×10^{-16}	[8,10]
I27	$O_2^+ + CO_3^- \rightarrow CO_2 + O_2 + O$	3.0×10^{-13}	[8,10]
I28	$CO_3^- + O \rightarrow CO_2 + O_2^-$	8.0×10^{-17}	[8,10]
I29	$CO_3^- + CO_2^+ \rightarrow CO_2 + CO_2 + O$	5.0×10^{-13}	[8,10]
I30	$CO_4^- + O \rightarrow CO_3^- + O_2$	1.1×10^{-16}	[8,10]
I31	$O^- + O_2^+ \rightarrow O + O + O$	2.6×10^{-14}	[8,10]
I32	$CO_4^- + O \rightarrow CO_2 + O_2 + O^-$	1.4×10^{-17}	[8,10]
I33	$CO_4^- + CO_2^+ \rightarrow 2CO_2 + 2O_2$	5.0×10^{-13}	[8,10]
I34	$O_2^+ + CO_4^- \rightarrow CO_2 + O_2 + O_2$	3.0×10^{-13}	[8,10]
I35	$O^- + O_3 \rightarrow O + O_3^-$	5.3×10^{-16}	[8,10]
I36	$O_2^- + CO_2 + CO_2 \rightarrow CO_4^- + CO_2$	1.0×10^{-35}	[8,10]
I37	$O_2^- + O^+ + CO_2 \rightarrow O_3 + CO_2$	2.0×10^{-37}	[8,10]
I38	$O^- + O^+ \rightarrow O + O$	4.0×10^{-14}	[8,10]
I39	$O^+ + CO_2 \rightarrow O_2^+ + CO$	9.4×10^{-16}	[8,10]
I40	$O^+ + CO_2 \rightarrow CO_2^+ + O$	4.5×10^{-16}	[8,10]
I50	$CO_4^- + O_3 \rightarrow CO_2 + O_3^- + O_2$	1.0×10^{-16}	[8,10]
I51	$O_2^- + CO_2 \rightarrow O_2 + CO_2 + e$	$2.7\times10^{-16}\sqrt{(T_g/300)}\times\exp(-5590/T_g)$	[9]
I52	$CO_4^- + O \rightarrow CO_2 + O_3^-$	1.4×10^{-16}	[8,10]

I53	$O_3^- + O \rightarrow O_3 + O^-$	1.0×10^{-19}	[8,10]
Neutral-Neutral reactions			
N1	$CO_2 + CO_2 \rightarrow CO + O + CO_2$	$3.91\times10^{-16}\ \exp(-49430/T_g)$	[10]
N2	$CO_2 + O_2 \rightarrow CO + O + O_2$	$1.81\times10^{-16}\ \exp(-49000/T_g)$	[10]
N3	$CO_2 + C \rightarrow CO + CO$	1.0×10^{-21}	[9]
N4	$CO_2 + O \rightarrow CO + O_2$	$2.8\times10^{-17}\ \exp(-26500/T_g)$	[12]
N5	$CO + O + CO_2 \rightarrow CO_2 + CO_2$	$16.4\times10^{-46}\ \exp(-1510/T_g)$	[12]
N6	$CO + O + CO \rightarrow CO_2 + CO$	$8.2\times10^{-46}\ \exp(-1510/T_g)$	[12]
N7	$CO + O + O_2 \rightarrow CO_2 + O_2$	$8.2\times10^{-46}\ \exp(-1510/T_g)$	[12]
N8	$CO + O_2 \rightarrow CO_2 + O$	$4.2\times10^{-18}\ \exp(-24000/T_g)$	[12]
N9	$O + O_2 + O_2 \rightarrow O_3 + O_2$	5.85×10^{-46}	[9]
N10	$O + O_2 + CO_2 \rightarrow O_3 + CO_2$	1.81×10^{-45}	[9]
N11	$O + O + CO_2 \rightarrow O_2 + CO_2$	1.04×10^{-44}	[9]
N12	$CO + Ar \rightarrow C + O + Ar$	$1.52\times10^{-10}(T_g/298)^{-3.1}\exp(-129000/T_g)$	[10]
N13	$CO_2 + Ar \rightarrow CO + O + Ar$	$1.27\times10^{-44}(T_g/300)^{-1}\ \exp(-170/T_g)$	[10]
N14	$O + O + Ar \rightarrow O_2 + Ar$	$4.39\times10^{-13}\exp(65000/T_g)$	[10]
N15	$O_2 + O + Ar \rightarrow O_3 + Ar$	$3.6\times10^{-46}(T_g/300)^{-1.93}$	[9]
N16	$O_2 + C_2O \rightarrow CO_2 + CO$	3.3×10^{-19}	[8]
N17	$O + C + Ar \rightarrow CO + Ar$	$2.14\times10^{-41}(T_g/300)^{-3.08}\ \exp(-2114/T_g)$	[9]
N18	$CO_2 + CO \rightarrow CO + O + CO$	$1.81\times10^{-16}\ \exp(-49000/T_g)$	[9]
N19	$O_3 + O \rightarrow O_2 + O_2$	8.5×10^{-21}	[9]
N20	$CO + O_3 \rightarrow CO_2 + O_2$	4.0×10^{-31}	[9]
N21	$O + O_3 \rightarrow O_2 + O_2$	8.5×10^{-21}	[9]
N22	$CO_2 + C + CO \rightarrow C_2O + CO_2$	6.3×10^{-44}	[13]
N23	$O + C_2O \rightarrow CO + CO$	5×10^{-17}	13]

IV.3.1 Surface reactions

Surface reactions at the wall strongly couple plasma kinetics with material properties. In dielectric barrier discharges, they govern charge neutralization, surface charging, and plasma–wall energy exchange, making them a critical component of both experimental analysis and numerical modeling.

Table IV.4: Surface reactions

N	Reaction
R1	$CO_2^+ \rightarrow CO_2$
R2	$CO^+ \rightarrow CO$
R3	$O^+ \rightarrow O$
R4	$O^- \rightarrow O$
R5	$O_2^+ \rightarrow O_2$
R6	$O_2^- \rightarrow O_2$
R7	$O_3^- \rightarrow O_2 + O$
R8	$Ar_2^+ \rightarrow Ar + Ar$
R9	$Ar^+ \rightarrow Ar$
R10	$Ars \rightarrow Ar$

IV.4 Simulation results

The spatiotemporal characteristics of DBD in pure CO_2 have been numerically studied. The simulation is carried for atmospheric pressure, external voltage amplitude of 6 kV, frequency of 2 kHz and a gas temperature equal to 300 °K.

IV.4.1 Current and voltage characteristics

Figure IV.4 presents the total current of the dielectric barrier discharge operating in pure carbon dioxide and illustrates the strong correlation between the applied voltage, the gas voltage, and the discharge current. The applied sinusoidal voltage governs the plasma dynamics, whereas the gas voltage exhibits a noticeable phase shift due to the presence of the dielectric barrier, confirming the capacitive nature of the discharge. The figure shows the simulated current during the second AC cycle. Electrical breakdown occurs on the rising negative half-cycle, leading to a sharp current pulse with a maximum at 0.55 ms. The simulated peak current reaches approximately 2.5 mA and shows good agreement with the experimentally measured current.

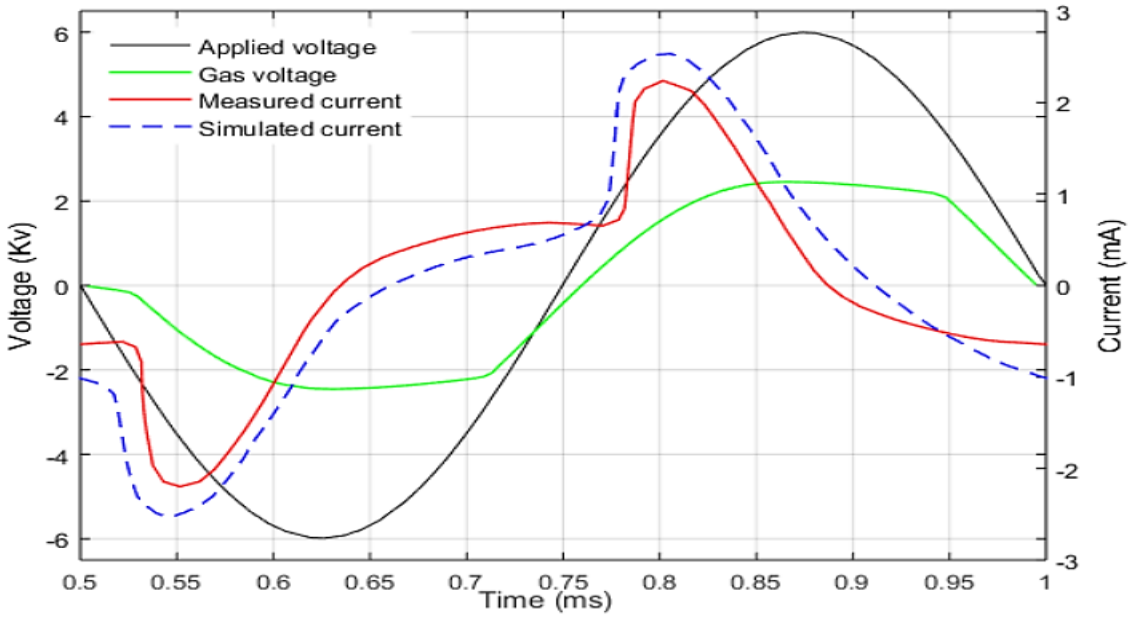

Figure IV. 4:Evolution during a single cycle of the applied and gas voltages, along with the simulated and measured discharge currents in pure CO_2 DBD.

Figure IV. 5 illustrates the time evolution of the power density. The maximum power deposition reaches approximately 4 $W \cdot cm^{-3}$, after which it rapidly decreases to nearly zero before the onset of the next cycle. This temporal behavior is typical of capacitive non-thermal discharges [39], in which energy is accumulated in the dielectric barrier and then abruptly transferred to the plasma during the breakdown phase. The observed asymmetry in peak intensity, with the first peak being slightly higher than the subsequent ones, indicates a stronger initial charging of the dielectric surface. As the discharge progresses, the accumulation of surface charges alters the local electric

field, resulting in a slight reduction of the breakdown intensity in later cycles while preserving the periodic nature of the discharge.

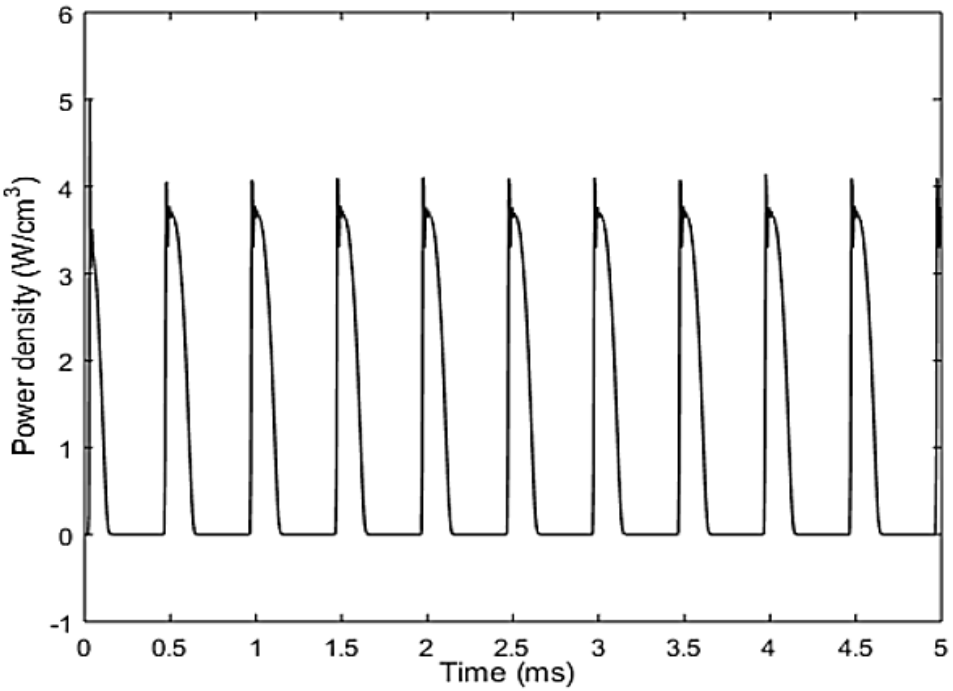

Figure IV.5: Time evolution of the power density.

IV.4.2 Temporal variation of plasma species densities

A comparison analysis was conducted to evaluate the impact of argon dilution on discharge dynamics in a gas combination of 90% CO_2 and 10% Ar, under the same operating conditions as pure CO_2.

Figure IV. 6 shows the time evolution of the number densities of neutral species over 100 discharge periods. The results reveal a rapid production of CO and O_2, which quickly reach steady-state concentrations on the order of 10^{20} m^{-3}, confirming their roles as the main products of CO_2 dissociation. Atomic oxygen (O) and ozone (O_3) appear at intermediate concentration levels, with O_3 displaying a gradual increase and a transient fluctuation around 0.03 s, which can be attributed to recombination processes. In contrast, minor species such as atomic carbon (C) and carbon suboxide (C_2O) remain at significantly lower concentrations throughout the discharge.

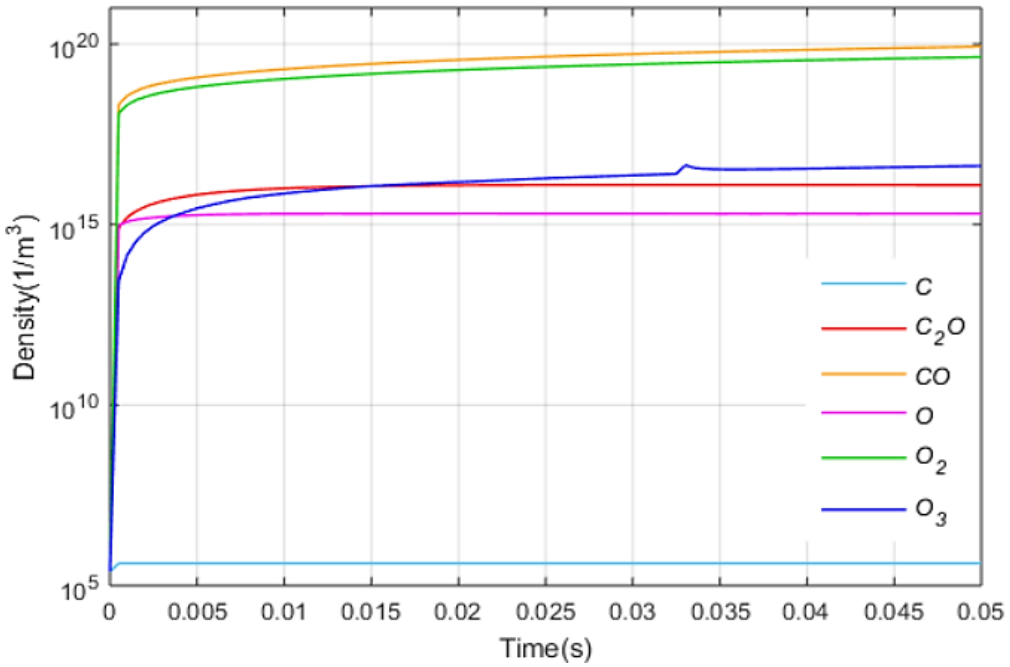

Figure IV.6: Time evolutions of neutral species.

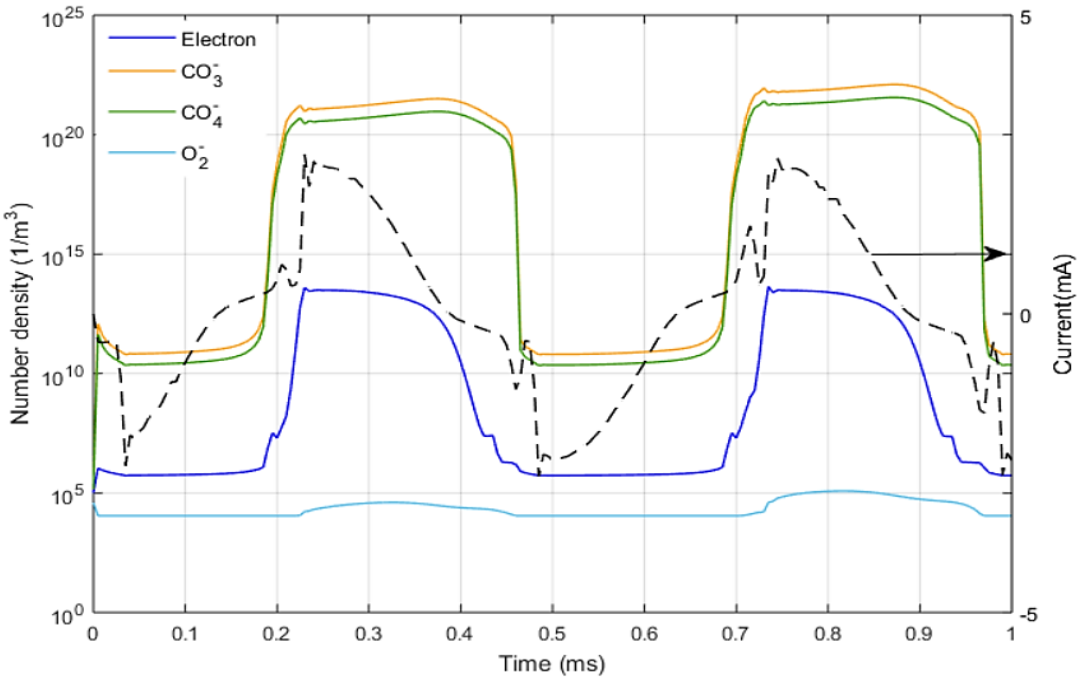

Figure IV. 7: Time evolutions of CO_2-derived negative ions.

Figure IV. 7 illustrates the transient evolution of selected charged species together with the discharge current over one complete AC cycle during the operation of a CO_2 dielectric barrier discharge. The numerical results show that the densities of the negative ions CO_3^- and CO_4^- increase rapidly during the discharge pulses, reaching peak values of approximately 10^{20} m^{-3}. The electron density exhibits a similar temporal behavior, although at lower levels, on the order of 10^{15} m^{-3}, reflecting the combined effects of ionization and electron attachment during breakdown

events. In contrast, the density of O_2^- remains relatively low and nearly constant, indicating a limited role of oxygen-based negative ion chemistry under the investigated conditions. The discharge current, shown by the black curve on the right axis, displays two pronounced peaks per cycle, corresponding to the breakdown events occurring during both the positive and negative half-cycles of the applied voltage. The close temporal correlation between the current maxima and the increases in charged species densities underscores the strong coupling between plasma kinetics and the electrical response of the DBD reactor.

Figure IV. 8 illustrates the concentrations of positively charged ions formed from CO_2. CO_2^+ is the predominant ion, reaching concentrations of 10^{16}–10^{17} m^{-3}, mostly generated through electron impact ionization and Penning events. In contrast, O_2^+ is produced at 10^{13} m^{-3} via dissociation and recombination processes, while CO^+ is a minor species.

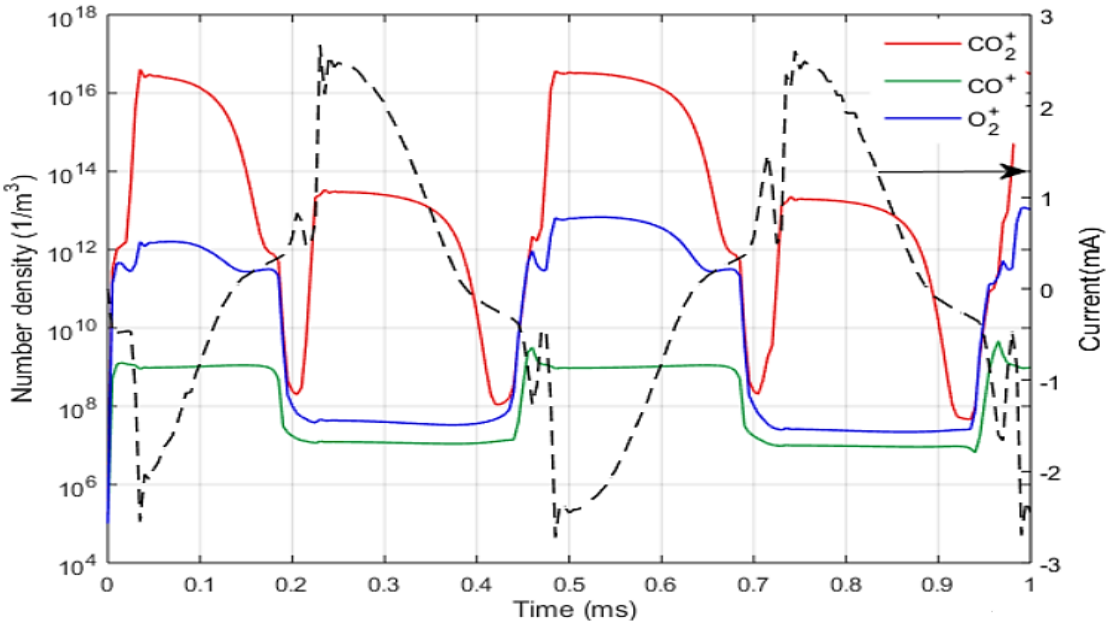

Figure IV.8: Time evolutions of CO_2-derived positive ions.

Figure IV. 9 illustrates the progression of argon species, with a significant concentration of metastable Ar at 10^{15} m^{-3} rapidly forming at each ignition peak and gradually decaying between discharges, which is crucial for maintaining the plasma via Penning ionization of CO_2. Ar^+ ions are ephemeral and are swiftly transformed into Ar_2^+ dimer ions, which emerge as the major argon cation with concentrations approaching 10^{12} m^{-3}.

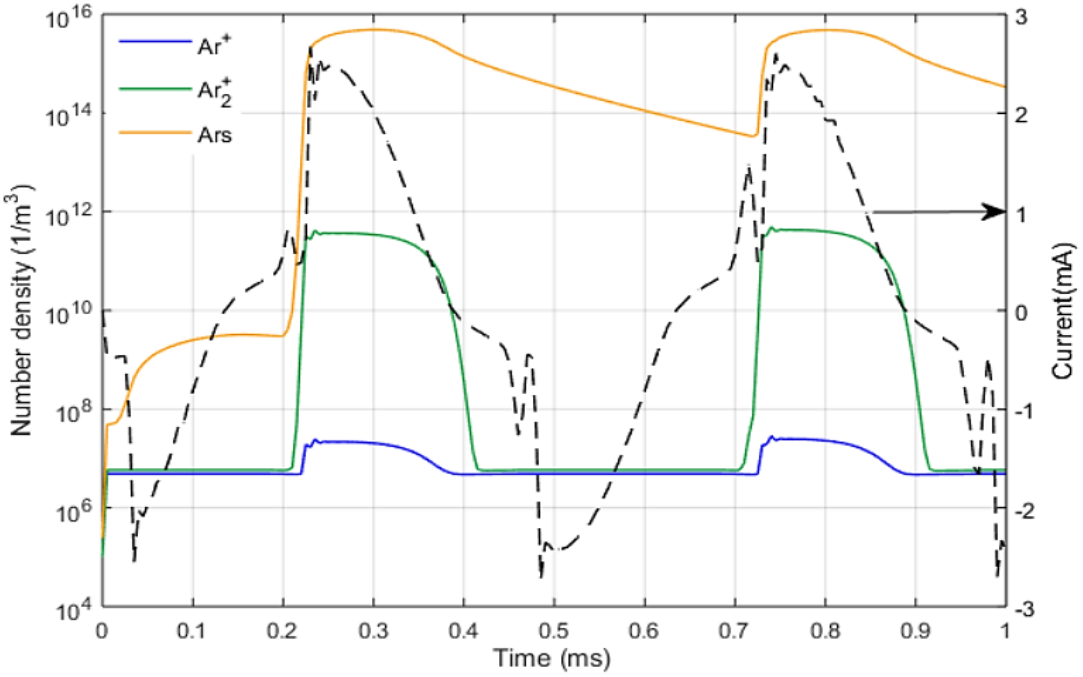

Figure IV. 9: Time evolutions of Ar excited species and positive ions.

IV.5 Analysis of operating parameters

A comprehensive parametric investigation was conducted to evaluate the influence of critical operating parameters on the behavior of the dielectric barrier discharge in a CO_2/Ar mixture at atmospheric pressure. The operating settings, such as applied voltage, excitation frequency, gas pressure, and gas composition, were systematically altered to evaluate their effects on electrical properties and species densities.

IV.5.1 Influence of Ar dilution

In this study, the discharge operating conditions were fixed at an applied voltage of 6 kV, an excitation frequency of 2 kHz, and a gas pressure of 760 Torr, while the argon concentration in the CO_2/Ar mixture was systematically varied from 10% to 90%. The effect of argon admixture on the electrical and plasma characteristics of the CO_2 dielectric barrier discharge is illustrated in Figure IV.10(a). As the argon fraction increases, a pronounced modification of the discharge behavior is observed. In particular, the current waveforms exhibit significantly higher amplitudes in argon-rich mixtures, indicating an intensification of microdischarge activity and enhanced plasma conductivity. This behavior can be primarily attributed to the lower ionization threshold of argon compared to CO_2, as well as its favorable electron collision cross sections, which promote the development of efficient electron avalanches and facilitate discharge ignition.

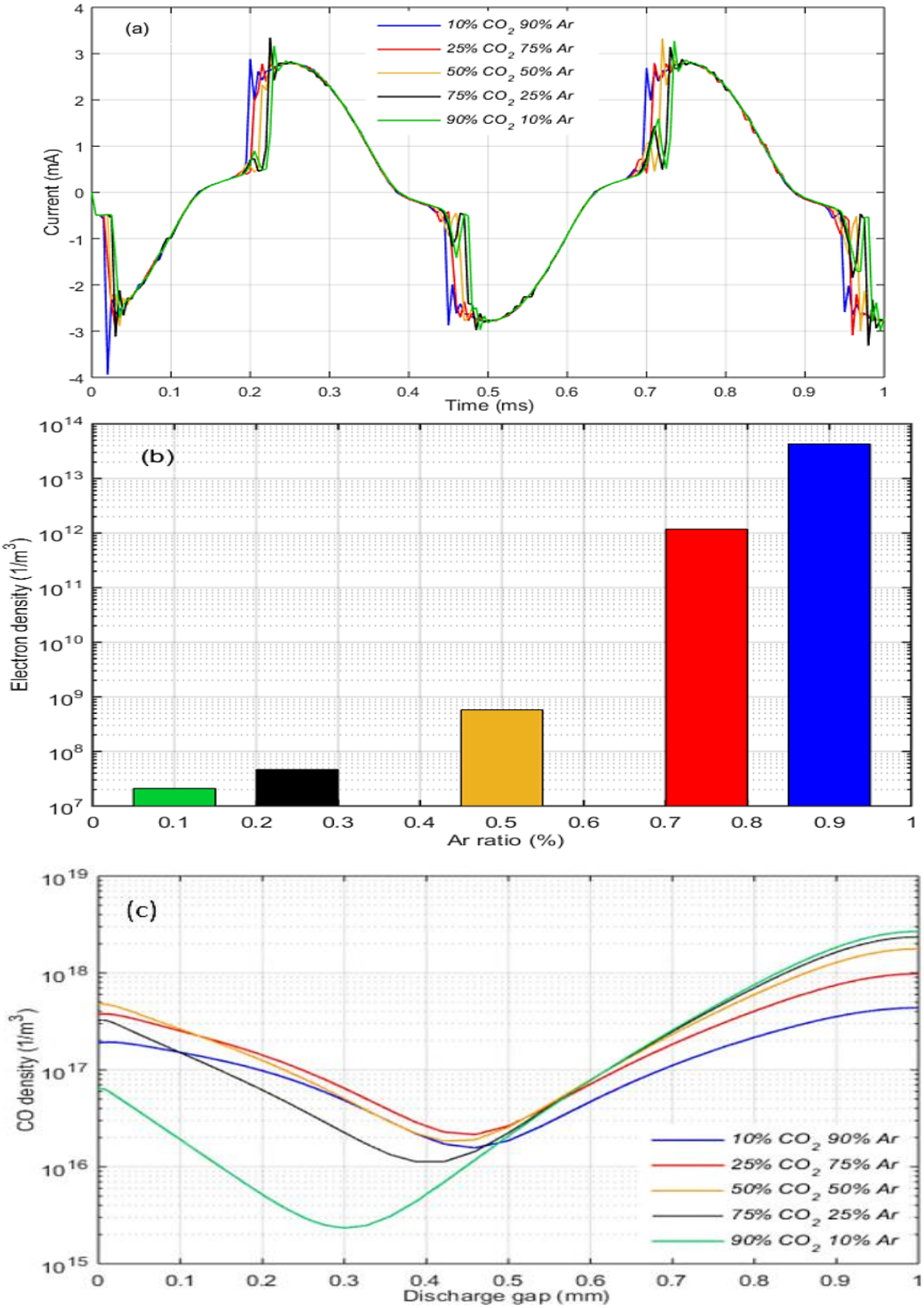

Figure IV. 10: Effect of Ar Dilution on: (a) Current waveform, (b) Electron concentration, (c) CO concentration.

The influence of argon addition is further evidenced by the evolution of the electron density, shown in Figure IV.10(b). The simulations reveal a significant increase in electron density by

nearly seven orders of magnitude when the argon content is raised from 10% to 90%. This substantial enhancement reflects the improved electron production and reduced electron energy losses in argon-rich environments, resulting in more stable and energetic discharge conditions. The elevated electron density plays a critical role in activating CO_2 molecules through electron impact processes, thereby enhancing the overall plasma reactivity.

Consequently, the intensified electron population significantly improves the dissociation of CO_2, as reflected in the spatial distributions of CO density presented in Figure IV.10(c). The highest CO concentrations are obtained for mixtures containing between 75% and 90% argon, where CO densities reach values on the order of 10^{18}–10^{19} m^{-3}. Under these conditions, an optimal balance is achieved between electron impact excitation and vibrational energy transfer mechanisms.

IV.5.2 Influence of frequency

In this study, the applied voltage (6 kV), argon fraction (10%), and operating pressure (760 Torr) were held constant, while the discharge frequency was varied from 2 to 4 kHz. The influence of discharge frequency on the temporal evolution and spatial characteristics of the DBD plasma during CO_2 conversion is presented in Figure IV. 11. At the lowest frequency of 2 kHz, the current waveform exhibits a relatively smooth and weak profile, with moderate peak amplitudes, as shown in Figure IV. 11(a). Under these conditions, the electron density remains low, on the order of 10^8–10^9 m^{-3} Figure IV. 11(b), resulting in limited CO production, as illustrated in Figure IV. 11(c).

When the frequency is increased to 3 kHz, the discharge becomes significantly more energetic, characterized by sharper and higher current peaks (Figure IV. 11(a)). This enhancement is accompanied by a substantial increase in electron density, reaching values up to 10^{12} m^{-3} near the cathode (Figure IV. 11b). The elevated electron population enhances electron-impact dissociation of CO_2, leading to increased CO densities throughout the discharge gap, as shown in Figure IV. 11(c).

At a higher frequency of 4 kHz, although the current amplitude further increases and exhibits pronounced fluctuations, the electron density decreases compared to the 3 kHz case, indicating reduced discharge stability. As a result, CO production is only slightly higher than that obtained at 3 kHz. These findings indicate that an intermediate frequency of 3 kHz offers an optimal compromise between discharge intensity and stability, thereby achieving the most efficient CO_2 conversion in the DBD reactor.

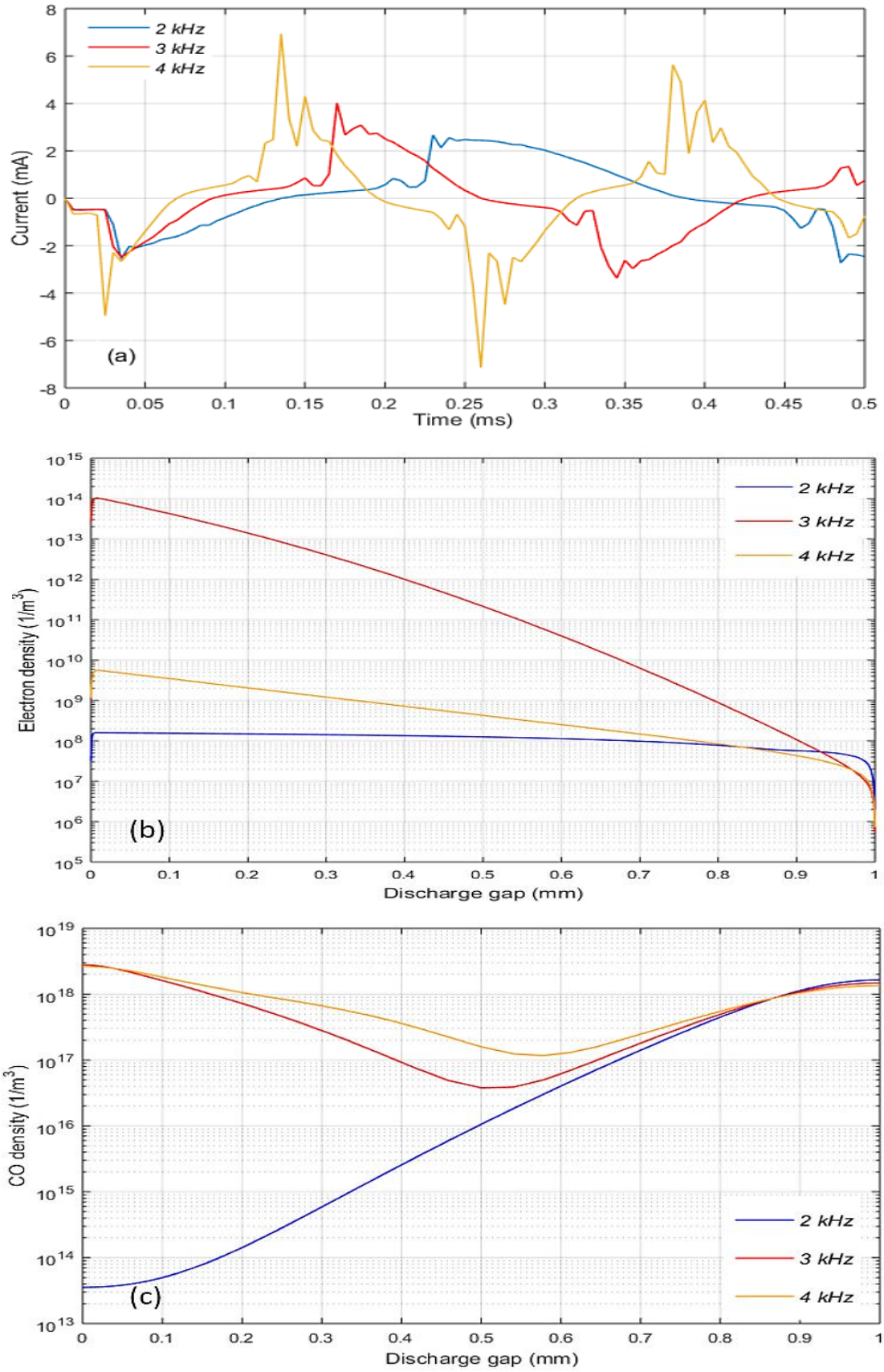

Figure IV. 11: Effect frequency on: (a) Current waveform, (b) Electron concentration, (c) CO concentration.

IV.5.3 Influence of applied voltage

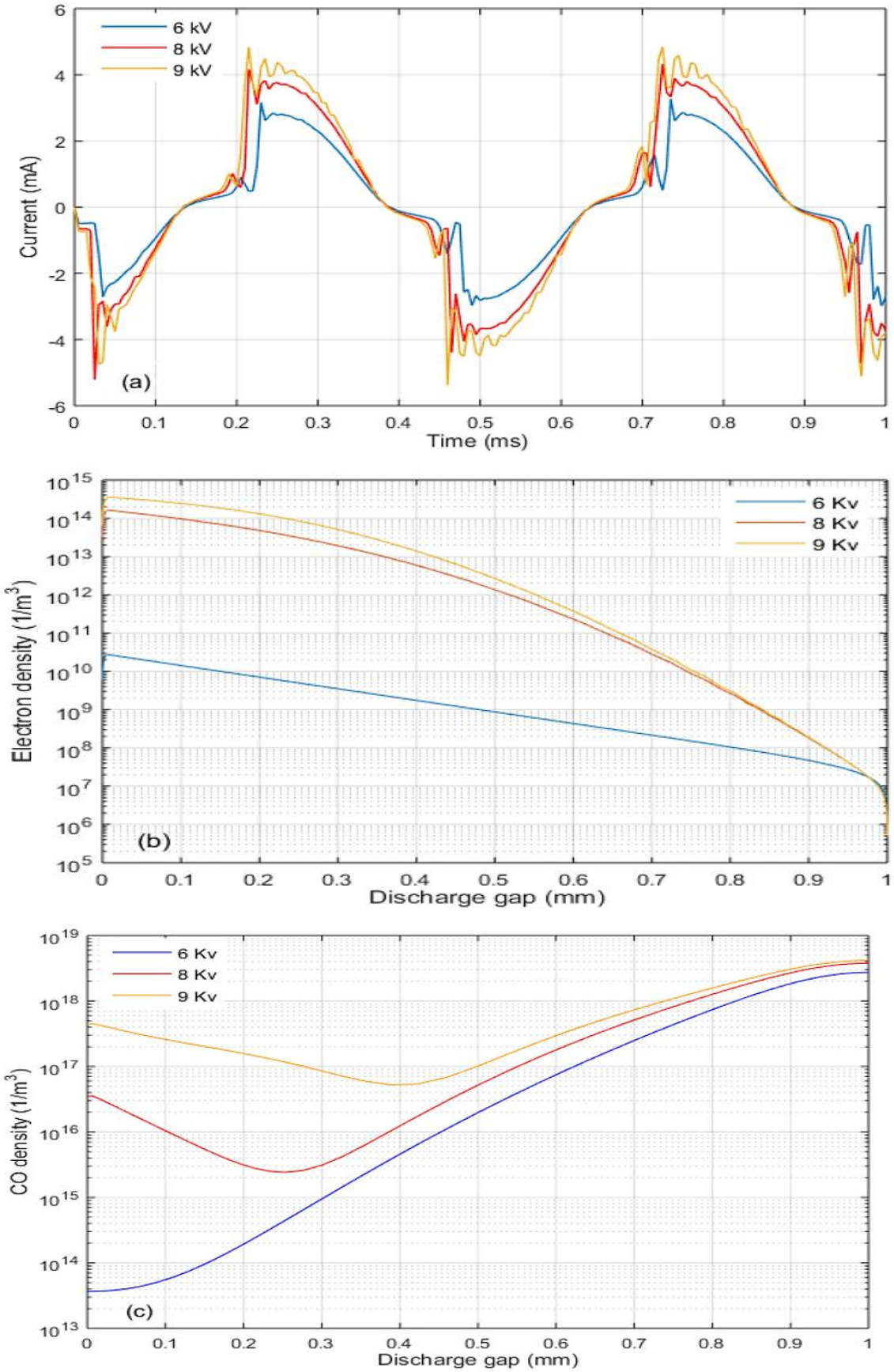

Figure IV. 12: Effect applied voltage on: (a) Current waveform, (b) Electron concentration, (c) CO concentration.

In this analysis, the discharge frequency (2 kHz), argon fraction (10%), and operating pressure (760 Torr) were kept constant, while the applied voltage was varied from 6 to 9 kV. Figure IV.12 (a) presents the discharge current waveforms corresponding to applied voltages of 6, 8, and 9 kV. The current signals display the characteristic periodic behavior of filamentary DBDs. As the applied voltage increases, the discharge current amplitude rises, indicating more intense microdischarge activity. However, at the highest voltage level (9 kV), a tendency toward partial saturation is observed, suggesting the onset of reduced discharge stability at elevated electric fields.

Figure IV. 12(b) shows that increasing the applied voltage leads to a substantial enhancement of the electron density, with increases of several orders of magnitude. This elevated electron population facilitates more effective electron-impact dissociation of CO_2. Consequently, CO production increases markedly with applied voltage, as illustrated in Figure IV. 12(c).

IV.5.4 Influence of gas pressure

In this study, the applied voltage (6 kV), discharge frequency (2 kHz), and argon fraction (10%) were kept constant, while the gas pressure was varied from 500 to 1000 Torr. Figure IV. 13a shows the discharge current waveforms at different pressures. At 500 Torr, the current pulses are sharper, indicating higher electron mobility and reduced collisional damping. In contrast, at 1000 Torr, the current waveforms become broader due to increased electron–neutral collisions, which slow down charge transport. The case of 760 Torr, corresponding to atmospheric pressure, exhibits intermediate behavior between these two regimes.

The spatial distributions of electron density are presented in Figure IV. 13b. At 500 Torr, the electron density reaches values of approximately 10^{14} m^{-3} near the cathode and decreases gradually across the 1 mm discharge gap. Increasing the pressure to 760 Torr reduces the peak electron density to about 10^{13} m^{-3}, accompanied by a steeper spatial decay. At 1000 Torr, the electron density further decreases to around 10^{11} m^{-3}, with a rapid decline along the discharge length. These results clearly demonstrate the strong influence of collisional processes at elevated pressures, which reduce the electron mean free path and suppress ionization.

The effect of pressure on CO production is shown in Figure IV. 13c. At 500 Torr, the CO density increases steadily along the discharge gap, reaching values above 10^{17} m^{-3}, indicating efficient CO_2 dissociation under low-pressure conditions. At atmospheric pressure (760 Torr), CO formation remains significant but decreases to approximately 10^{16} m^{-3}. At 1000 Torr, CO densities drop sharply to about 10^{14} m^{-3}, confirming that enhanced collisional quenching at high pressures strongly limits the generation of reactive species.

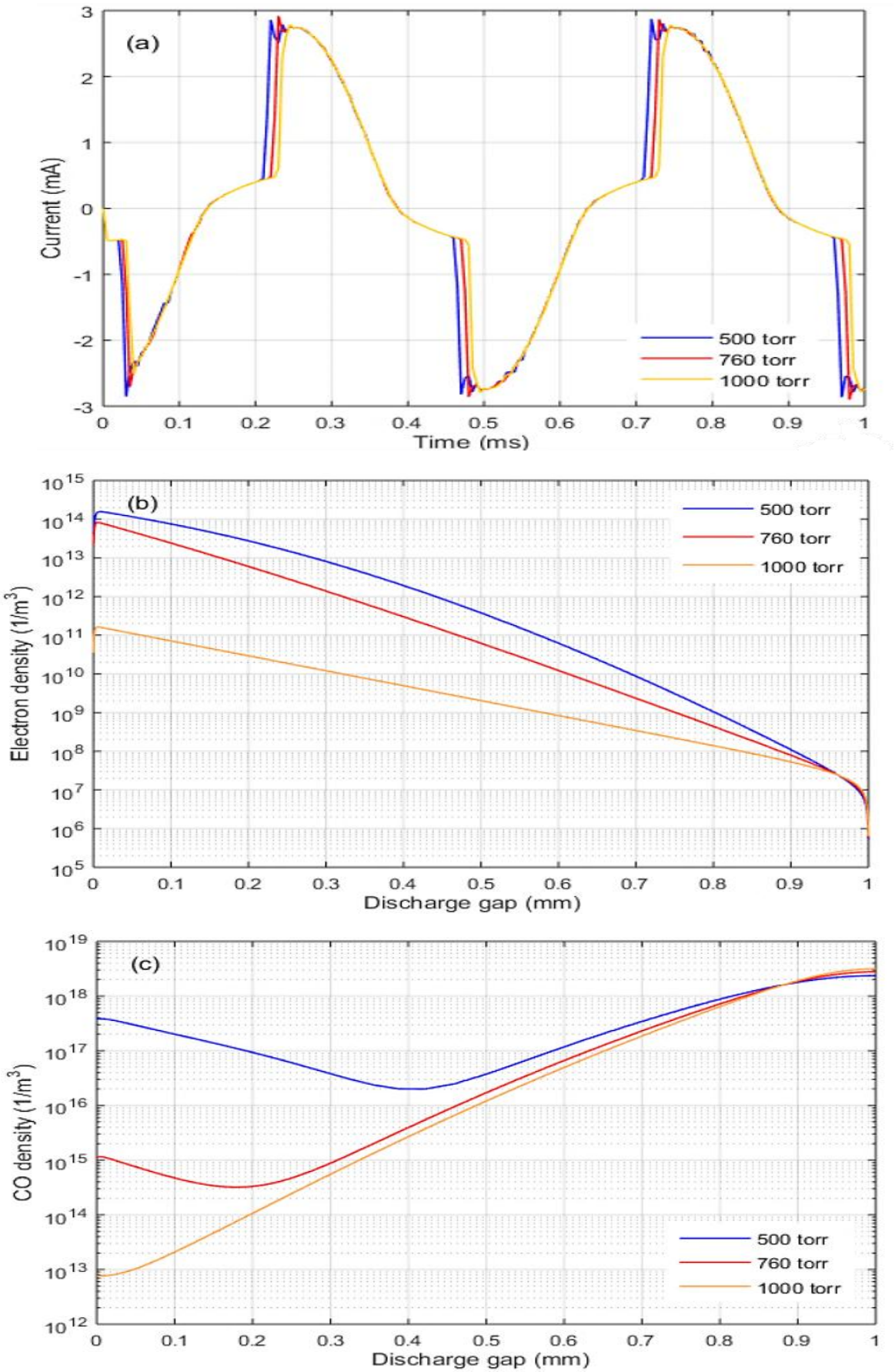

Figure IV. 13: Effect of the gas pressure on: (a) Current waveform, (b) Electron concentration, (c) CO concentration.

IV.5.4 Influence of dielectric material

Figure IV.14 (a) illustrates the time evolution of the discharge current for different dielectric barrier materials characterized by increasing relative permittivity (ε_r). The results show that materials with higher dielectric constants (alumina and gallium arsenide) lead to higher current amplitudes and more pronounced current peaks compared to quartz and glass. This behavior is attributed to the enhanced capacitive coupling of the dielectric barrier: a higher ε_r increases the surface charge accumulation on the dielectric, which strengthens the local electric field in the gas gap and promotes more intense microdischarge activity.

Consequently, gallium arsenide ($\varepsilon_r = 12$) exhibits the strongest current oscillations, indicating a higher discharge intensity.

Figure IV.14 (b) presents the spatial distribution of electron density across the discharge gap. For all dielectric materials, the electron density decreases monotonically from the powered electrode toward the opposite electrode, which is typical of DBD systems due to electron losses by recombination and attachment processes. However, at any given position in the gap, higher dielectric permittivity results in a systematically higher electron density. This confirms that stronger electric fields generated by high dielectrics enhance electron production through impact ionization, leading to a denser plasma.

Figure IV.14 (c) shows the CO number density profile along the discharge gap. The CO density exhibits a minimum near the center of the gap and increases toward the electrodes. This spatial behavior reflects the balance between CO production via CO_2 dissociation and its consumption through recombination and secondary reactions. Importantly, higher permittivity dielectrics lead to significantly higher CO densities over the entire gap, with gallium arsenide producing the maximum CO concentration. This result highlights the strong coupling between plasma electrical properties and chemical conversion efficiency: increased electron density and discharge intensity enhance CO_2 dissociation pathways.

Taken together, these results demonstrate that the dielectric material plays a crucial role in controlling DBD plasma behavior. Increasing the dielectric permittivity:

- Intensifies discharge currents and microdischarge activity
- Enhances electron density within the plasma
- Promotes more efficient CO_2 dissociation and higher CO production

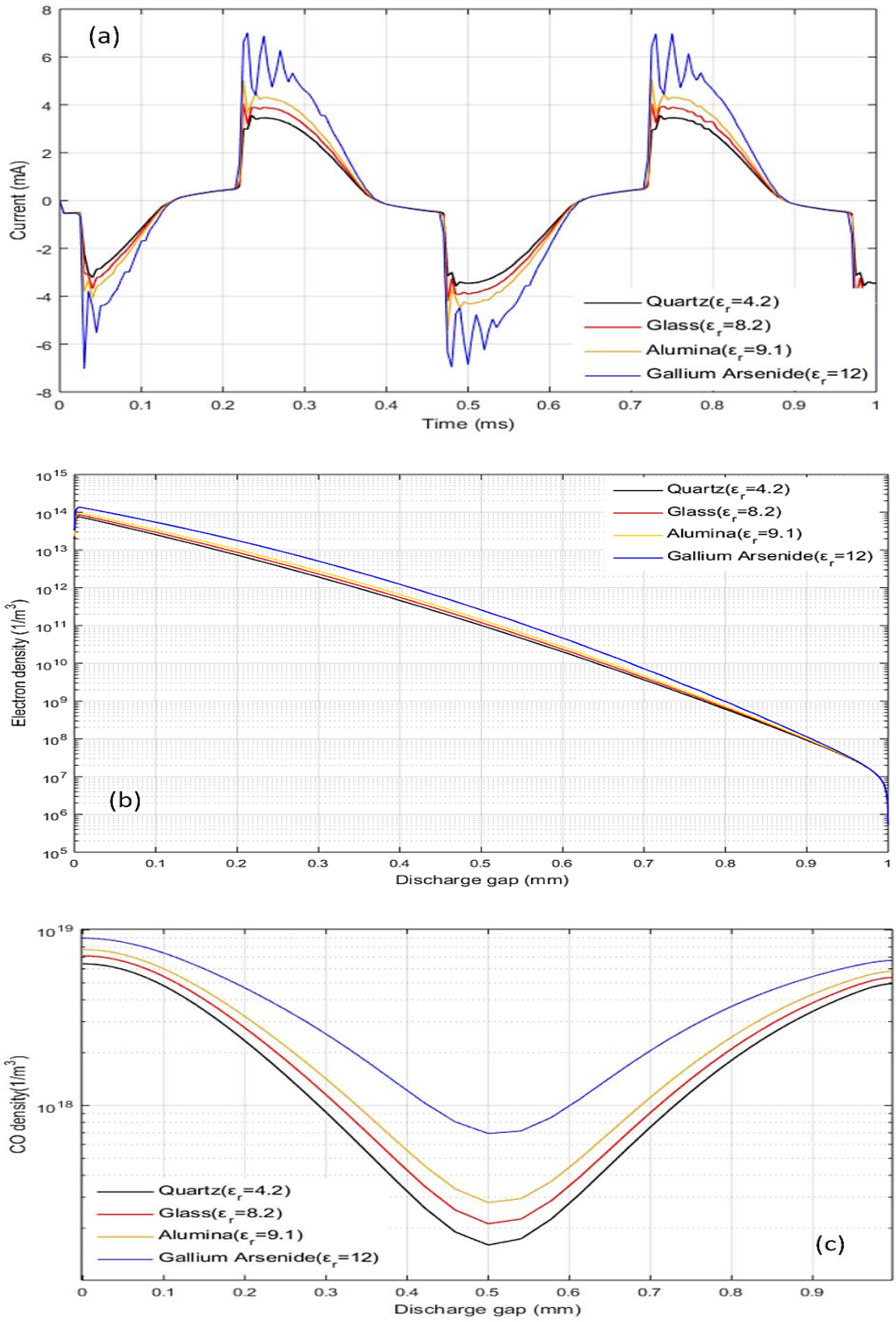

Figure IV.14: Effect of dielectric material on: (a) Current waveform, (b) Electron concentration, (c) CO concentration.

Therefore, high ε_r dielectric materials such as gallium arsenide and alumina are more favorable for plasma-assisted CO_2 conversion applications. However, the associated increase in discharge intensity may also lead to stronger filamentation and higher dielectric stress, which must be considered in reactor design and long-term operation.

IV.6 Conclusion

This study examined the electrical and physicochemical behavior of dielectric barrier discharges operating in pure CO_2 and CO_2/Ar mixtures at atmospheric pressure through numerical simulations validated by comparison with experimental data. The results demonstrate that the proposed model accurately reproduces the main discharge characteristics, including the phase shift between the applied and gas voltages, the occurrence of current peaks associated with plasma breakdown, and the formation of the primary reaction products, namely CO and O_2.

Parametric investigations show that the addition of argon markedly increases the electron density and enhances CO production. The discharge frequency plays a critical role in determining discharge stability, with optimal CO_2 conversion observed around 3 kHz. Increasing the applied voltage improves CO_2 dissociation efficiency up to a saturation regime, beyond which further voltage increases do not lead to additional conversion due to energy losses associated with gas heating, recombination processes, and reduced discharge stability. Moreover, higher operating pressures are found to suppress CO_2 conversion as a result of enhanced collisional quenching.

Overall, these findings emphasize the necessity of optimizing key operating parameters particularly argon concentration, discharge frequency, and applied voltage to achieve efficient CO_2 splitting in DBD reactors. The results provide valuable guidance for the design and optimization of plasma-based CO_2 conversion systems.

References

[1] Talviste, R., Reino, C. R., Paris, P., Raud, J., Plank, T., & Jõgi, I. (2023b). Study of apparent effective ionization coefficient in CO_2 and Ar gas mixtures. Physics of Plasmas, 30(11).

[2] Hasan, M. I., & Walsh, J. L. (2016). Numerical investigation of the spatiotemporal distribution of chemical species in an atmospheric surface barrier-discharge. Journal of Applied Physics.

[3] Grosch, H., Hoder, T., Weltmann, K. -d., & Brandenburg, R. (2010). Spatio-temporal development of microdischarges in a surface barrier discharge arrangement in air at atmospheric pressure. The European Physical Journal D, 60(3), 547–553.

[4] Bajon, C., Dap, S., Belinger, A., Guaitella, O., Hoder, T., & Naudé, N. (2023). Homogeneous dielectric barrier discharge in CO_2. Plasma Sources Science and Technology, 32(4), 045012.

[5] LXCAT, electron scattering database, University of Toulouse, France. www.lxcat.net. retrieved on January 23, 2025.

[6] Phelps database, www.lxcat.net, retrieved on May 4, 2025.

[7] Biagi database, www.lxcat.net, retrieved on May 4, 2025.

[8] Moss, M. S., Yanallah, K., Allen, R. W. K., & Pontiga, F. (2017b). An investigation of CO2splitting using nanosecond pulsed corona discharge: effect of argon addition on CO2conversion and energy efficiency. Plasma Sources Science and Technology, 26(3)

[9] Elahi, R., Simasiku, E. M., & Trelles, J. P. (2023b). Computational modeling of CO_2 conversion by a solar-enhanced microwave plasma reactor. Plasma Sources Science and Technology, 32(6), 065018.

[10] Brezmes, A. O., & Breitkopf, C. (2019b). Numerical analysis of atmospheric pressure plasma produced by a dielectric barrier discharge in a mixture of AR/CO_2. IEEE Transactions on Radiation and Plasma Medical Sciences, 4(4), 498–511.

[11] Beuthe, T. G. B. T. G., & Chang, J.-S. C. J.-S. (1997). Chemical kinetic modelling of Non-Equilibrium AR-CO_2 thermal plasmas. Japanese Journal of Applied Physics, 36(7S), 4997.

[12] Vermeiren, Vincent. Chemical kinetics modeling of non-equilibrium and thermal effects in vibrationally active CO_2 plasmas. Diss. University of Antwerp, 2020.

[13] Saidia, L., Belasri, A., Baadj, S., & Harrache, Z. (2019). Physico-chemical investigation of pulsed discharge in CO_2/O_2 gas mixture. Plasma Physics Reports, 45(5), 501–516.

[14] LAHOUEL, M. H. A. (2021). Modélisation et simulation d'une décharge à barrière

diélectriques dans un Mélange gazeux à la pression atmosphérique (Doctoral dissertation, Djilali BENYOUCEF/Hocine TEBANI).

[15] Chenoui.M. Tebani, H., & Benyoucef, D Zero-dimensional Modeling of Dielectric Barrier Discharge in Pure Carbon Dioxide, The 3rd edition of the international conference on materials science and engineering and their impact on the environment, Djilali Lyabes University of Sidi-Bel-Abbes, 29-30-May 2024.

[16] Dawson, J. M. (1983). Particle simulation of plasmas. Reviews of modern physics, 55(2), 403.

[17] Brown, L. S., Preston, D. L., & Singleton Jr, R. L. (2005). Charged particle motion in a highly ionized plasma. Physics Reports, 410(4), 237-333.

[18] Kee, R. J., Rupley, F. M., Meeks, E., & Miller, J. A. (1996). CHEMKIN-III: A FORTRAN chemical kinetics package for the analysis of gas-phase chemical and plasma kinetics (No. SAND-96-8216). Sandia National Lab.(SNL-CA), Livermore, CA (United States).

[19] Wende, K., von Woedtke, T., Weltmann, K. D., & Bekeschus, S. (2018). Chemistry and biochemistry of cold physical plasma derived reactive species in liquids. Biological Chemistry, 400(1), 19-38.

[20] Cortez, A. (2020). A Practical Approach to Ion Mobility. New Horizons in Time Projection Cambers, Santiago de Compostela (Spain).

General Conclusion

General conclusion

In this thesis, a comprehensive numerical investigation of dielectric barrier discharge plasmas operating in CO_2 and CO_2/Ar mixtures at atmospheric pressure has been conducted. A self-consistent plasma model was developed to describe the coupled electrical, kinetic, and chemical processes occurring within the discharge. The model successfully reproduces key discharge features, including current waveforms, electron density evolution, and the formation of reactive species, and shows good agreement with experimental observations.

The first chapter provides a general overview of plasmas and electrical discharges, introducing fundamental plasma concepts, classification of discharge regimes, and voltage–current characteristics of gas discharges. Particular emphasis is placed on non-thermal plasmas and their advantages for gas treatment and environmental applications.

The second chapter is devoted to the fundamentals of dielectric barrier discharges. It reviews the historical development of DBDs, their operating principles, discharge regimes, reactor configurations, and the role of dielectric materials in stabilizing the discharge and preventing arc formation, The chapter further examines the different operating regimes of DBDs, highlighting the filamentary, homogeneous, and multi-peak modes, which are critical for determining plasma uniformity and reactivity. Finally, major application areas of DBD technology are presented, with particular emphasis on environmental processes and carbon dioxide conversion.

In the third chapter, the plasma modeling framework is presented. The governing equations, boundary conditions, and numerical solution strategies are detailed. The computational approach adopted allows for the self-consistent simulation of electrical, kinetic, and chemical phenomena occurring in CO_2/Ar DBD systems.

The fourth chapter focuses on the modeling and electrical characterization of CO_2/Ar dielectric barrier discharges, plasma chemistry, transport coefficients. Simulation results are analyzed and compared with experimental data to validate the model. The effects of key operating parameters, including applied voltage, excitation frequency, gas composition, pressure, and dielectric properties, are systematically investigated.

The results demonstrate that the addition of argon plays a significant role in enhancing discharge stability and increasing electron density, thereby improving CO_2 dissociation and carbon monoxide production. The influence of operating parameters such as applied voltage, excitation frequency, gas pressure, and dielectric material properties was systematically analyzed. It was shown that optimal CO_2 conversion is achieved at intermediate voltages and frequencies, where efficient energy transfer to electrons is maximized while minimizing losses due to gas heating and

recombination. Conversely, higher gas pressures were found to suppress ionization processes due to increased collisional quenching, leading to reduced conversion efficiency.

Overall, this work highlights the importance of carefully optimizing operating conditions and reactor design to achieve efficient plasma-assisted CO_2 conversion. The findings contribute to a deeper understanding of non-thermal DBD plasma behavior and provide a solid foundation for the development of advanced plasma-based systems for environmental protection and carbon utilization.

Future Works

Although this study provides important insights into the modeling and optimization of CO_2/Ar dielectric barrier discharge plasmas, several avenues remain for future research. Model extensions to higher-dimensional geometries could better capture discharge non-uniformities and filamentary behavior. Incorporating detailed plasma surface interactions and expanded plasma chemistry would further improve accuracy and relevance to industrial conditions. Experimental validation using advanced diagnostics is also essential to refine model predictions. Finally, exploring alternative gas mixtures, and integration with renewable energy sources offers promising pathways toward more efficient and sustainable plasma-based CO_2 conversion technologies.